COLLAPSE RISK ESTIMATION OF REINFORCED CONCRETE BUILDINGS

by

Tamer İzzet Beyazoğlu

B.S., Civil Engineering, Yıldız Technical University, 2005

Submitted to the Kandilli Observatory and
Earthquake Research Institute in partial fulfillment of
the requirements for degree of
Master of Science

Graduate Program in Earthquake Engineering
Boğaziçi University
2013

To my family,

ACKNOWLEDGEMENTS

I would like to express my gratitude to Professor Nuray Aydınoğlu for his guidance and help during the preparation of this dissertation. It is very hard to describe the honor of working with such a valuable scientist. I would also like to thank for his understanding. Also, I would like to express my gratefulness to the department of Earthquake Engineering during my M.S. education with whom I had the chance to take courses and work with, Prof. Erdal Şafak, Prof. Atilla Ansal, Prof. Uğur Ersoy, Prof. Semih Tezcan, Ass. Prof. Gülüm Tanırcan. Their support is greatly acknowledged.

I would like to express my special thanks to Cüneyt Tüzün for his valuable contributions to my experience in engineering practice, his support in all aspects made me feel like at home in Kandilli rather than a school.

I would also like to express my special thanks to Şeref Polat, and ErenVuran for their help about preparation of computer model and guidance for the problems.

I would like to express my thanks to my colleagues Serkan Görk, Kenan Turandar, Barbaros Çetiner and Tarık Tufan for their support during the preparation of this dissertation.

I would like to express my special thanks to my mother, my father and all of my family for their supports, their encouragement about this dissertation.

ABSTRACT

COLLAPSE RISK ESTIMATION OF REINFORCED CONCRETE BUILDINGS

In this study, collapse risks of five-storey RC frame buildings are estimated analytically using advance mathematical model. The concentration of this study is on advanced nonlinear analysis of the building including nonlinear modeling of columns and beams with their shear capacities. Collapse fragility curves are obtained in terms of spectral acceleration corresponding to dominant natural period of the building. The collapse risk of the building is obtained through integration of collapse fragility curves of models and corresponding hazard curve.

In the first chapter of this study, the scope of the work and literature survey have been given. In the second chapter, the methodology of estimating collapse risk in an analytical way has been introduced. The steps of the proposed methodology for collapse risk estimation have been explained briefly. In the third chapter, mathematical modeling of the buildings has been given in details in terms of non-linear material properties, lump and distributed plasticity approach for structural members. In the fourth chapter, objectives of the analysis, the strong ground motion records and hazard curves used in the analysis phase have been presented. In the fifth chapter, fragility curves are obtained and the collapse risk has been calculated for each building under consideration. In the last chapter, the conclusions are presented.

ÖZET

BETONARME BİNALARIN YIKILMA RİSKİNİN TAHMİN EDİLMESİ

Bu çalışmada, yapının gelişmiş matematiksel modeli kullanılarak, beş katlı betonarme çerçeveli binaların göçme riskleri tahmin edildi. Yoğunluklu olarak bu çalışmada, yapının elastik ötesi davranışının modellenmesi üzerinde durulmuştur. Kolon ve kirişlerin kesme kapasiteleri de göz önüne alınarak elastik ötesi davranışları incelenmiştir. Yapının birinci doğal titreşim periodunа karşı gelen spektral ivmeye göre, yapı hasar görebilirlik eğrileri çıkarılmıştır. Modelin göçme hasar görebilirlik eğrisi ve buna karşılık gelen depremsellik eğrisinin birlikte entegre edilmesiyle yapının göçme riski elde edilmiştir.

Bu çalışmanın ilk bölümünde, çalışmanın genel çerçevesi çizilmiştir. İkinci bölümünde, analitik olarak göçme analizinin metodolojisi tanıtılmıştır. Göçme riskinin tahminiyle ilgili adımlar kısaca açıklanmıştır. Üçüncü bölümünde, yapının matematiksel modeli detaylı bir şekilde verilmiştir. Malzeme ve elastik ötesi şekilde yük taşıyan elemanlar, detaylı bir şekilde açıklanmıştır. Dördüncü bölümünde, "Artımsal Dinamik Analizi" açıklanarak, çalışmada kullanılan deprem kayıtları ve depremsellik eğrisi verilmiştir. Beşinci bölümünde, hasar görebilirlik eğrileri oluşturularak yapıların göçme riskleri hesaplanmıştır. Son bölümünde ise sonuçlar sunulmuştur.

TABLE OF CONTENTS

LIST OF FIGURES

LIST OF TABLES

LIST OF SYMBOLS / ABBREVIATIONS

a_1	Unscaled accelerogram
a_i	Spacing between longitudinal reinforcements around the core
a_λ	Scaled accelerogram
A_{ch}	Concrete core area
A_s	Area of longitudinal reinforcement
b_o	Confined core dimension
C	Damping matrix
E_c	Tangent modulus of elasticity of the concrete
f	Nonlinear internal force
f_c	Longitudinal compressive concrete stress
f_{cc}	Compressive strength of confined concrete
f_{co}	Unconfined concrete strength
f_{ctk}	Characteristic design strength of concrete
f_e	Effective lateral confining stress on the concrete.
f_G	Equivalent P-delta force
f_{yw}	Yield strength of transverse reinforcement
f_{ywk}	Characteristic yield strength of transverse reinforcement
h	Height of column
h_o	Confined core dimension
im	Intensity measure
k	Stiffness of the element
k_e	Confinement effectiveness coefficient
K	Stiffness matrix
$\mathbf{K}_G$	Global geometric-stiffness matrix
$\mathbf{K}_{initial}$	Global initial stiffness maxrix
M	Mass matrix
M_w	Moment magnitude
P	Probability
s	Clear vertical spacing between spiral or hoop bars

S_a (T_1, 5%)	5 % damped first-mode spectral acceleration
V_r	Shear force
Δ	Lateral displacement
Φ	Log-normal probability function
λ	Non-negative scalar
λ_C	Mean annual frequency of collapse
μ	Mean of the natural logarithm of random variable
σ	Standard derivation of the natural logarithm of random variable
ρ_s	Volumetric ratio of total transverse reinforcement
ρ_{sh}	Volumetric ratio of transverse reinforcement
ε_c	Longitudinal compressive concrete strain
ε_{cc}	Longitudinal compressive concrete strain at compressive strength of confined concrete
ε_{co}	Longitudinal compressive concrete strain at compressive strength of unconfined concrete
ε_{cu}	Ultimate strain of confined concrete
ε_{su}	Ultimate strain of confinement reinforcement

ATC	Applied Technology Council
CDF	Cumulative Distribution Function
FEMA	Federal Emergency Management Agency
IDA	Incremental Dynamic Analysis
IM	Intensity Measure
IN2	Incremental N2 method
K-Net	Strong-motion seismograph networks in Japan
NGA	Next- Generation Attenuation
NRHA	Nonlinear Response History Analysis
PGA	Peak Ground Acceleration
PGMD	PEER Ground Motion Database
PGV	Peak Ground Velocity
RTR	Record-to-record

1. INTRODUCTION

The primary objective of this study to estimate the collapse risks of five-story modern reinforced concrete moment frame buildings in terms of mean annual frequency of collapse. For this purpose, advanced nonlinear structural models of the buildings are developed. The nonlinear modeling of structural members is done by using fiber model for columns and plastic hinges for beams.

Collapse risk is estimated in two steps. In the first step, a collapse fragility curve is obtained with respect to spectral acceleration corresponding to dominant natural period of the building in a given earthquake direction. In the formation of fragility curve, a set of strong ground motion records has been used in order to consider record to record variability. The second step involves the evaluation of the so called risk integral. The fragility curves and derivative of the hazard curve are integrated to obtain the mean annual collapse frequency of the building.

In the literature many different methodologies have been introduced to obtain fragility curves. In ATC-13 (1985), the proposed fragility curves are obtained based on expert judgment. P. Fajfar (Matjaz *et al.*, 2004) has proposed an analytical methodology to obtain fragility curves by using IN2 method. This method is based on a probabilistic framework in which the pushover of the system is converted to IDA curve. In another analytical methodology proposed by A.K. Chopra (Han *et al.*, 2004) fragility curves are obtained based on a Single Degree of Freedom (SDOF) oscillator which is constructed from the pushover curve of the system through multi-mode pushover method with superposing effects of different modes independently. Then a classical IDA procedure is applied to this SDOF oscillator of each mode.

In this study, the fragility curves are obtained through an analytical methodology by using nonlinear response history analysis details of which are given in Chapter 2.

On the other hand, an efficient method for easy estimation of the collapse risk is applied. Since the fragility curve is log-normally distributed, the entire fragility curve can be clearly defined by two parameters: a median value and a standard derivation. Instead of these two independent variables, two random points on the cumulative distribution function can also represent the log-normally distributed curve. This efficient method is also applied to obtain the mean annual collapse frequency of the building.

2. METHODOLOGY

2.1. Collapse Risk Estimation

The mean annual frequency of collapse can be calculated using integration of fragility and hazard curves with given Equation 2.1;

$$\lambda_C = \int_0^\infty P(C|im) \cdot |d\lambda_{IM}(im)| \tag{2.1}$$

where P(C | *im*) is the probability of collapse (C) when excited by an earthquake with intensity measure *im* and λ_{IM} is the mean annual frequency of exceedance of ground motion intensity *im* (Eads *et al.*, 2013).

The Equation 2.1 can be rewritten as Equation 2.2 to use hazard curve in an easy way when calculating annual frequency of collapse, λ_C.

$$\lambda_C = \int_0^\infty P(C|im) \cdot \left|\frac{d\lambda_{IM}(im)}{d(im)}\right| d(im) \tag{2.2}$$

where λ_{IM} *(im)/d(im)* is the slope of the seismic hazard curve at the site. Generally the closed-form solution of integration given at Equation 2.2 cannot be represented. Therefore the numerical integration is used to obtain annual frequency of collapse, λ_C.

The probability of collapse in a desired period, namely collapse risk, is calculated using Equation 2.3 assuming Poisson distributions for occurrence of earthquakes in years. For buildings, the probability of desired damage level in one-year is almost the same as λ_C (Eads *et al.*, 2013).

$$Pr_C(in\ t\ years) = 1 - \exp(-\lambda_C\, t) \tag{2.3}$$

2.2. Fragility Curve Formation

A fragility curve can be defined as a cumulative distribution function (CDF) which associates the probability of the selected damage level with ground motion intensity. This curve is obtained from the all IDA curves that represent every individual ground motion. (Ibarra and Krawinkler, 2005). Studies shows that fragility curve, namely cumulative distribution function, can be sufficiently well represented by two parameters of a lognormal distribution function. In that curve, the intensity measure can be represented by many parameters such as peak ground acceleration, PGA, peak ground velocity, PGV, the normalized factor $R=\lambda/\lambda_{yield}$ or the 5 % damped first-mode spectral acceleration S_a (T_1, 5%).

IDA is an analysis method to estimate structural response under seismic excitations (Vamvatsikos and Cornell, 2002). This method includes a structure subjected to strong ground motions, each of which is scaled to different levels of intensity in time domain for a given ground motion parameter. Intensity measure should be selected carefully to represent ground motion with one parameter. Then, IDA curves are generated as response of structure parameterized various intensity levels. Extreme increment in response of structure with very small increase in intensity level of ground motion is used as indicator of collapse in IDA curves for ductile structures.

In this study, collapse has been selected as the desired damage level. The dynamic instability of structure is concerned with suitable material and member force-deformation relationships. The intensity measure is taken the 5 % damped first-mode spectral acceleration, S_a (T_1, 5%). Using these damage and intensity measures, the IDA curves are obtained for the four five-storey building models used in this study.

When the collapse state is concern, collapse fragility curves describe the building's probability of collapse conditioned on the intensity of the ground motion. Generally, collapse state is reached due to loss of vertical load carrying capacity which is a special case of the dynamic instability. In this case, collapse damage level depends on both the structural system and ground motion. At a given intensity measure, collapse probability is calculated by dividing the number of records causing collapse to total number of records (Krawinkler, 2013). Briefly, collapse fragility curve can be defined as a diagram which

presents information how the probability of collapse develops with increasing ground motion intensity.

2.3. Hazard Curve

The mean annual frequency of exceeding ground motion parameters at a site is described by seismic hazard. Selected ground motion parameter in hazard curve should be same as intensity measure (IM) to be used for scaling of ground motion records. Using same parameter, risk of exceeding any damage level can be calculated by integration of fragility and hazard curves.

There are basically four steps for obtaining a hazard curve for a given site. Firstly, earthquake sources affecting the site are identified. These sources can be defined as area, line and rarely point sources. Second step is establishment of a magnitude recurrence relationship for each source. This relationship gives the temporal behavior of earthquake at selected source. Gutenberg and Richter (1954) recurrence model is widely used. Third step is selection of ground motion attenuation models. Ground motion attenuation models give the change of ground motion parameters with seismological parameters, which are properties of earthquake (magnitude, style-of-faulting), distance and site conditions. In recent seismic hazard analysis studies next generation attenuation (NGA) relationships (2008) are widely used. At the last step, all three steps mentioned above are integrated over all possible magnitude and earthquake locations to find seismic hazard at the site. These steps are represented seen schematically in Figure 2.1.

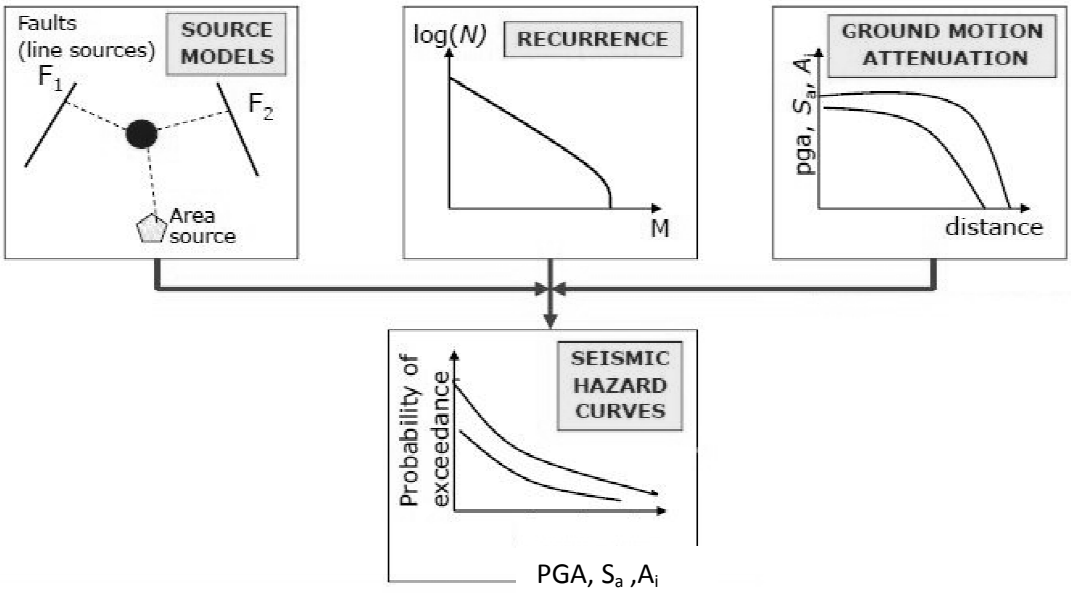

Figure 2.1. Basic steps of establishment of hazard curve (Tanırcan, 2010).

2.4. Nonlinear Structural Modeling

It is a well known fact that structures respond beyond their elastic limit under earthquake excitation. In order to capture the inelastic response of structures up to collapse level nonlinear modeling is of great importance. Additionally, some simplifications can be used such as rigid-diaphragm modeling and neglecting stiffness of infill walls and other nonstructural elements while their masses and weights are taken into consideration.

Basically there are two main approaches for nonlinear modeling such as lumped and distributed plasticity. In lumped plasticity approach plastic deformations of the structural members are assumed to be concentrated at predefined location called plastic hinges. This approach is generally used for frame elements, i.e. beams and columns. In the distributed plasticity approach structural members are modeled by using fiber elements which is defined along the member.

Determination of nonlinear modeling approach depends on the complexity of structural members. As the fiber approach is more complicated than the plastic hinge assumption, it should be used carefully in order to avoid long computational time.

2.4.1. Lumped Plasticity

The lumped plasticity known as plastic hinge which is a zero length component is widely used because of its simplicity and less computational time. In this type of modeling, the nonlinear behavior is assumed to be concentrated at center of plastic zone while the plastic hinge is defined at the each end of clear length of a structural member. Plastic hinge behavior can be represented by a moment-curvature relationship, moment-rotation relationship or axial load - bending moment interaction. Generally, these relationships are bilinearized in the form of with or without strain hardening.

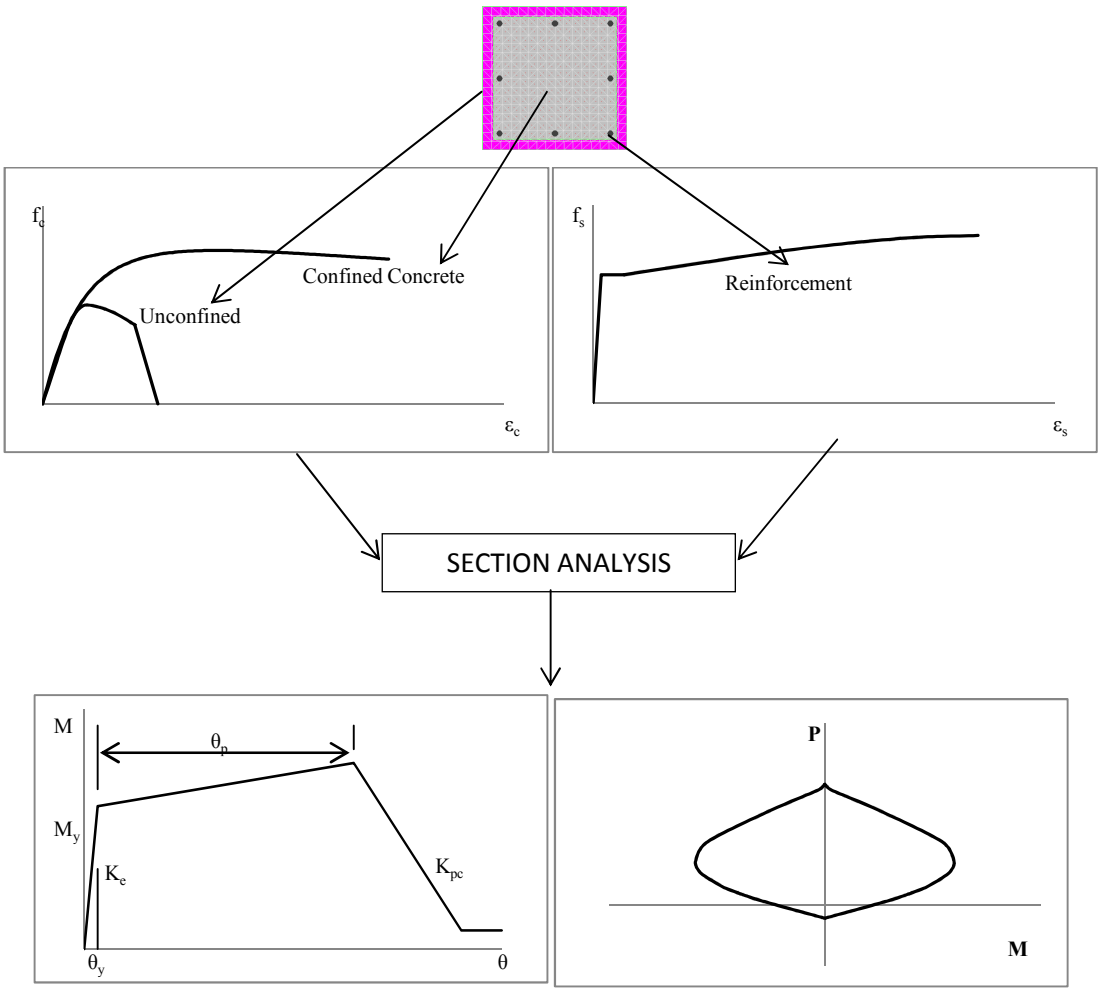

Figure 2.2. Lumped plasticity definition.

Plastic hinges can be defined in different degrees of freedom such as axial force hinge, shear hinge and most commonly moment hinges. For the members whose yield condition is defined by interaction of axial load and bending moment, yield surfaces should be defined in 2-D and 3-D form.

For practice oriented nonlinear analysis procedures such as pushover analysis, all these yielding criteria defined by curves or surfaces in the form of typical moment rotation relationships for plastic sections are sufficient On the other hand, cyclic hysteresis of plastic hinges are also needed to represent unloading and reloading branches of the real behavior of hinges in the Nonlinear Response History Analysis (NRHA). There are many hysteresis rules for different type of members available in the literature, such as standard bi-linear model, peak-oriented model with or without pinching and Takeda type models.

2.4.2. Distributed Plasticity

The most popular distributed plasticity model used for nonlinear modeling is the fiber model. In this model, cross sections are divided into concrete and steel fibers given in Figure 2.3. The force-deformation relationships of each fiber are defined by the uniaxial stress-strain relationships of concrete and reinforcement fibers. There are many material models are available for unconfined concrete, confined concrete and steel.

As it is indicated above, the fiber model is more advanced model than the plastic hinge model. It is used commonly for rectangular and U or L shaped flexural walls in plan while it is not preferred in frame elements, especially for beams, because of longer computational time. In performance evaluation of these walls, the concrete and steel strain capacities can be used directly without any transformation from curvature or rotation to strain.

In lumped plasticity approaches, shifting of the neutral axis cannot be modeled because plastic hinge model assumes that all rotations occur around the predetermined point at the centroidal axis of the frame section. Also, strains due to axial force must be thought independently from strains due to bending moment. As such, the plasticity theory used in plastic hinge analyses overestimates the amount of axial elongation for reinforced

concrete in cyclic loading. On the other hand, fiber sections modeled with nonlinear uniaxial fiber segments overcome all these problems more realistically (PERFORM-3D, 2011).

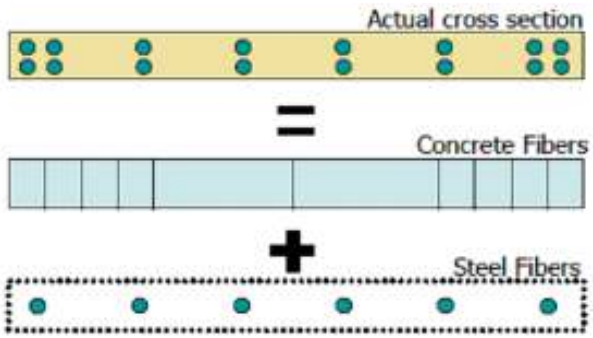

Figure 2.3. Fiber model of cross-section.

3. MODELING

3.1. Description of Buildings

Four five-story reinforced concrete residential buildings used in this collapse risk analysis is selected from existing building stock of Bolu city which has been struck by 12th November 1999 Düzce earthquake with M_w=7.2 magnitude. These buildings are named with the number of 411, 617,668 and 1472 from the database. All those four buildings are monolithic beam-column connection frame structures. It can be asset that the selected structures symbolize the regional engineering capabilities for typical Turkish practice. This practice is generally settled the position of beams according to the position of infill-walls in plan. Therefore regular frame system in elevation can not be formed. Design drawings and design reports were obtained from previously studied structure database at Bolu city (Tüzün, 2008). By using the design drawings of these real structures, the nonlinear design parameters such as framework plans, loads, material strength, longitudinal and transverse reinforcement detailing are determined. Some basic properties, framing plan views and 3D-views of those four building shown in Table 3.1 and Figure 3.1 to Figure 3.8 respectively.

The effects of the foundation and local site condition are neglected in this study. The story heights vary from three meter to five meter. In modeling and analysis of the building, the Perform-3D V5 by CSI software is used. Rayleigh damping in which damping matrix is assumed to be proportional to stiffness and mass matrices is preferred as the damping model in the nonlinear time history analysis with five percent damping coefficient.

Some modeling assumptions can be listed as:

- The nonlinear behavior of the columns is defined by fiber elements.
- The nonlinear behaviors of beams are defined by rigid plastic hinges.

- All hinges of the beams are located at the ends of the members. The masses of all structural and non-structural members are assumed to be lumped at the mass center of the rigid diaphragms for every storey level.
- Through section analysis, plastic hinge properties are determined by considering material strength, cross-section dimensions, longitudinal and transverse reinforcement configuration.
- All beams are modeled as frame elements with forty percent of their gross section stiffness of uncracked section stiffness.
- At the beam-column joints, rigid end zone are defined.
- Detailed information about modeling of the five-storey building is given in the proceeding parts of this study.

Table 3.1. Some basic properties of the buildings.

Building Name	**Storey height (m)**					**Concrete Strength**	**Reinforcement Strength**	**Period (Sec)**	
	1	**2**	**3**	**4**	**5**			**X direction**	**Y direction**
411	2.80	2.80	2.80	2.80	2.80	C14	S220	0.906	0.673
617	2.80	2.80	2.80	2.80	2.80	C16	S220	0.732	0.609
668	3.30	2.80	2.80	2.80	2.80	C14	S220	0.659	0.859
1472	3.40	3.40	3.40	3.40	3.40	C12	S220	0.549	0.923

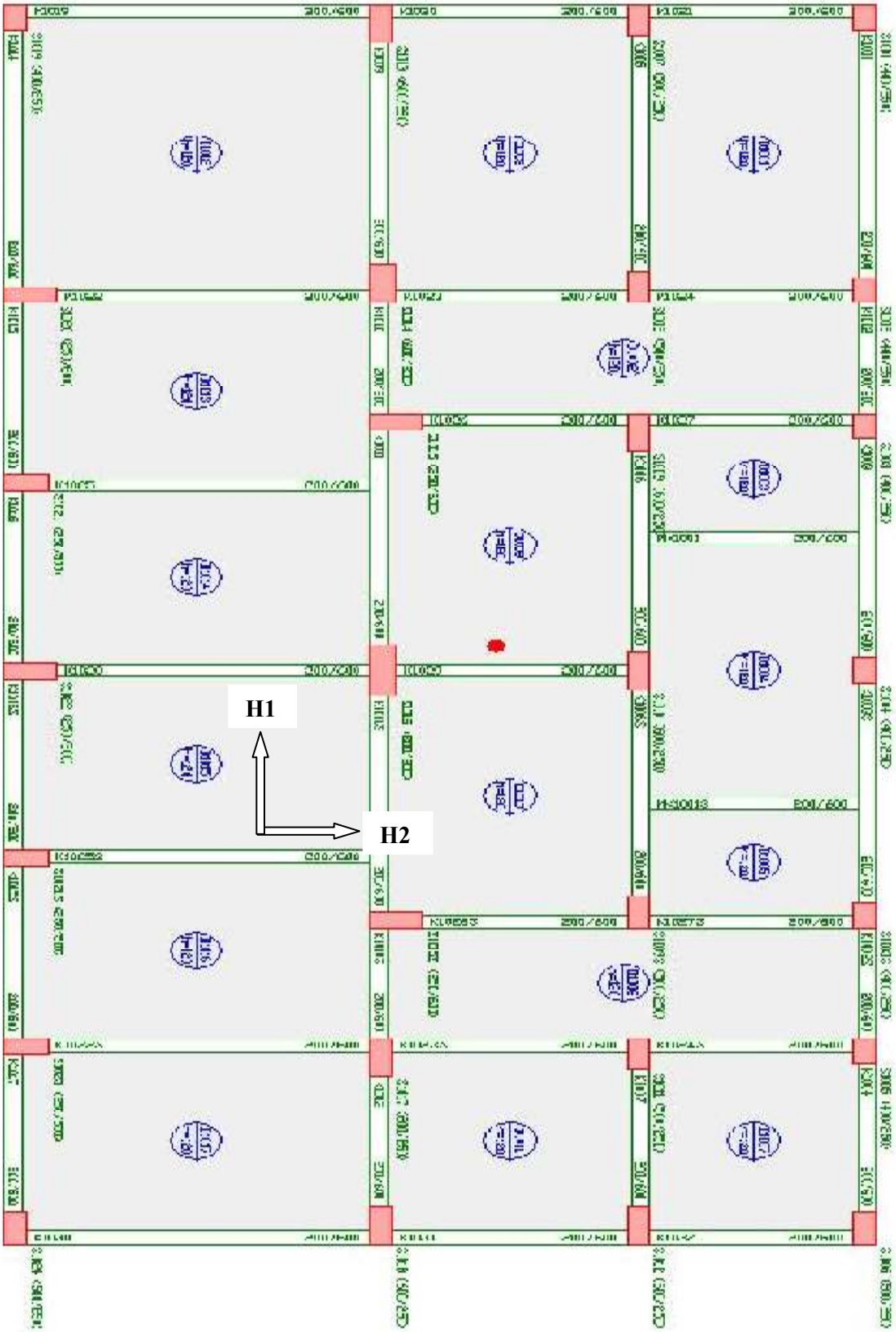

Figure 3.1. Typical framing plan of building 411.

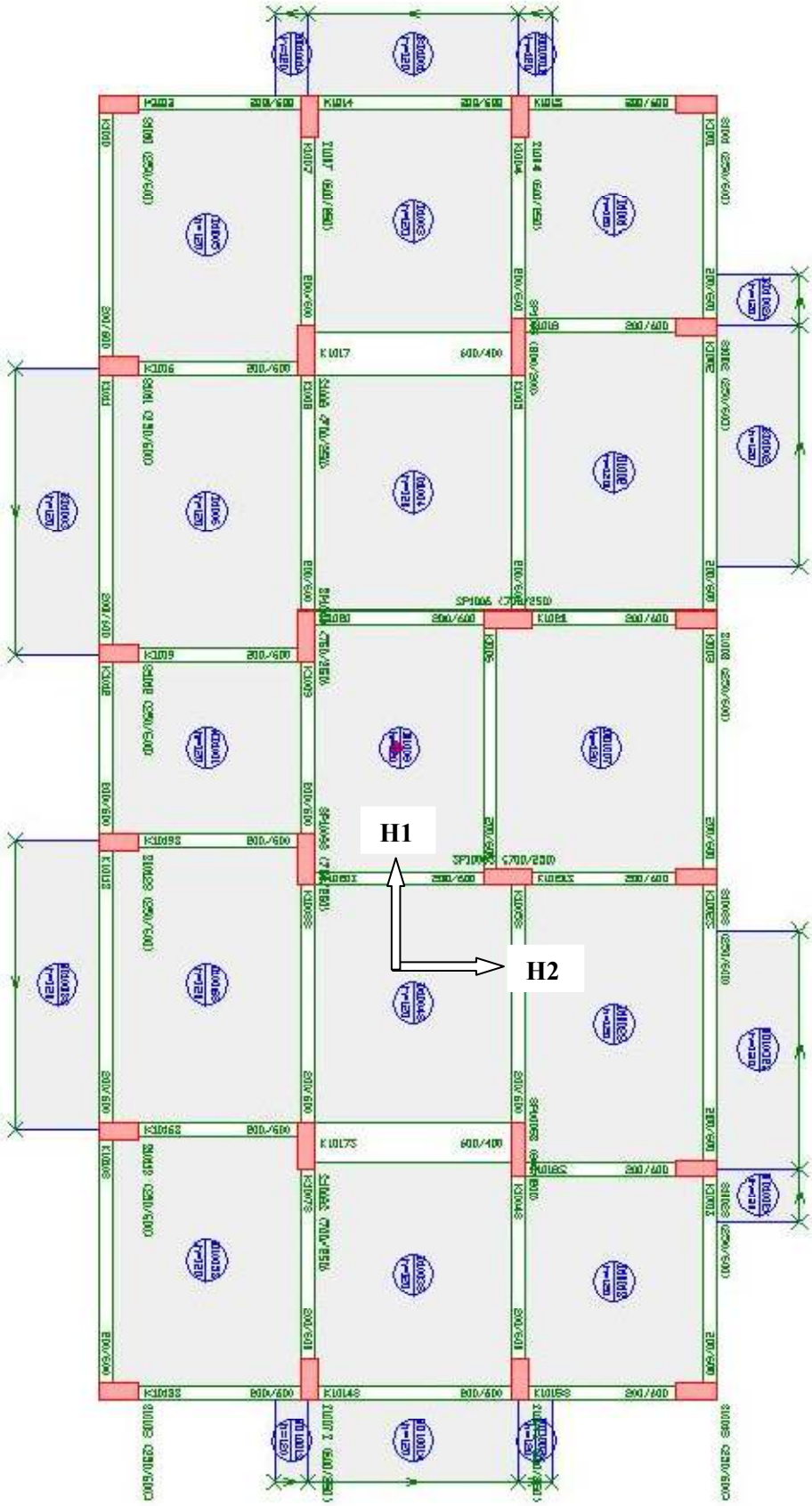

Figure 3.2. Typical framing plan of building 617.

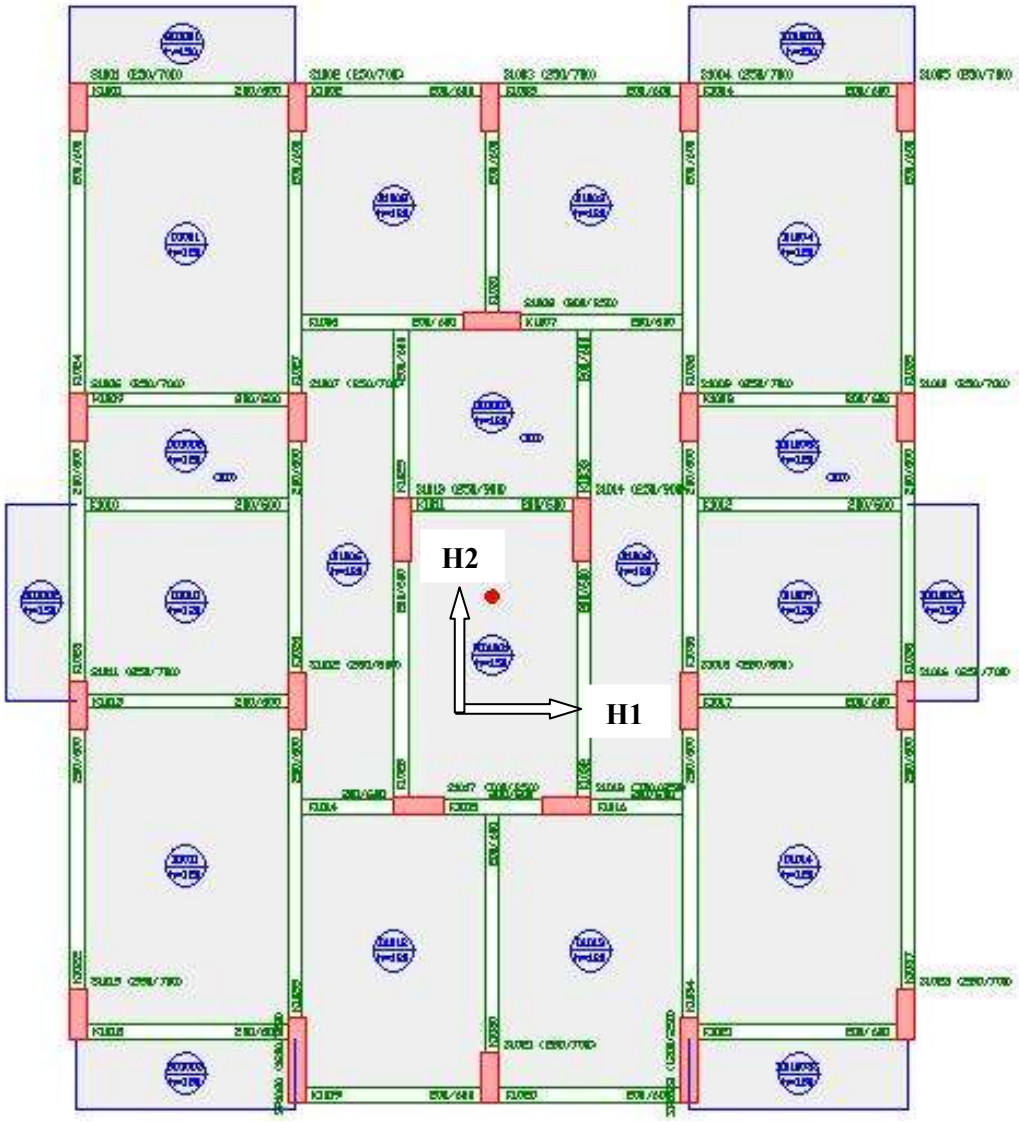

Figure 3.3. Typical framing plan of building 668.

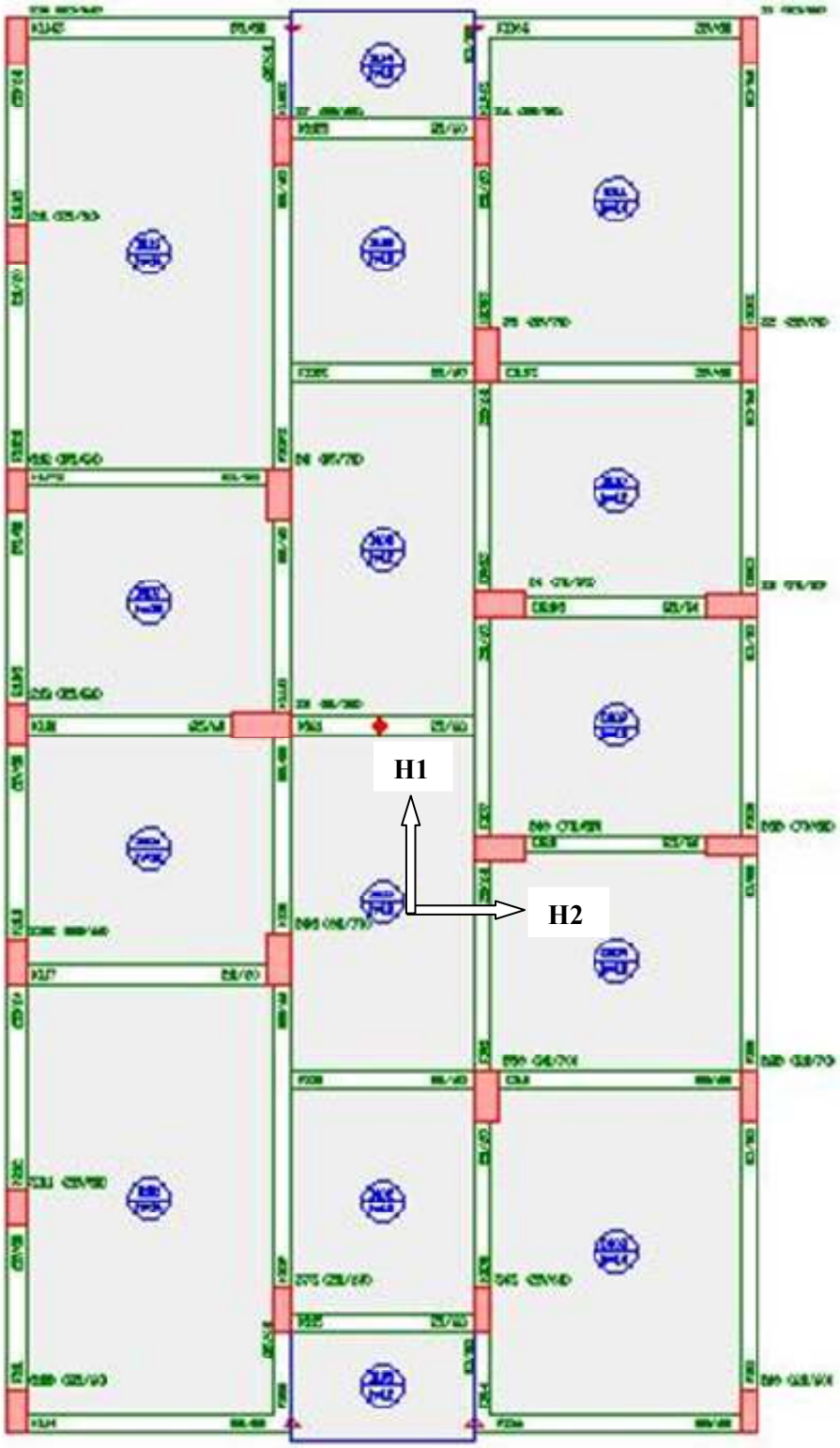

Figure 3.4. Typical framing plan of building 1472.

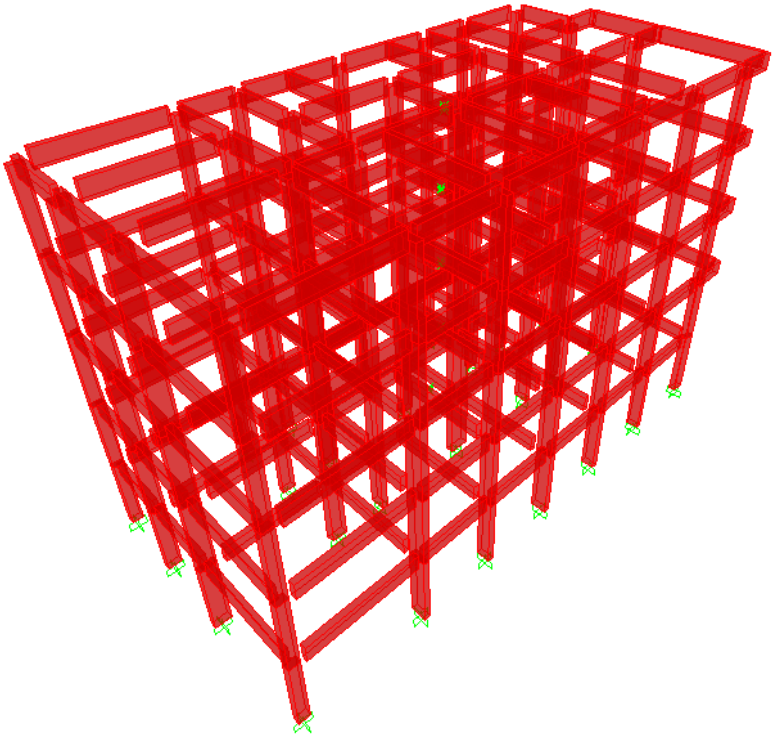

Figure 3.5. 3-D view of building 411.

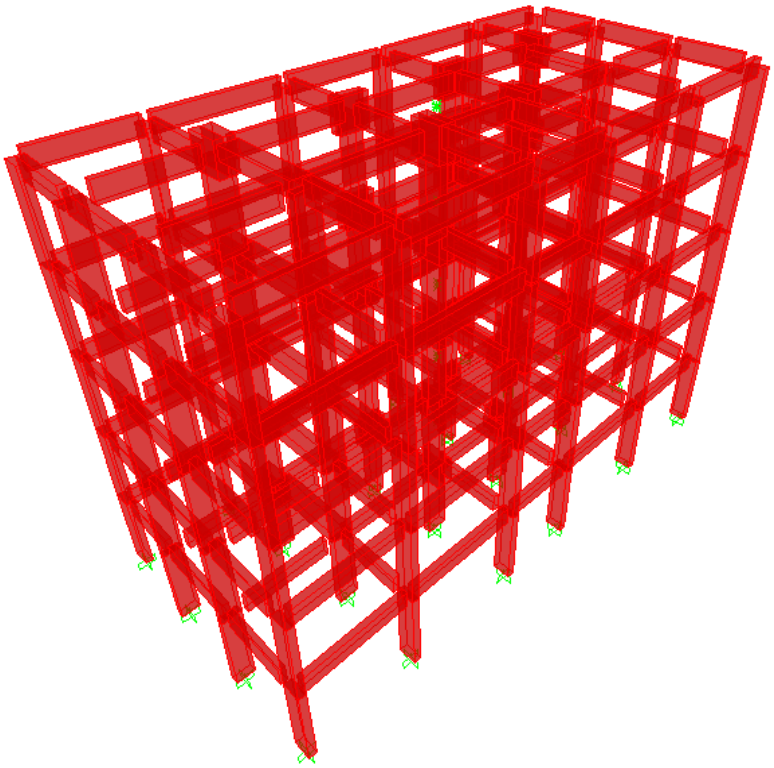

Figure 3.6. 3-D view of building 617.

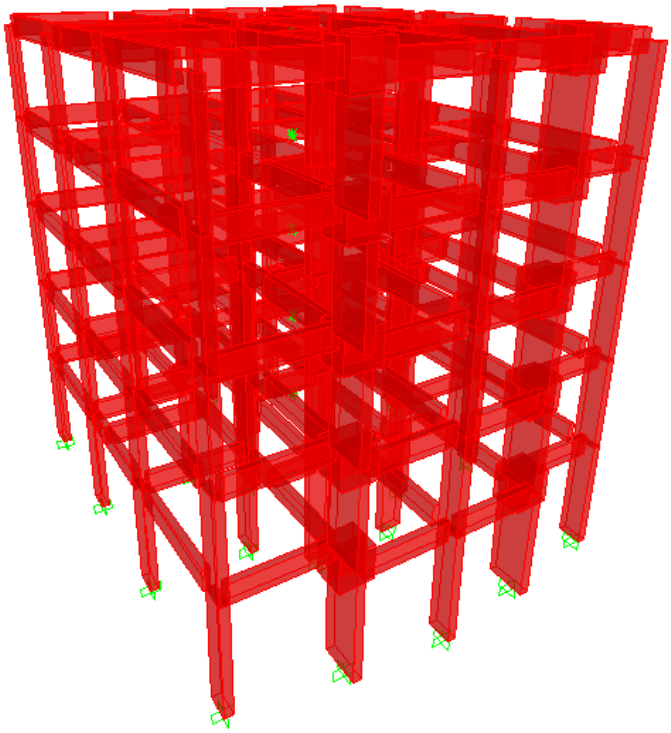

Figure 3.7. 3-D view of building 668.

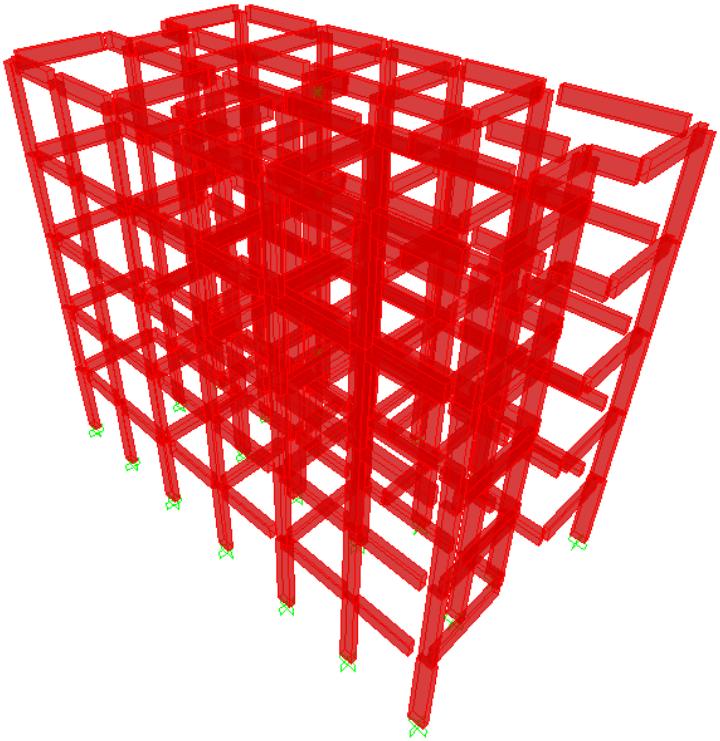

Figure 3.8. 3-D view of building 1472.

3.2. Material Properties

The mechanical properties of concrete and reinforcement materials are given in Table 3.2 and Table 3.3. Poisson ratio is taken 0.20 and shear modulus of the concrete is assumed 40 % of the elasticity modulus as it is defined in TS-500.

Table 3.2. Mechanical properties of concrete.

Mechanical Properties	Characteristic compressive strength, f_{ck} (MPa)	Characteristic tensile strength, f_{ctk} (MPa)	Elasticity Modulus, E_c (MPa)
C12	12	1.2	25250
C14	14	1.3	26160
C16	16	1.4	27000

Table 3.3. Mechanical properties of steel reinforcement.

Mechanical Properties	Minimum yield strength, f_{yk} (MPa)	Minimum ultimate strain ,ε_{su}(%)	Elasticity Modulus, E_s (MPa)
S220a	220	18	200000

The confined and unconfined concrete model is used as it is defined Turkish Seismic Code (2007). The proposed confined concrete model is known as Mander concrete model (Mander, 1988). Used unconfined and confined concrete models are shown below Figure 3.9.

The longitudinal compressive concrete stress is defined using the Equation 3.1.

$$f_c = \frac{f_{cc}\, x\, r}{r - 1 + x^r} \tag{3.1}$$

The required parameters for this equation are "f_{cc}", "x" and "r" values. These parameters are explained below. Compressive strength of confined concrete "f_{cc}" can be calculated using given equations.

$$f_{cc} = \lambda_c f_{co} \tag{3.2}$$

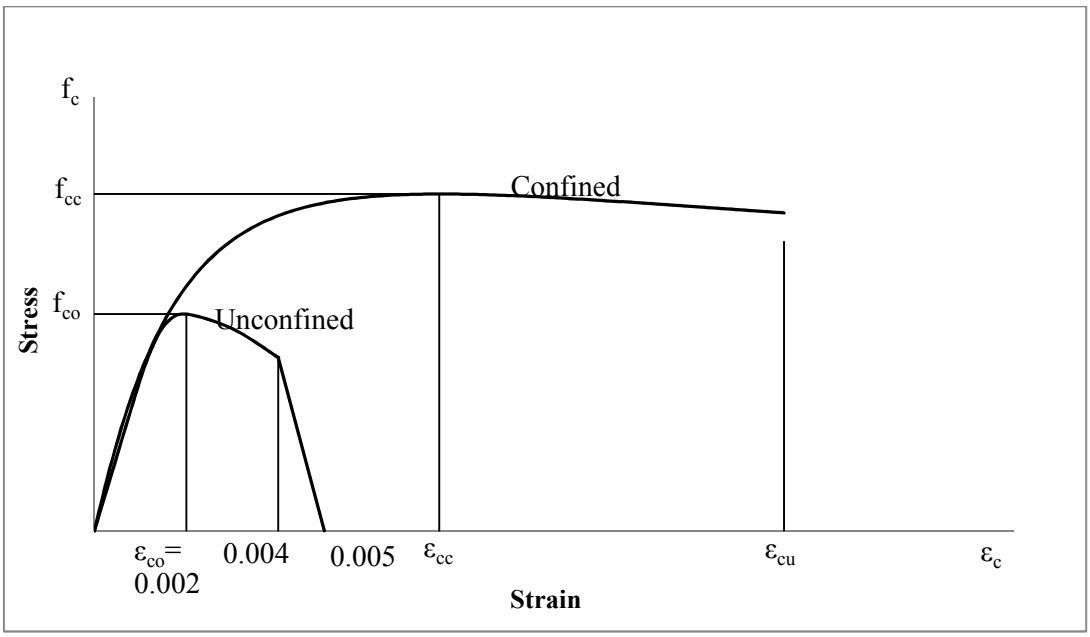

Figure 3.9. Unconfined and confined concrete models.

$$\lambda_c = 2.254\sqrt{1 + 7.94\frac{f_e}{f_{co}}} - 2\frac{f_e}{f_{co}} - 1.254 \tag{3.3}$$

where

f_{co} : unconfined concrete strength

f_e : effective lateral confining stress on the concrete.

Effective lateral confining stress "f_e" can be taken as average of about x and y axes stresses "f_{ex}, f_{ey}":

$$f_{ex} = k_e \rho_x f_{yw} \;\; ; \;\; f_{ey} = k_e \rho_y f_{yw} \tag{3.4}$$

where

f_{yw} : yield strength of transverse reinforcement

ρ : volumetric ratio of transverse reinforcement about corresponding axis

k_e : confinement effectiveness coefficient

Confinement effectiveness coefficient "k_e" is calculated using equation given below.

$$k_e = \left(1 - \frac{\sum a_i^2}{6b_o h_o}\right)\left(1 - \frac{s}{2b_o}\right)\left(1 - \frac{s}{2h_o}\right)\left(1 - \frac{A_s}{b_o h_o}\right)^{-1} \tag{3.5}$$

where

a_i : spacing between longitudinal reinforcements around the core

h_o, b_o : confined core dimensions

s : clear vertical spacing between spiral or hoop bars

A_s : area of longitudinal reinforcement

"x" and "r" coefficients for stress-strain diagram of confined concrete are:

$$x = \frac{\varepsilon_c}{\varepsilon_{cc}} \;\; ; \;\; \varepsilon_{cc} = \varepsilon_{co}[1 + 5(\lambda_c - 1)] \;\; ; \;\; \varepsilon_{co} \cong 0.002 \tag{3.6}$$

$$r = \frac{E_c}{E_c - E_{sec}} \;\; ; \;\; E_c \cong 5000\sqrt{f_{co}}[MPa] \;\; ; \;\; E_{sec} = \frac{f_{cc}}{\varepsilon_{cc}} \tag{3.7}$$

where

ε_c : longitudinal compressive concrete strain

ε_{cc} : longitudinal compressive concrete strain at compressive strength of confined concrete

ε_{co} : longitudinal compressive concrete strain at compressive strength of unconfined concrete, taken as 0.002

E_c : the tangent modulus of elasticity of the concrete in MPa

The ultimate strain of confined concrete "ε_{cu}" is calculated using below equation:

$$\varepsilon_{cu} = 0.004 + \frac{1.4\rho_s f_{yw} \varepsilon_{su}}{f_{cc}} \tag{3.8}$$

where

ρ_s : volumetric ratio of total transverse reinforcement

ε_{su} : ultimate strain of confinement reinforcement

Using above equations, confined concrete stress-strain parameters models are found for every confinement configuration that is determined from longitudinal and transverse reinforcement detailing. Then, these concrete models are represented with five different parameters:

- Compressive strength of confined concrete. "f_{cc}"
- Compressive strength of confined concrete at ultimate strain. "f_{cu}"
- Concrete strain at confined concrete compressive strength. "ε_{cc}"
- Ultimate concrete strain capacity for confined concrete." ε_{cu}"

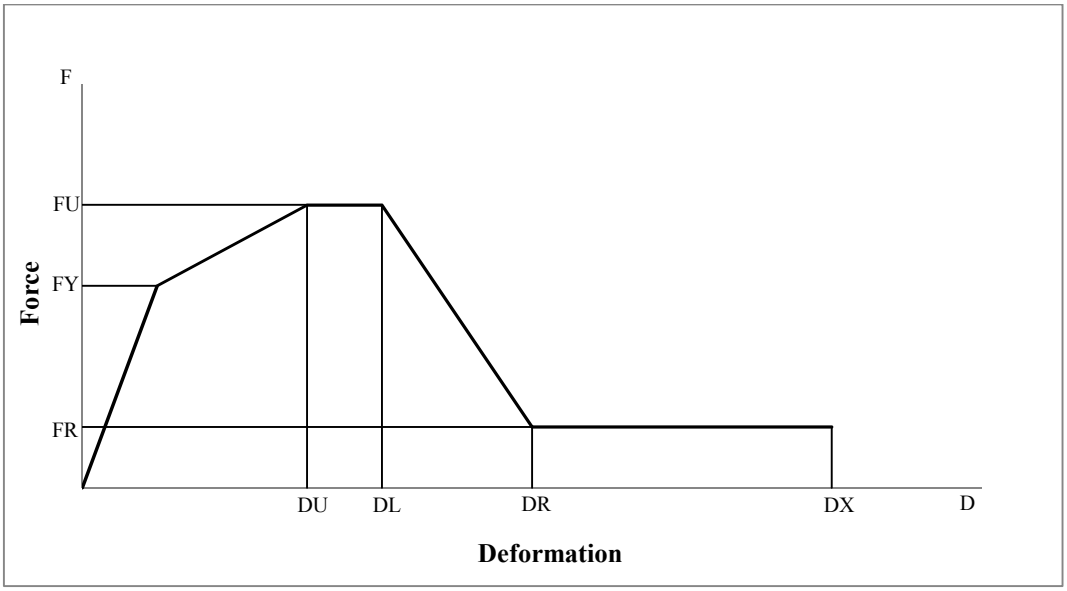

Figure 3.10. Sample material model used in Perform-3D.

FU strength in Figure 3.10 is chosen as average of stress value at ultimate strain and maximum stress value. FY strength is taken as characteristic strength value of the concrete. DU value is the strain at the first FU stress of Mander confined concrete model. DL strain is ultimate strain of Mander model. DR strain is assumed to be one and a half multiplier of DL in order to avoid sudden strength loss that may cause some computational problem. DX strain is preferred to have large value in order to avoid computational problem in response history analysis. FR namely residual strength is assumed to be one-tenth of the FU. All Perform-3D concrete material model parameters are calculated for every

confinement configurations. The comparison of Mander and assumed Perform concrete models are seen at Figure 3.11. Tensile strength of the confined concrete is not taken into consideration to be on the safe side.

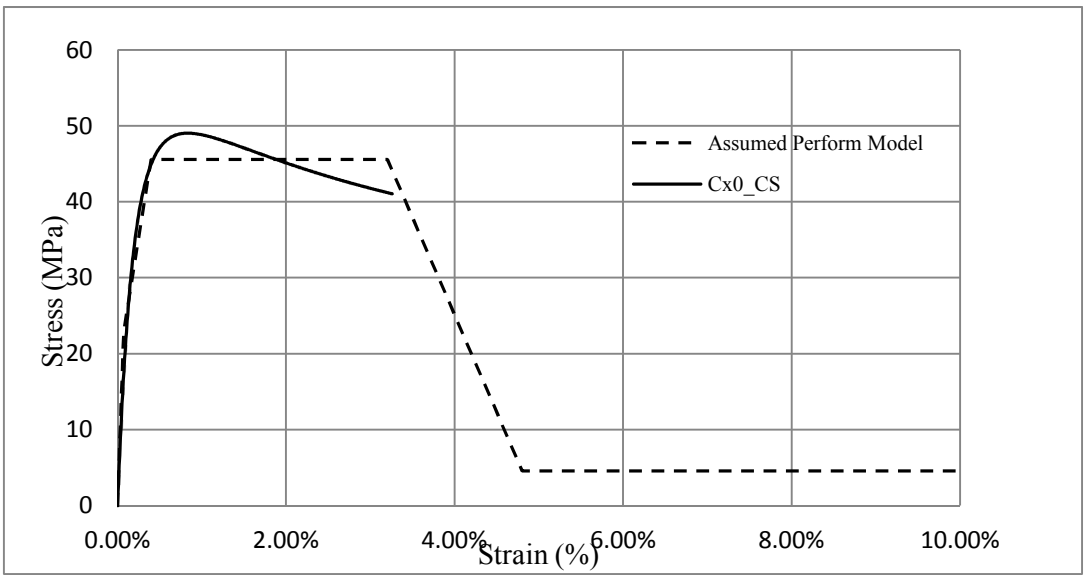

Figure 3.11. Comparison of Perform and Mander concrete models.

Also, the reinforcement model used in this study is taken from Turkish Seismic Code 2007 Part 7.B. The reinforcement model is given in Figure 3.12.

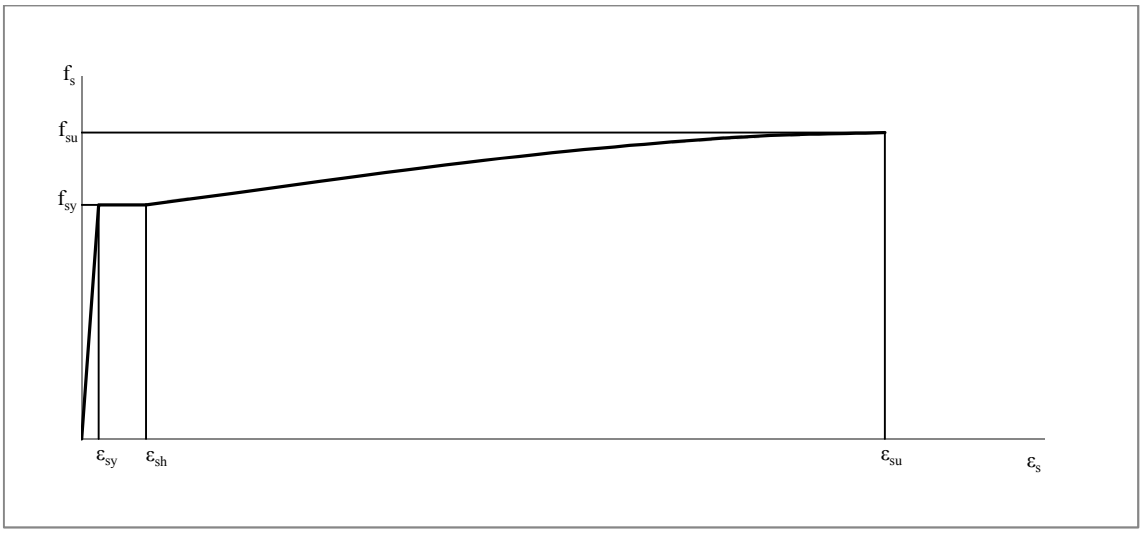

Figure 3.12. Reinforcement model.

The parameters to define stress-strain curve of reinforcement is given Table 3.4 .

Table 3.4. Stress-strain curve parameters of reinforcement.

	f_{sy} (MPa)	ε_{sy}	ε_{sh}	ε_{su}	f_{su} (MPa)
S220	220	0.0011	0.011	0.16	275

The stress-strain curve parameters of reinforcement in the Code are adopted to stress-strain curve parameters of Perform-3D, as it can be seen in Figure 3.12. FY is taken f_{sy} and FU is taken f_{su}. The modulus of elasticity of reinforcement is used as 200000 MPa. DU is same as and DL is taken as very close value to DU. DX is assumed close to DL. The strength loss is assumed 90 % of its original value, i.e. FR/FU is 0.1.

Table 3.5. Stress-strain parameters of reinforcement in Perform-3D.

		Stress (MPa)		Strain (%)				
	E_c (MPa)	F_Y	F_U	D_U	D_L	D_R	D_X	FR/FU
S220	200000	220	275	14	15	17	18	0.1

3.3. Column Sections

Column sections are typical rectangle and they were designed with two different types of concrete fibers: cover fibers and core fibers. Cover fibers were modeled with unconfined concrete material that has no strength at 0.005 strain in any stage of the time history analysis. Core fibers were also modeled with confined concrete material that has the same strength and strain limitations as Mander confined concrete model. Reinforcements also were modeled with non-buckling nonlinear reinforcement materials

one by one at the original locations where it is given in the reinforcement detailing drawings.

Columns are modeled using fiber sections. In this type of modeling, cross section of structural elements is divided into small sub areas named with fibers and each fiber has their own material properties. The schematic division of the any column is given in Figure 3.13. Column cross sections are divided into approximately square meshed fibers in confined part of column section. The size of he these confined fiber section change from five centimeters to ten centimeters, but there should be at least two confined fiber section in order to take into consideration of nonlinear bending behavior at both directions. Also every individual longitudinal reinforcement bars are implemented in the section separately at original location by using reinforcement fibers. The unconfined concrete of any column cross section are taken into consideration by four or six fibers.

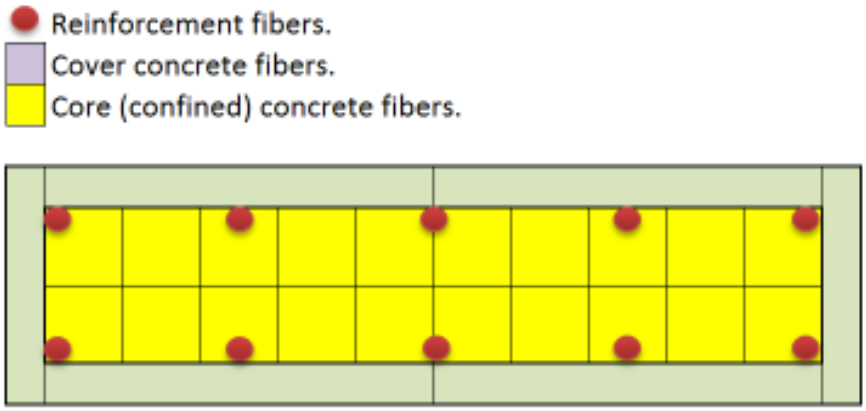

Figure 3.13. General division of column cross section into fibers.

Every individual column element is divided into sub-parts named segment along the frame member axis. Rigid-end-zone segments which assume that the connection interface of the frame members is fully rigid are added at the edge of the frames. Fiber segments which are finite length parts with a uniform fiber cross-section also are included to observe distributed nonlinear behavior. Fiber segment lengths are taken equal to plastic hinge length that is assumed the half of the section depth. The mild part between the fiber segments is modeled as elastic section in order to reduce computation time. As a summary, frame member are modeled with that sequence: rigid-end-zone, fiber segment, elastic

section segment, shear hinge, elastic section segment, fiber segment, rigid-end-zone, as shown in Figure 3.14.

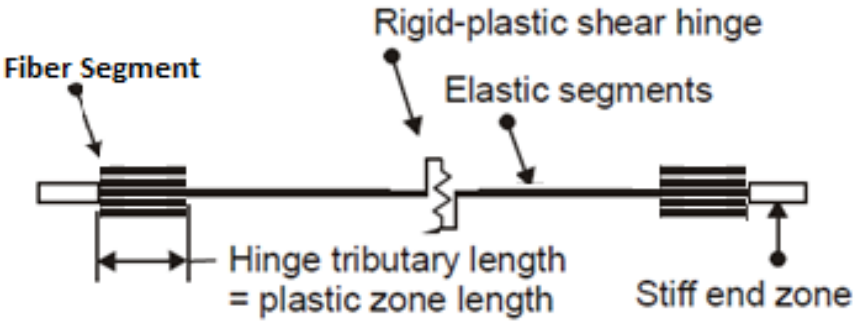

Figure 3.14. Schematic segmentation of column element.

3.3.1. Shear Capacity of Column

Shear capacity of columns are calculated from Equation 3.9 as given in TS500 at the mild section of the column since that section has the least transverse reinforcement in spite of the fact that shear force is the same value along the column height in earthquake loading. Shear hinges are assigned to each column in order to capture the shear failure. Due to ultimate strength design approach, the shear capacity of the members is determined based on ultimate bending moment capacity at the ends of the members rather than analysis results. Thus there are not occur shear failure in frame members.

$$V_r = A_{ch}\left(0.8 * 0.65 f_{ctk} + \rho_{sh} f_{ywk}\right) \tag{3.9}$$

3.4. Beam Cross Sections

Plastic hinge and fiber models are two different approaches used for nonlinear modeling. Once distributed plasticity approach named as fiber model is preferred, rigid diaphragm modeling can not be used since it will prevent axial elongation of beam members. As such in order to use the rigid diaphragm modeling concentrated plasticity approach named as plastic hinge has been used in beam members. Under cyclic loading reinforced concrete beams deformed in axial direction but since the in-plane stiffness of

surrounding slabs is relatively high in comparison to beam element, this axial deformations can be neglectibally small. However; if lumped plasticity model named plastic hinge is preferred, this issue could be solved at computation time significantly decrease.

In this study, plastic hinge approach is used in modeling nonlinear beam elements. All plastic hinge properties are determined from nonlinear section analysis by considering material strength, cross-section dimensions, longitudinal and transverse reinforcement configuration, and the nonlinear material stress-strain relationships. Also, Rigid-plastic hinge approach is preferred. In this approach, hinges at each side of the members have no initial elastic relative rotation named hinge rotation, and plastic rotation occurs once the yield moment has been reached, as shown in Figure 3.15.

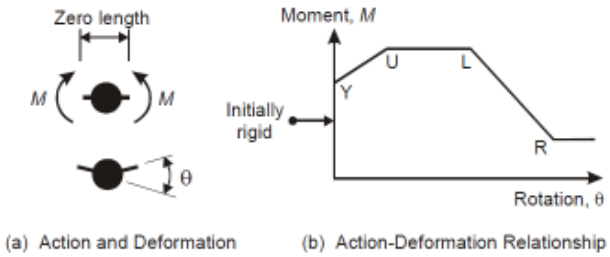

Figure 3.15. Schematic rigid plastic hinge representation (Perform-3D,2011).

Similar to columns, every individual beam element is divided into sub-parts named segment along the frame member axis. Beam members also are modeled with that sequence: rigid-end-zone, plastic hinge, elastic section segment, shear hinge, elastic section segment, plastic hinge, rigid-end-zone, as shown in Figure 3.16.

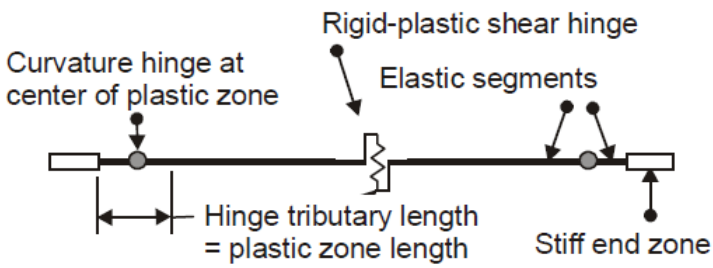

Figure 3.16. Schematic segmentation of beam element (Perform-3D, 2011).

Shear hinge parameters of the beams are determined with the same procedure in column shear hinge. Calculated capacities from the Equation 3.9, shear hinges are defined at both orthogonal directions.

3.5. Shear Hinges Definition

For columns and beams, the shear capacities are calculated as it is defined in Section 3.3.1. Using these capacities, shear hinges are assigned at both orthogonal directions. The force-deformation relationship and required parameters for shear hinge definition are:

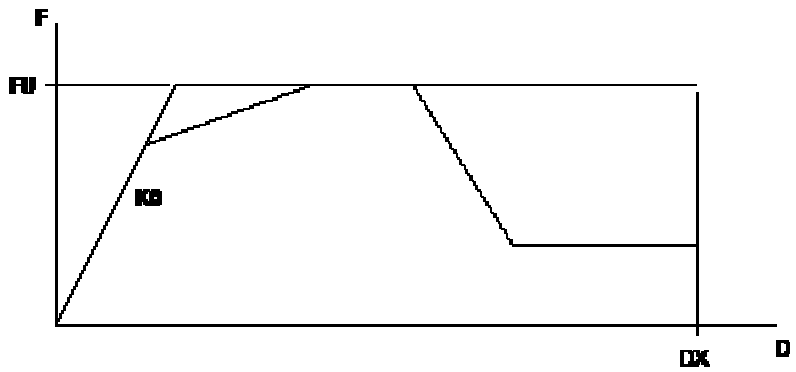

Figure 3.17. Schematic explanation of a shear hinge (Perform-3D, 2011).

In shear hinge definition, the basic parameters to be defined are ‘FU’ and ‘DX’ values. The ‘FU’ value is calculated based on shear capacity of the members. In order to avoid problem in the analyses process, ‘DX’ value is taken as 0.001 m. Once the shear capacity of the members is exceeded, the analysis will not continue. So shear failure could be captured at any element in the structural system.

4. ANALYSIS

4.1. Analysis Objectives

On the purpose of having prediction about every possible performance level that the structure could experience under corresponding seismic excitation, “Incremental Dynamic Analysis” (IDA) offered by (Vamvatsikos and Cornelll, 2002) is one of the most realistic analytical method. Construction of IDA curves is also the most time consuming part of the analytical risk assessment analysis. In IDA method huge number of nonlinear response history analyses with ground motion data scaled to several increasing intensity levels are performed. The nonlinear response history analyses can be in the form of pushover based or time history based. In this study, nonlinear history analyses methodology details of which are given in the proceeding sections.

4.2. Nonlinear Response History Analysis

In this study, IDA curves are independently estimated for each orthogonal direction of the structures by applying scaled ground motion accelerations from only one direction. As the finite element software Perform-3D V5 by CSI has been preferred for nonlinear time history analysis by integrating equilibrium equation step-by-step in time domain. General procedure of this method is explained in detail on proceeding sections.

4.2.1. Strong Ground Motion Records

With the advancement in the nonlinear time history analysis as a common analysis method, selection of the acceleration time histories takes important place in the quantification of building seismic performance and analytical derivation of the vulnerability functions. Quantification of Building Seismic Performance Factors FEMA-P695 (2009), is used in the stage of selecting record set and restrictions. The objectives about composing record sets and characteristics of records are based on FEMA-P695

(2009). Far-field record set given in FEMA-P695 (2009) is examined carefully. This set can be applicable for many studies about nonlinear time history analyses. The far-field record set composed of 22 records is used in this study.

The selection of seismic input is the crucial part of nonlinear time history analyses. There are mainly three methods of obtaining seismic input: accelerograms from real earthquakes, synthetic records from seismological models and spectrum compatible simulated records. Earthquake records can be obtained from some ground motion databases, such as PEER Ground Motion Database (PGMD) and strong-motion Seismograph Networks in Japan (K-Net). However, there may not be sufficient number of the earthquake records that are suitable in terms of magnitude, local site conditions, faulting type and fault distance for region under consideration. In this case synthetic records and spectrum compatible simulated records can be used.

There are five different basic objectives to be satisfied when composing records set for time history analysis within FEMA-P695 (2009). Firstly, the ground motions should satisfy the criteria given in the Code. Such as average response spectrum of the selected ground motions should be compatible with the Code spectrum. Secondly, the records should be selected to characterize intensity of the expected strong ground motion. If there are no enough records at that expected level, selected records can be scaled up to this level. Thirdly, representing record-to-record (RTR) variability and median value of the evaluation results, the number of records should be adequate. Fourthly, the selected record set could be used for seismic evaluation of many types of structures. The record set should not be selected in terms of building properties, such as period or material of the structures. Finally, the applicability of earthquake records should not be restricted to some specific site conditions, hazards and source.

To fulfill the objectives given at the previous paragraph, some criteria are used in selecting earthquake records from databases. It is the fact that earthquakes which have moment magnitude greater than 6.5 could cause some damage on new structures. These earthquakes are called as strong ground motions and their duration of strong shaking is relativity longer than smaller magnitude earthquakes. Large magnitude events also affect large region and large number of structures.

The source type of earthquakes of the record set should be same as the source type of expected earthquake of the studied area. In the databases, the most of earthquakes are from shallow crustal earthquakes with strike-slip or reverse source type. The records from other source types are few.

The site characteristics of the earthquake excitations in the ground motion set should be compatible with the site conditions of the region under consideration. Earthquake motions recorded on rock, soft rock or stiff soils could be used since earthquake record do not change significantly from hypocenter of earthquakes to the ground level. But the earthquake motions recorded on soft soil and sites susceptible to failure should not be taken into record set.

The records can be divided into two subgroups in terms of distance as Near-field and Far-field records. Records having source-to-site distance less than 10 km is generally named as Near-field records. Also, there are many fault distance definition in the literature, such as (Campbell, 1997) and (Joyner-Boore, 1981). The far-field records sets are used in this study.

Strong-motion recorders are not evenly distributed across active seismic zones. In the databases, the number of recording from each earthquake is unevenly distributed. Therefore, number of records from some earthquakes is very large number. To avoid event-based bias of taking many records from same earthquake, two records from any earthquake should betaken into the record set.

With magnitude of earthquake, peak ground acceleration (PGA) and peak ground velocity (PGV) thresholds can be used to select strong ground motions. Threshold values such as 0.2g for PGA and 15 cm/sec for PGV can be used to identify the ground motions which may cause structural damage.

When selecting earthquake records, the location of strong-motion instruments can be crucial. Some instruments are located inside buildings such as at ground floor or basement. So they are affected from soil-structure-foundation interaction and their records are not

same as the records at ground level. Alternatively, records from free-field strong ground motion instrument could be used.

Some older strong ground motion devices do not have capability of recording long-period vibration efficiently. When selecting records, this capability should be taken into consideration especially for nonlinear analysis of long-period structures, such as tall buildings.

Based on the criteria defined above a set of strong ground motion has been taken from the FEMA-P695 (2009) and their properties are given in Table 4.1 and Table 4.2.

Table 4.1. Some major properties of the ground motion used in analyses.

ID No	Earthquake				Site Data		Source
	M	Year	Name	Station	NEHRP Class	Vs_30 (m/sec)	Fault Type
1	6.7	1994	Northridge	Beverly Hills-Mulhol	D	356	Thrust
2	6.7	1994	Northridge	Canyon Country-WLC	D	309	Thrust
3	7.1	1999	Düzce, Turkey	Bolu	D	326	Strike-slip
4	7.1	1999	Hector Mine	Hector	C	685	Strike-slip
5	6.5	1979	Imperial Valley	Delta	D	275	Strike-slip
6	6.5	1979	Imperial Valley	El Centro Array #11	D	196	Strike-slip
7	6.9	1995	Kobe, Japan	Nishi-Akashi	C	609	Strike-slip
8	6.9	1995	Kobe, Japan	Shin-Osaka	D	256	Strike-slip
9	7.5	1999	Kocaeli, Turkey	Duzce	D	276	Strike-slip
10	7.5	1999	Kocaeli, Turkey	Arcelik	C	523	Strike-slip
11	7.3	1992	Landers	Yermo Fire Station	D	354	Strike-slip
12	7.3	1992	Landers	Coolwater	D	271	Strike-slip
13	6.9	1989	Loma Prieta	Capitola	D	289	Strike-slip
14	6.9	1989	Loma Prieta	Gilroy Array #3	D	350	Strike-slip
15	7.4	1990	Manjil, Iran	Abbar	C	724	Strike-slip
16	6.5	1987	Superstition Hills	El Centro Imp. Co.	D	192	Strike-slip
17	6.5	1987	Superstition Hills	Poe Road (temp)	D	208	Strike-slip
18	7.0	1992	Cape Mendocino	Rio Dell Overpass	D	312	Thrust
19	7.6	1999	Chi-Chi, Taiwan	CHY101	D	259	Thrust
20	7.6	1999	Chi-Chi, Taiwan	TCU045	C	705	Thrust
21	6.6	1971	San Fernando	LA-Hollywood Stor	D	316	Thrust
22	6.5	1976	Friuli, Italy	Tolmezzo	C	425	Thrust

Table 4.2. The other properties of the ground motion used in analyses.

ID No.	Site-Source Distance (km)				Recorded Motions			As-Recorded Parameters	
	Epicentral	Closest to Plane	Campbell	Joyner-Boore	PGA (g)		PGV_{max} (cm/sec)	1-Sec. Spectral Acceleration (g)	
					Comp.1	Comp.2		Comp.1	Comp.2
1	13.3	17.2	17.2	9.4	0.42	0.52	41	1.02	0.94
2	26.5	12.4	12.4	11.4	0.41	0.48	38	0.38	0.63
3	41.3	12	12.4	12	0.73	0.82	39	0.72	1.16
4	26.5	11.7	12	10.4	0.27	0.34	46	0.35	0.37
5	33.7	22	22.5	22	0.24	0.35	43	0.26	0.48
6	29.4	12.5	13.5	12.5	0.36	0.38	43	0.24	0.23
7	8.7	7.1	25.2	7.1	0.51	0.50	39	0.31	0.29
8	46	19.2	28.5	19.1	0.24	0.21	42	0.33	0.23
9	98.2	15.4	15.4	13.6	0.31	0.36	41	0.43	0.61
10	53.7	13.5	13.5	10.6	0.22	0.15	54	0.11	0.11
11	86	23.6	23.8	23.6	0.24	0.15	51	0.50	0.33
12	82.1	19.7	20	19.7	0.28	0.42	49	0.20	0.36
13	9.8	15.2	35.5	8.7	0.53	0.44	38	0.46	0.28
14	31.4	12.8	12.8	12.2	0.56	0.37	39	0.27	0.38
15	40.4	12.6	13	12.6	0.51	0.50	43	0.35	0.54
16	35.8	18.2	18.5	18.2	0.36	0.26	40	0.31	0.25
17	11.2	11.2	11.7	11.2	0.45	0.30	42	0.33	0.34
18	22.7	14.3	14.3	7.9	0.39	0.55	36	0.54	0.39
19	32	10	15.5	10	0.35	0.44	47	0.49	0.95
20	77.5	26	26.8	26	0.47	0.51	38	0.30	0.43
21	39.5	22.8	25.9	22.8	0.21	0.17	40	0.25	0.15
22	20.2	15.8	15.8	15	0.35	0.31	44	0.25	0.30

These twenty-two pairs of two-component ground motions are the Far-Field record set includes only the horizontal components. On the other hand; both of fault parallel and fault normal components are applied in each direction on the structure under consideration separately. Therefore, the total number of ground motions used in analyses has been increased to 44 and record-to-record (RTR) variability has been provided better. As it is indicated in FEMA-P695 (2009) document, all strong motion records have 0.2g or larger PGA, 15 cm/sec or larger PGV and 6.5 or larger magnitude. Also, all these ground motion data are taken from Pacific Earthquake Engineering Research Center (PEER) Next-Generation Attenuation (NGA) database (PEER, 2006). Acceleration response spectrum of each 44 time history is given in Figure 4.1.

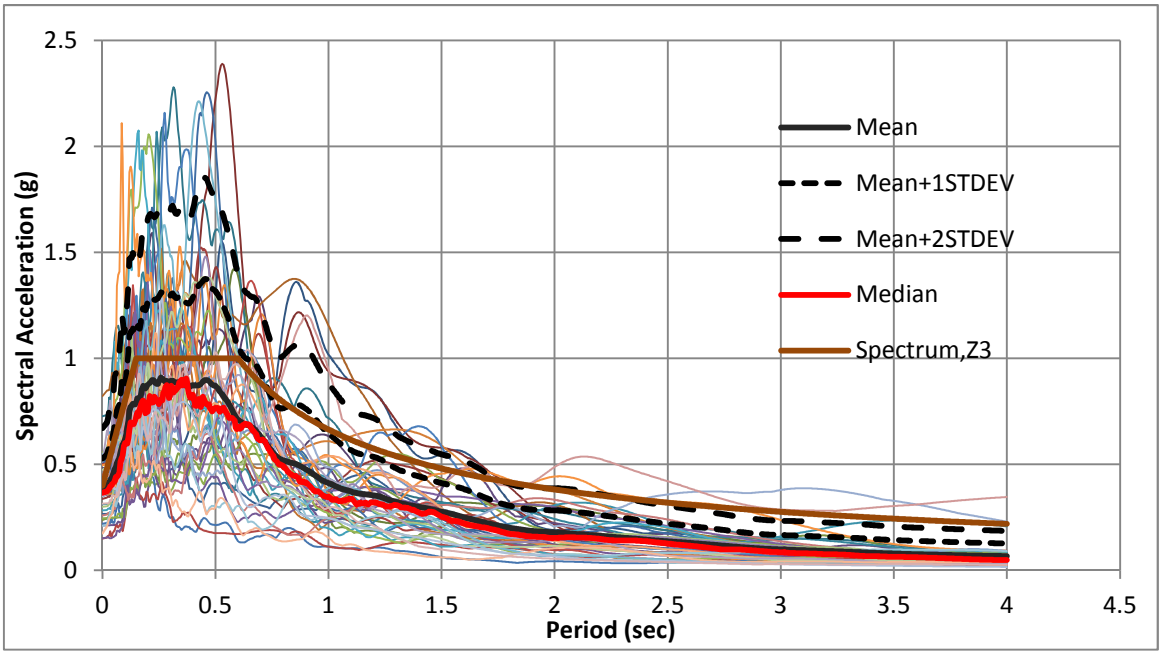

Figure 4.1. Far-field record set response spectra with median, one standard deviation and two standard deviation.

4.2.2. Scaling Method

For the purpose of estimating all possible damage levels in IDA method, each strong ground motion data is needed to be scaled to represent every intensity level of the earthquake (Vamvatsikos and Cornell, 2002). There are many intensity parameters for earthquake records such as PGA, PGV, spectral displacement at the first natural period $S_d(T_1,5\%)$ and spectral acceleration at the first natural period $S_a(T_1,5\%)$ that are used in scaling procedure. In this study the engineering demand parameter is selected as spectral acceleration at the first natural period $S_a(T_1,5\%)$. Also this intensity measure $S_a(T_1,5\%)$ used in scaling should be compatible with intensity axis of the hazard curve in order integrate the fragility curve over hazard curve.

In this study, uniform scaling procedure in time domain is preferred in order not to change the frequency content of the earthquake excitation. Once more or less severe ground motions are needed, the earthquake acceleration time history can uniformly be scaled up or down by using a scalar. Also, frequency content of earthquake data is not

distorted by keeping phase information of the data intact. This process can be done as below;

$$a_\lambda = \lambda \cdot a_1 \tag{4.1}$$

where a_λ is the scaled accelerogram, λ is non-negative scalar and a_1 is the unscaled accelerogram (Vamvatsikos and Cornell, 2002).

4.2.3. Damping

In the direct integration of the equation of motion, Rayleigh damping is used as one of the widely known damping type. Rayleigh damping assumes that damping matrix is composed of liner combination of system stiffness and mass matrix as given in Equation 4.2;

$$C_i = \alpha M_i + \beta K_i \tag{4.2}$$

where **C** is the damping matrix, **M** is the mass matrix, **K** is the stiffness matrix and sub indexes represent the mode number. In this study, stiffness matrix is considered initial stiffness without updating it at each step due to the limitation on the analysis program. α and β coefficients can be calculated for specified damping ratios ξ_i and ξ_j by the following Equation 4.3.

$$\xi_i = \alpha\frac{1}{2\omega_i} + \beta\frac{\omega_i}{2} \quad \text{or} \quad \xi_i = \alpha\frac{T_i}{4\pi} + \beta\frac{\pi}{T_i} \tag{4.3}$$

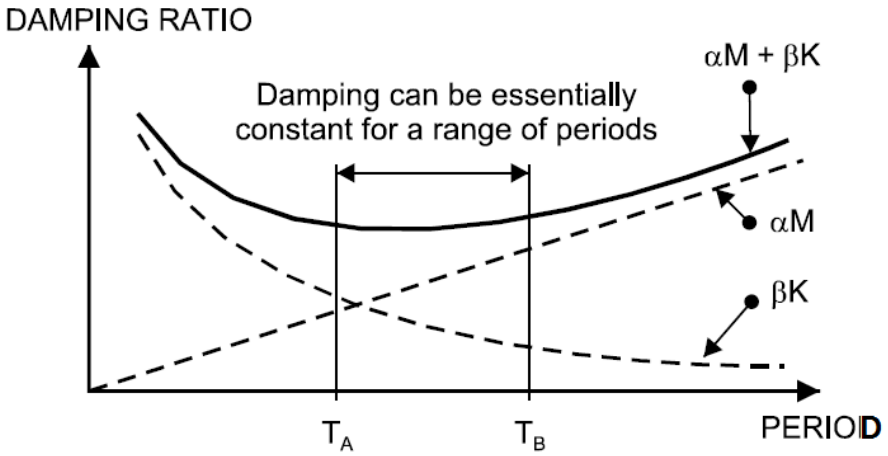

Figure 4.2. Variation of damping ratio with period (Perform 3-D, 2011).

In this type of damping approach, determination of the shorter period value, T_A, and the longer period, T_B, is a crucial point. As the nonlinearity of the structure increases, the elastic periods of the structure are elongates. Once the T_B value has been chosen lower than the first period of the structure, the damping could be over estimated as shown in Figure 4.2 (Perform 3-D, 2011). In this study, 5 % damping points T_A and T_B are chosen so that T_A period is equal to $0.2T_1$ and T_B period is equal to $1.5T_1$. Consequently, the damping can be approximately the 5 % near the T_A and T_B.

4.2.4. P-Delta Effects

Engineering structures respond in linear range under service loads but in some loading cases such as seismic actions respond maybe inelastic. In this case lateral deformations may have significantly high values such that geometric nonlinearity should be taken into consideration due to change in the geometry of the structure. In the first order small displacement theory, equations of equilibrium are formed based on undeformed structure geometry. On the other hand, geometric change in the geometry can be included in the equilibrium equations through the help of two different analysis methods: P-Δ analysis and true large displacement analysis. P-Δ analysis only considers horizontal deformations to form equilibrium equation. True large displacement also consider the axial deformations in the formation of equilibrium equations (Perform 3-D, 2011), as shown in Figure 4.3.

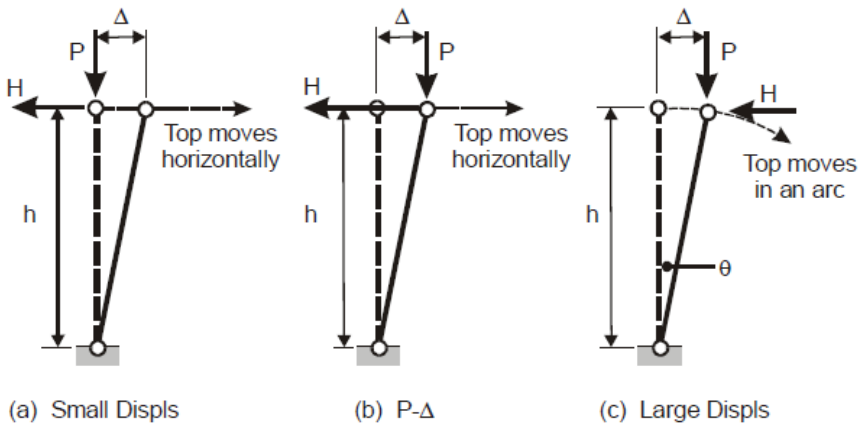

Figure 4.3. Geometric nonlinearity types (Perform 3-D, 2011).

P-Δ phenomenon generally has significant effect on vertical elements due to additional bending moment which is the product of axial-load and Δ-displacement. In the beam element second order moments are negligible due to very small axial loads.

P-Δ effect can be included into the system stiffness by introducing geometric stiffness term which has negative effect. This can be expressed as:

$$f_s = f - f_G \tag{4.4}$$

where f is the nonlinear internal force, f_G is the equivalent P-delta force. For single degree of freedom systems this force can be expressed by the following equations:

$$f_G = k \cdot \Delta \tag{4.5}$$

$$f_G = \frac{P}{\mathrm{h}} \cdot \Delta \quad ; (P \cdot \Delta = f_G \cdot \mathrm{h}) \tag{4.6}$$

where k refers to stiffness of the element, Δ represents the lateral displacement, P is the axial force and h is the height of element. From these equations:

$$f_s = k \cdot \Delta - \frac{P}{\mathrm{h}} \cdot \Delta = (k - k_G) \cdot \Delta \tag{4.7}$$

So,k_G named as the geometric stiffness coefficient reveals as P/h $(P \approx m \cdot g)$.

On the other hand, for multi degree of freedom systems this phenomena can be represented in matrix form as Equation 4.8;

$$\{f_s(u,\bar{u})\} = \{f\} - \{f_G\} = ([\boldsymbol{K}_{initial}] - [\boldsymbol{K}_G]) \times \{u(t)\} \tag{4.8}$$

where $\mathbf{K}_G$ is the geometric-stiffness matrix of the whole structure and $\mathbf{K}_{initial}$ is the initial stiffness matrix of the whole structure for each increment. As it can be seen in Equation 4.9, the general form of the geometric stiffness has a tridiagonal form due to the contribution of upper and lower storey columns (Calugh&Penzien, 1995).

$$\{f_G\} = \begin{Bmatrix} f_{G_1} \\ f_{G_2} \\ \vdots \\ f_{G_i} \\ \vdots \\ f_{G_n} \end{Bmatrix} = \begin{bmatrix} \frac{P_o}{h_o} + \frac{P_1}{h_1} & -\frac{P_1}{h_1} & 0 & \cdots & 0 & \cdots \\ -\frac{P_1}{h_1} & \frac{P_1}{h_1} + \frac{P_2}{h_2} & -\frac{P_2}{h_2} & \cdots & 0 & \cdots \\ \vdots & \vdots & \vdots & \ddots & \vdots & \vdots \\ 0 & 0 & 0 & \cdots & \frac{P_{i-1}}{h_{i-1}} + \frac{P_i}{h_i} & \cdots \\ \vdots & \vdots & \vdots & \ddots & \vdots & \vdots \\ 0 & 0 & 0 & \cdots & 0 & \cdots \end{bmatrix} \begin{Bmatrix} u_1(t) \\ u_2(t) \\ \vdots \\ u_i(t) \\ \vdots \\ u_n(t) \end{Bmatrix} \tag{4.9}$$

In the analyses phase of this study true large displacement analysis is neglected but P- Δ analysis is included. The second order moment due to geometric nonlinearity of the system may reach up to considerable values especially in the range of Collapse-Prevention performance level. One of the most common lateral dynamic instability types, sidesway collapse can be precisely captured through IDA process, by considering geometric nonlinearity. As far as sidesway collapse is concerned, P-Δ phenomena can significantly affect the response of ductile systems due to second order moments. The contribution of the P-Δ effect on collapse behavior of the structure can be seen in Figure 4.4.

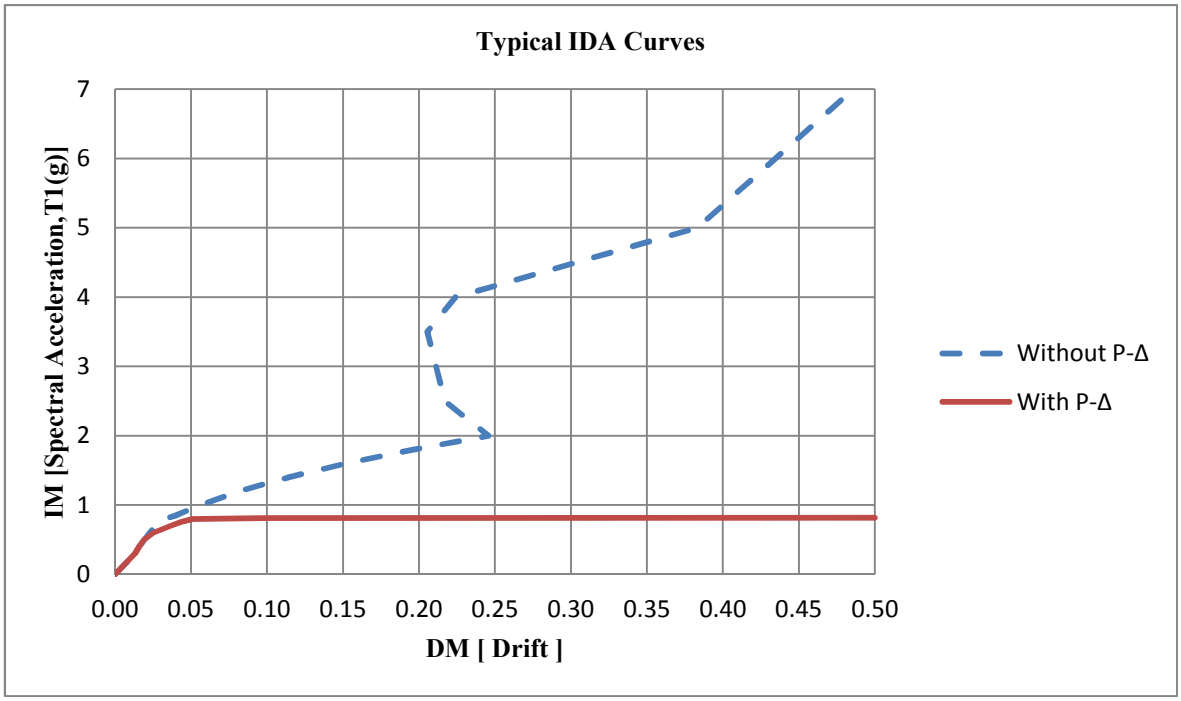

Figure 4.4. Two sample IDA curves with and without P-Δ effect.

As it can be seen in the Figure 4.4, when the P-Δ effect is considered, the structure cannot withstand more than 5 % drift ratio. Because the second order moment due tothe P-Δ effect causes loss of lateral stiffness by drastically accelerating sidesway-story drifts of deteriorating systems.

4.2.5. Determination of Collapse State

In the Incremental Dynamic Analysis, detection of the global instability is a most fundamental problem because of the computational time. When the static analysis or equivalent static analysis is concerned, static instability can be clearly determined with the existence of the negative eigen-value in the solution of the stiffness matrix. On the other hand; during dynamic analysis this check is not enough to identify dynamic instability. At the dynamic instability phase, the structure starts to tilt in one direction without vibrating (FEMA-P440A). Also, non- convergence of the time integration, in other words numerical instability, can be the simplest way of the prediction of the collapse (Vamvatsikos and Cornell, 2002).

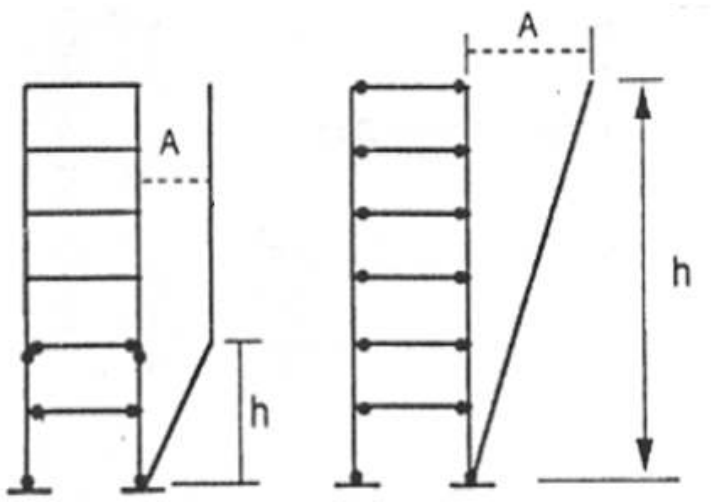

Figure 4.5. Two sample collapse mechanism shapes (FEMA-P440A).

As it can be seen in Figure 4.5 above, the framed structures may reach mechanism stage either all of the columns and beams become plastic at one storey or all beams in the structure and foundation connection of the all columns. With the help of the P-Δ effect, the structural drifts continue to increase excessively without vibration after one of the mechanism shapes occurs.

In this study, sudden and excessive increment in the drift ratios is defined as the collapse state. The high drift values cause numerical convergence problem named as lateral dynamic instability in the nonlinear response history analysis.

Moreover, with the small increase in the intensity measure $S_a(T_1,5\%)$, the structure suddenly reaches dynamic instability since the structure is stumbled by the negative effect due to geometric nonlinearity. This situation can clearly observed in Figure 4.6 that the structure-1472 collapses with 0.05 (g)-increase in the intensity measure in H1 direction.

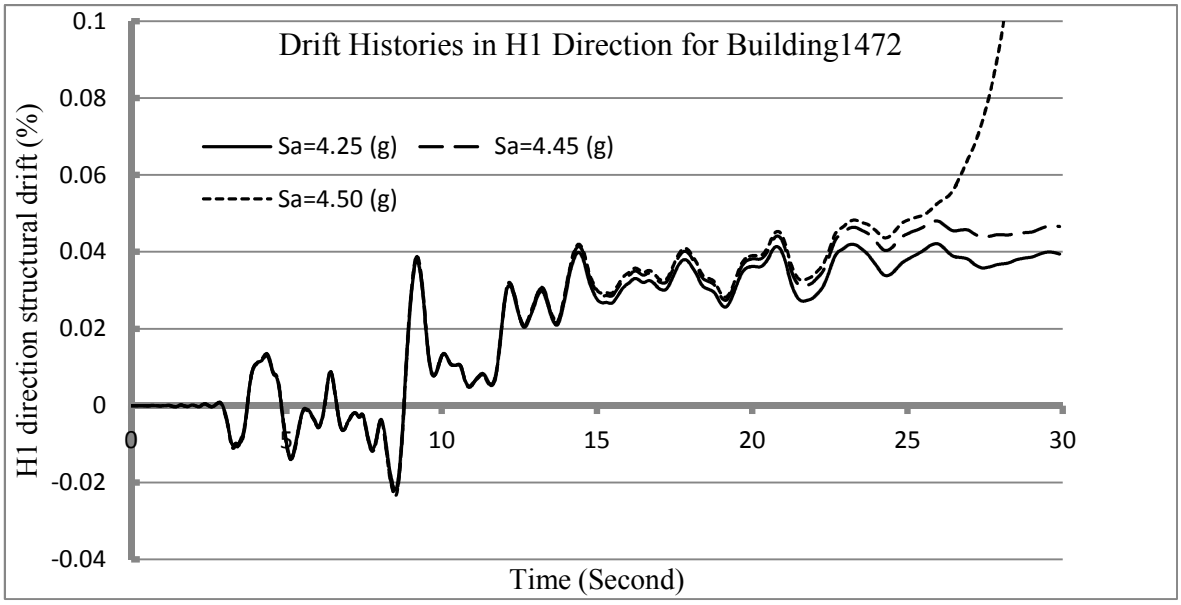

Figure 4.6. Three sample drift histories for collapse detection.

4.3. General IDA Procedure

In this study, nonlinear response history analysis based on IDA method is preferred in order to capture the nonlinear response and final global instability level in a more realistic manner. P-delta effect is also included. The ξ=5 percent damped Spectral Acceleration at the first mode period of the structure ($S_a(T_1,5\%)$) is preferred as the intensity measure that represent the increasing effect of the seismic input. Also, as the engineering demand parameter representing the response of the structure, peak inter-storey drift ratio is selected.

Some major steps of the Incremental Dynamic Analysis (IDA) procedure is given below:

- Selection the ground motion ($u_g(t)$).
- Determination of Spectral Accelerations corresponding to the first mode period of the structure under consideration.
- Determination intensity measure steps , ($S_a(T_1,5\%)$), as 0.10g, 0.25g, 0.5g, 1.00g, 1.50g, 2.00g, 2.50g, 3.00g for IDA.

- Determination of scale factor for each selected intensity measure.
- Performing nonlinear response history analysis for each scaled ground motion.
- Checking any dynamic instability in the response history process analyses.
- Determination refined $S_a(T_1,5\%)$ value that cause collapse of the structure by using bisection method in between the collapsed and non-collapsed $S_a(T_1,5\%)$ value with 0.05g error tolerance.
- Once dynamic instability cannot be captured in any step, the intensity measure should be increased until the dynamic instability is reached.

The above mentioned steps are repeated for each ground motions and building under consideration in order to obtain IDA curves.

Sets of IDA curves obtained from that analyses are given in Figure 4.7 to Figure 4.14 for each building for each orthogonal direction.

As it can be observed from IDA-curves given below, the maximum drift capacities varies at the range of 7 % to 12 % depending on structures.

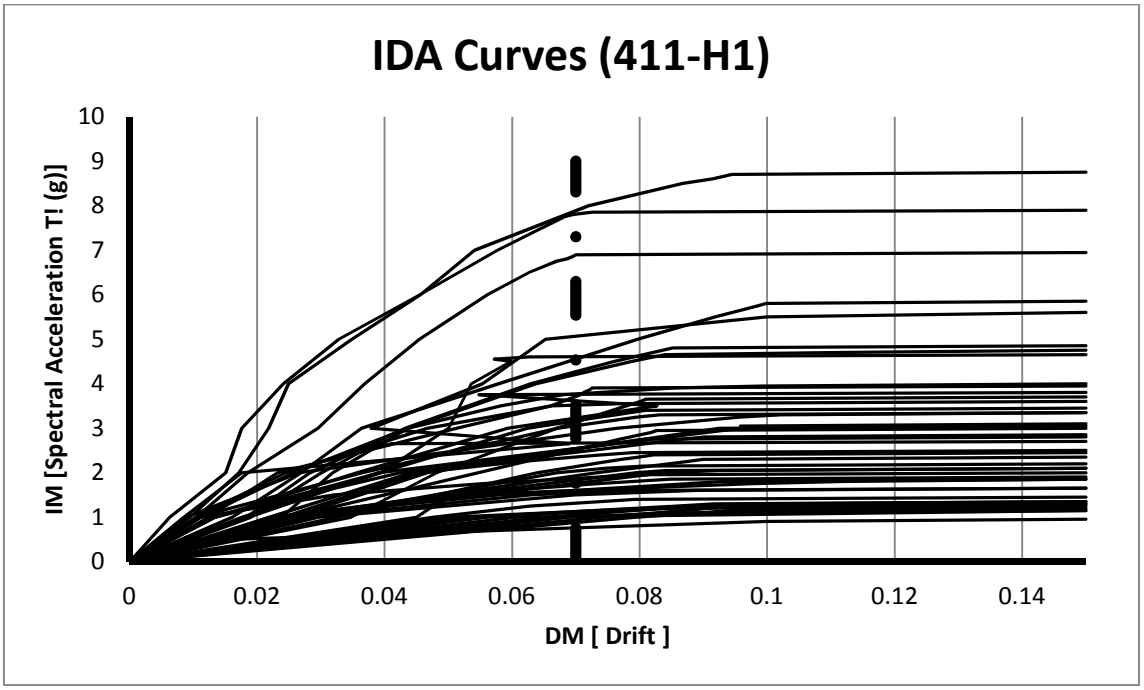

Figure 4.7. IDA curves for building-411 in H1 direction.

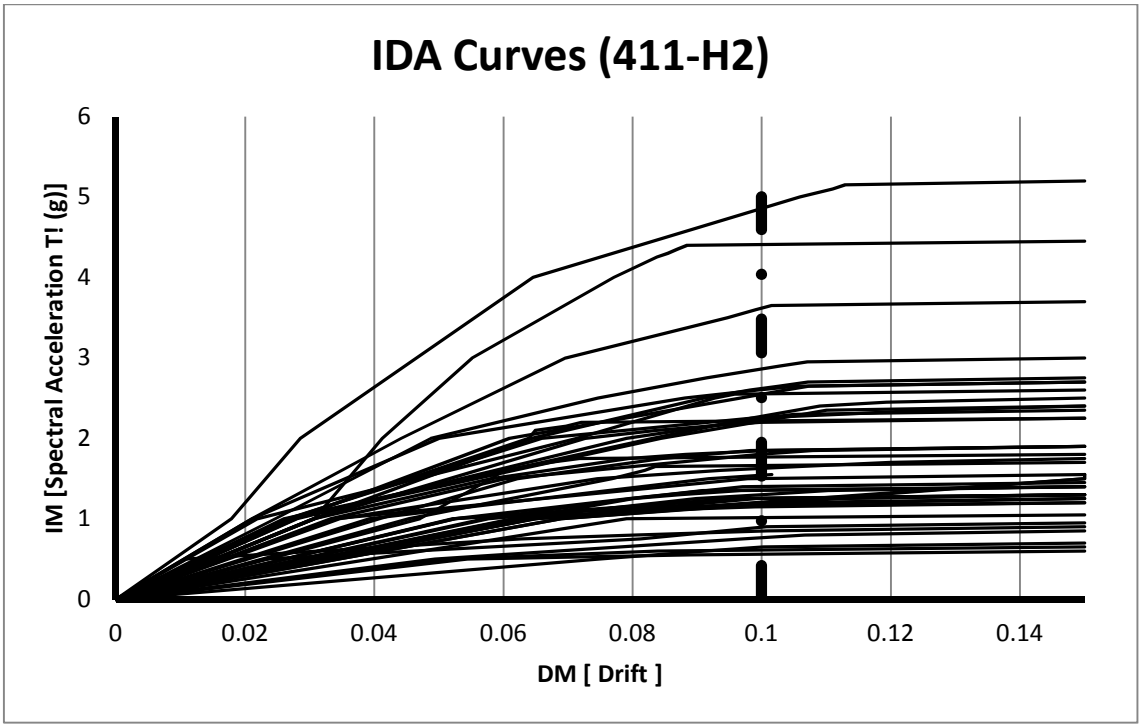

Figure 4.8. IDA curves for building-411 in H2 direction.

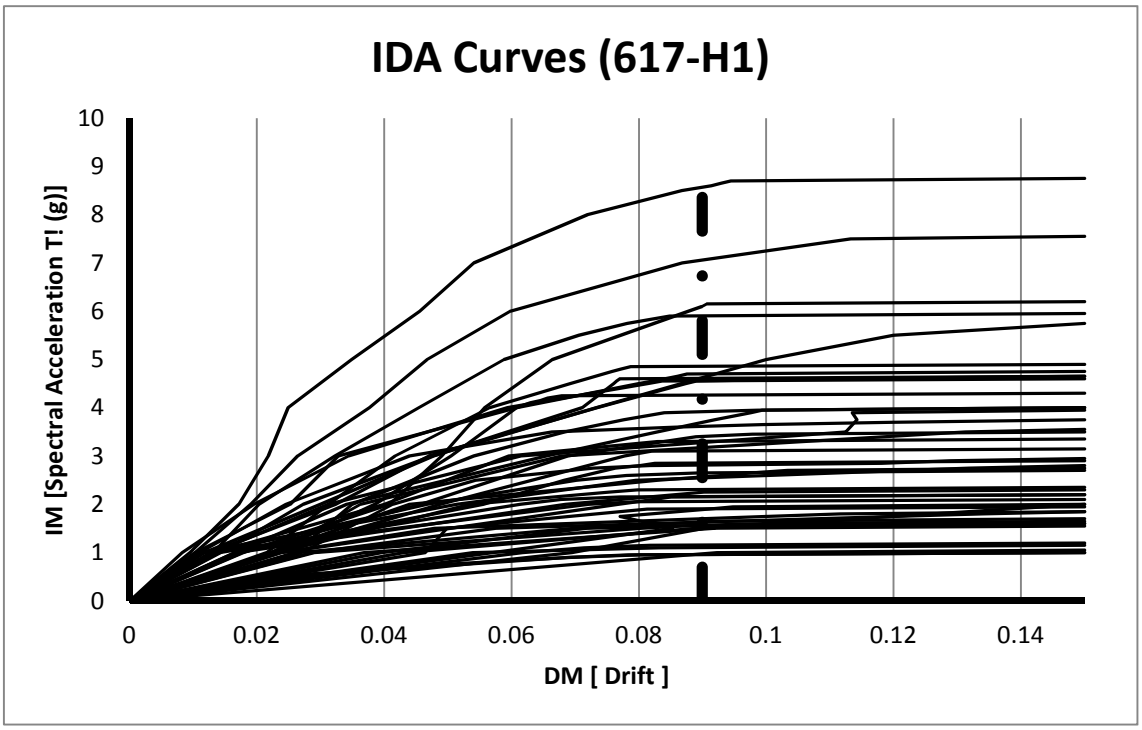

Figure 4.9. IDA curves for building-617 in H1 direction.

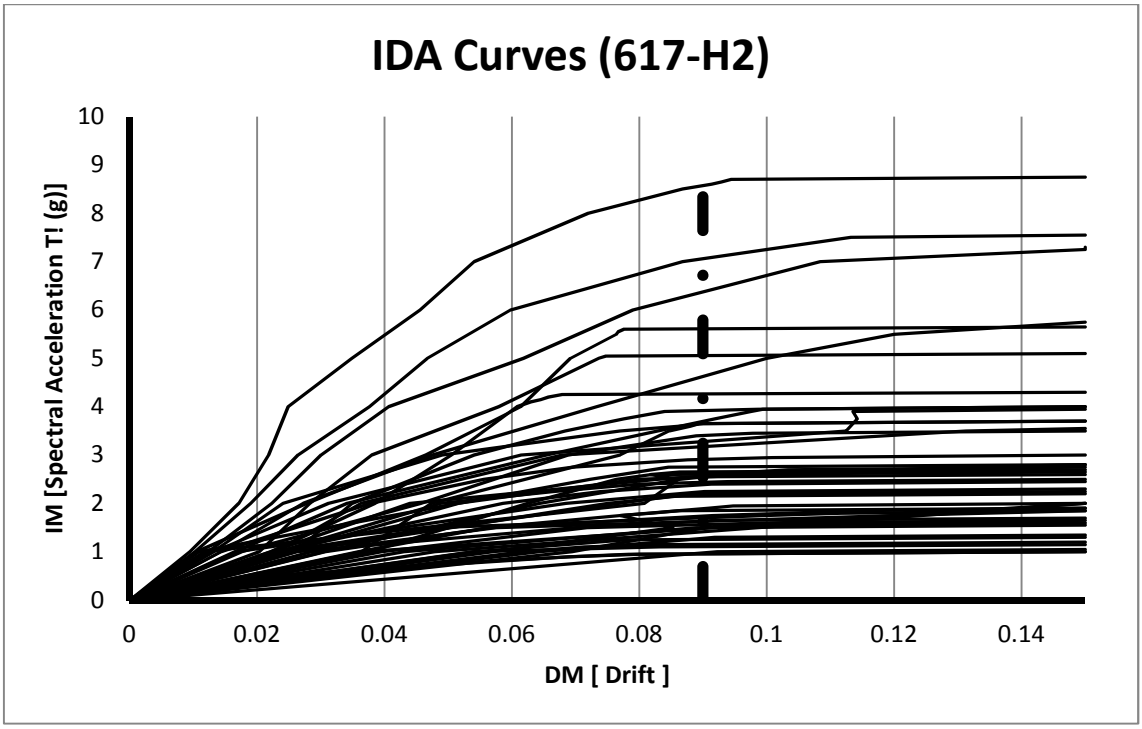

Figure 4.10. IDA curves for building-617 in H2 direction.

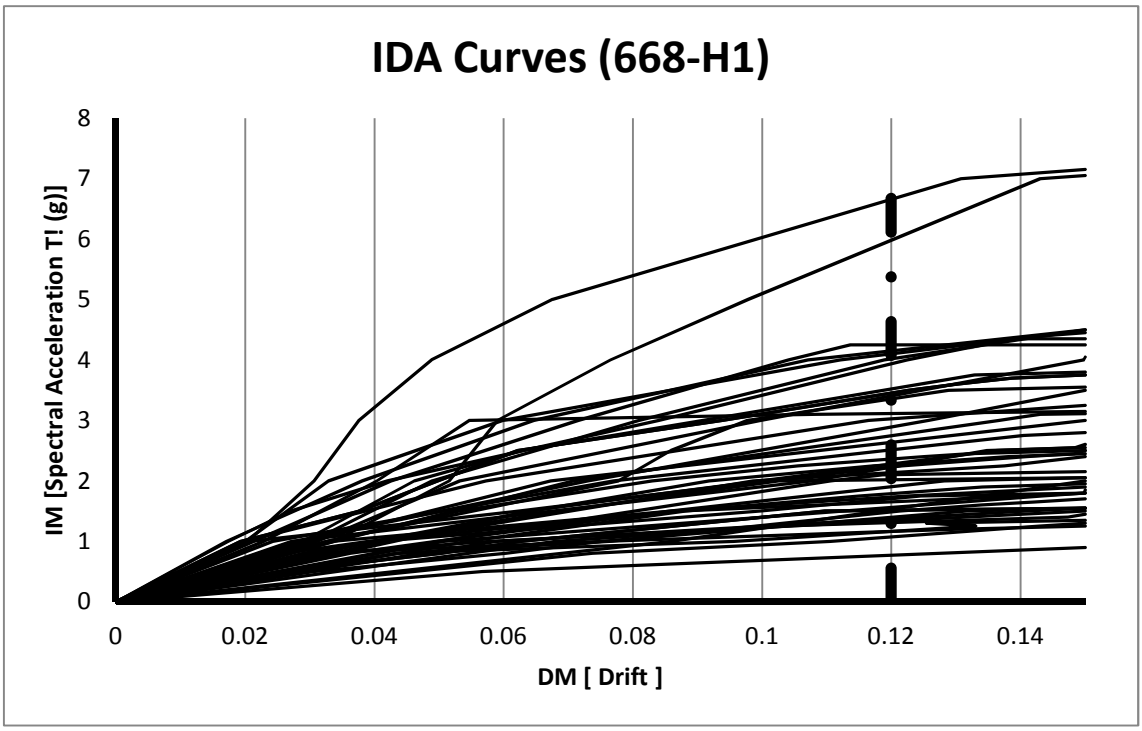

Figure4.11. IDA curves for building-668 in H1 direction.

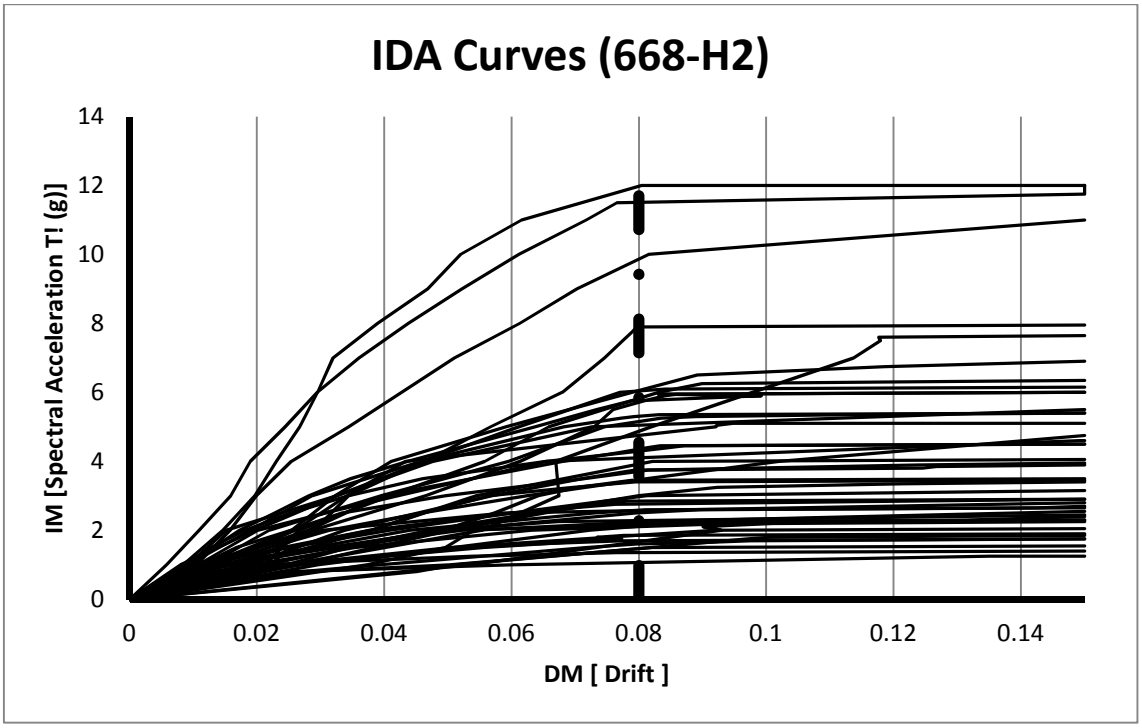

Figure 4.12. IDA curves for building-668 in H2 direction.

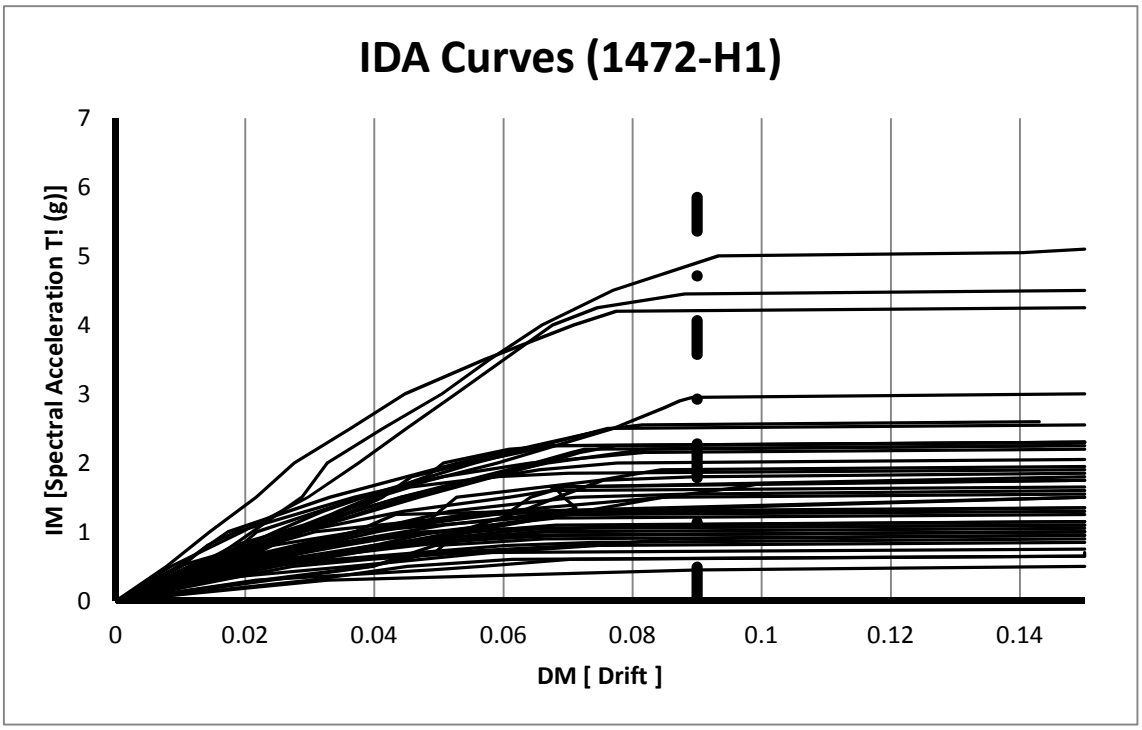

Figure 4.13. IDA curves for building-1472 in H1 direction.

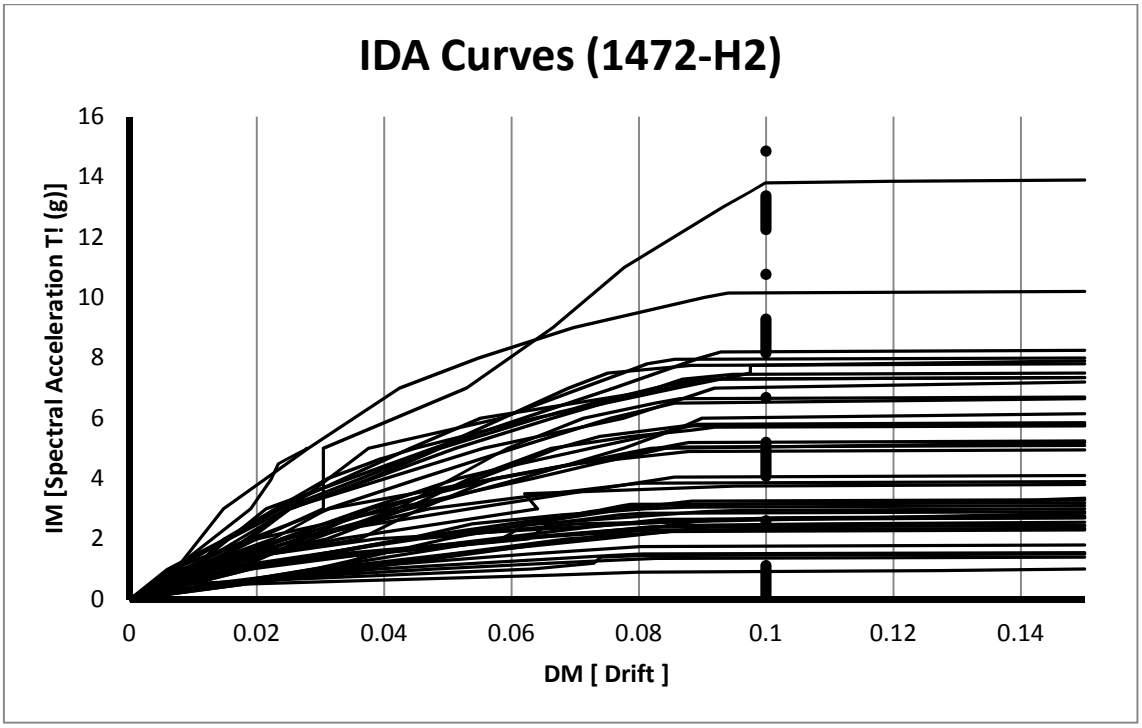

Figure 4.14. IDA curves for building-1472 in H2 direction.

5. PROCESS OF COLLAPSE RISK ASSESSMENT

5.1. General Information about Risk Assessment

In the previous section IDA curves are calculated and presented graphically to represent the distribution of the damage with respect to strong ground motion intensity. The demand parameter is chosen as maximum inter-story drift ratio and, the seismic intensity parameter is chosen as Spectral Acceleration at the first mode period of the structure ($S_a(T_1,5\%)$). In this section, estimation of the collapse risk is statistically evaluated by integrating collapse fragility curve of the structure over the seismic hazard curve.

Fragility curve is formed by calculating the probability of reaching collapse for each level of intensities of the selected ground motions. Major steps for estimation of the collapse risk calculation are listed below:

- Hazard curve calculation to identify seismic risk of the region.
- Formation of fragility curves for collapse state through obtained by IDA curves.
- Calculation of annualized probability of collapse by integrating fragility curve over the hazard curve.

On the other hand, another efficient method recommended by (Eads *et al*., 2013) for estimating the collapse risk can be used in calculation of the collapse risk assessment. The main assumption in this method is that the fragility curve is distributed log-normally. In order to evaluate log-normal distribution assumption, the discrete result obtained from "Incremental Dynamic Analysis" (IDA) procedure proposed by (Vamvatsikos and Cornelll, 2002) are graphically compared with the efficient method offered by (Eads *et al.*, 2013).

5.2. Seismic Hazard Curve

The collapse risk for the example structures can be calculated combination of collapse fragility curve and site-specific hazard curve. Hazard curve represents the probability of occurrence of the intensity measure which is five percent damped spectral acceleration of the records at the first mode period of the structure ($S_a(T_1,5\%)$) in this study. The hazard curves of Düzce city used in this study were provided by Prof. Dr. S. Akkar (personal communication, January 31, 2013). Also, each hazard curve utilized in this study are plotted in the form of ground motion intensity versus annual rate of exceedances for twenty different period levels as 0.0001, 0.001, 0.01, 0.02, 0.05, 0.07, 0.1, 0.2, 0.3, 0.4, 0.5, 0.6, 0.7, 0.8, 0.9, 1.0, 2.0, 3.0, 4.0, 5.0 at soft site (V_s=250m/sec) on Düzce city. The uniform hazard spectrum obtained by using each hazard curves is given in Figure 5.1. Also hazard curves for selected periods are given Figure 5.2.

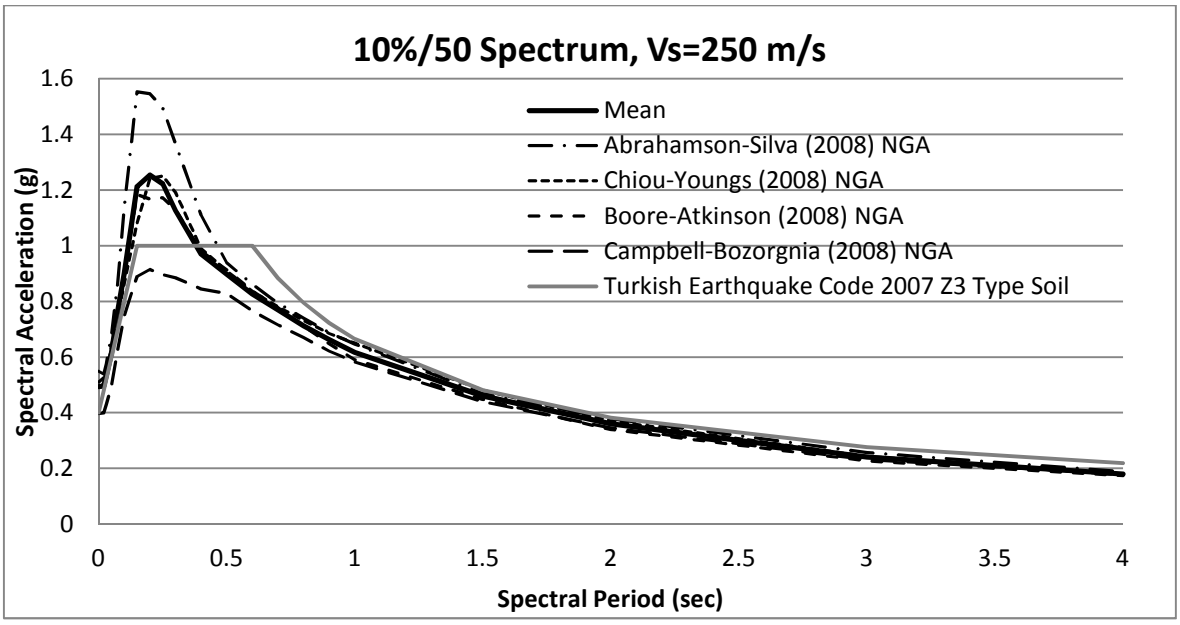

Figure 5.1. Uniform hazard spectra for Düzce city.

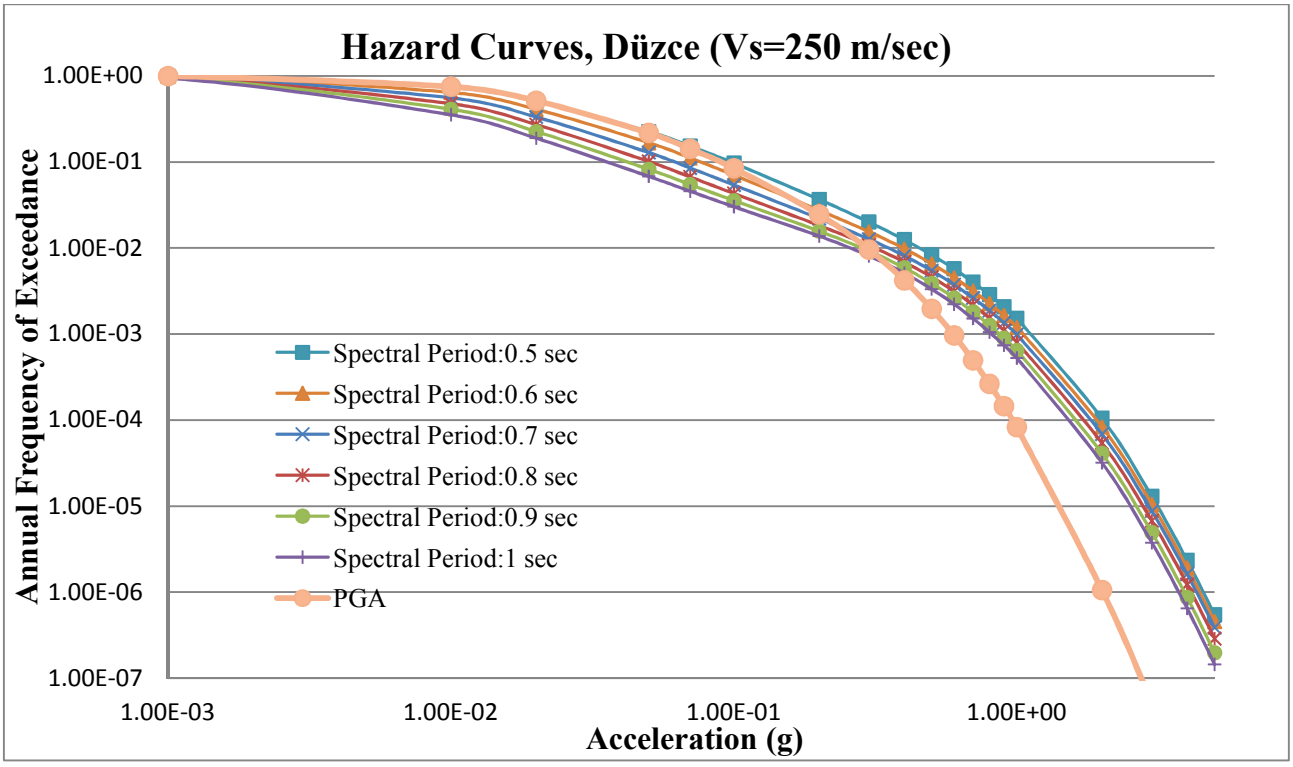

Figure 5.2. Some hazard curves for Düzce city.

5.3. Probabilistic Evaluation of the IDA Curve

To built relationship between collapse probability and intensity measure, the collapse fragility curve can be used in the form of a Cumulative Distribution Function (Ibarra and Krawinkler, 2002). The IDA results obtained in the previous section for each structure can be easily converted to the fragility curves at specified damage level which is collapse in this study. The probabilities of reaching and exceeding to pre-determined damage level are calculated for every intensity measure level. For this study, the damage level measured as maximum inter-story drift ratio is the sidesway collapse, and the intensity measure of the scaled ground motions is five percent dumped spectral acceleration at the first mode period of the structure ($S_a(T_1,5\%)$). Since generally sidesway collapse is the major mechanism type, dynamic instability or numerical convergence problem is accepted as the collapse level in IDA analysis. Repeated calculation steps for each ground motion intensity measures are given in the following steps:

- Determination of total number of IDA curves representing an individual ground motion for every structure. In this study that number is forty-four.
- Determination of total number of the number of the collapsed IDAs at every Spectral Acceleration level of the first mode period of the structure ($S_a(T_1,5\%)$).
- Calculation of collapse probability of reaching or exceeding to collapse state for each $S_a(T_1,5\%)$ value.

By repeating those steps, each point on fragility curve is estimated with 0.05g accuracy.

Moreover lognormal distributions of the fragility curves can be clearly defined by a median value and a standard deviation parameter. By utilizing the statistical program EasyFit, a lognormal probability distribution function could be fitted to represent the discrete result obtained from "Incremental Dynamic Analysis" (IDA). The median collapse intensity, $(S_a(T_1,5\%))_{50\%}$, indicates the point that half of the ground motions cause collapse on the structure, or vice versa. Also the dispersion parameter represent the record-to-record variability.

The probability density function and the cumulative distribution function can be calculated by using these two representative parameters: the median collapse intensity and dispersion parameter. The probability density function of the random variable "*x*" is given in Equation 5.1 in the form of the probability distribution of the natural logarithm of the random variable;

$$f_x(x) = \frac{1}{\sqrt{2\pi}\cdot \sigma x} \cdot e^{-\frac{1}{2}\left(\frac{lnx-\mu}{\sigma}\right)^2} (x > 0) \tag{5.1}$$

where μ represents the mean of the natural logarithm of "*x*" and σ represents standard derivation of the natural logarithm of "*x*". The probability of the random variable "*x*" in the interval of (a,b) is calculated from the Equation 5.2.

$$P(a \leq X \leq b) = \int_a^b \frac{1}{\sqrt{2\pi}\cdot \sigma x} \cdot e^{-\frac{1}{2}\left(\frac{lnx-\mu}{\sigma}\right)^2} dx \tag{5.2}$$

The log-normal probability function "Φ" can be expressed in the form of Equation 5.3 through applying following transformations;

$$s = \frac{lnx - \mu}{\sigma} \quad and \quad dx = x\sigma ds$$

$$P(a \leq X \leq b) = \frac{1}{\sqrt{2\pi}} \int_{(lna-\mu)/\sigma}^{(lnb-\mu)/\sigma} \cdot e^{-s^2/2} ds = \Phi\left(\frac{lnb - \mu}{\sigma}\right) - \Phi\left(\frac{lna - \mu}{\sigma}\right) \tag{5.3}$$

Since a collapse-state fragility curve is constructed by computing the conditional probabilities of reaching or exceeding to the collapse state at various level of ground motion namely the scaled ground motions, the fragility curve can be explained in the form of a log-normal cumulative distribution function as in Equation 5.4;

$$P(Collapse|im) = \Phi\left[\frac{1}{\sigma} ln\left(\frac{im}{im_{median}}\right)\right] \tag{5.4}$$

where $P(Collapse|im)$ represents the probability of the collapse for the given ground motions represented by intensity measure of ground motion "*im*" and σ is the lognormal dispersion.

In this study intensity measure is five percent damped spectral acceleration corresponding to the first mode, and damage measure is maximum inter-story drift radio for collapse detection. The cumulative distribution function representing the fragility curve can be re-written for parameters used in this study as given in Equation 5.5.

$$P\left(Collapse \middle| S_{ae}(T_1, 5\%)\right) = \Phi\left[\frac{1}{\sigma} ln\left(\frac{S_{ae}(T_1, 5\%)}{S_{ae}(T_1, 5\%)_{median}}\right)\right] \tag{5.5}$$

The discrete result obtained from "Incremental Dynamic Analysis" (IDA) procedure proposed by (Vamvatsikos and Cornelll, 2002) are plotted on the same graph with probabilities obtained from cumulative distribution function in Equation 5.5 for comparison. These graphs are given in Figure 5.3 to Figure 5.10 for all buildings evaluated in this study.

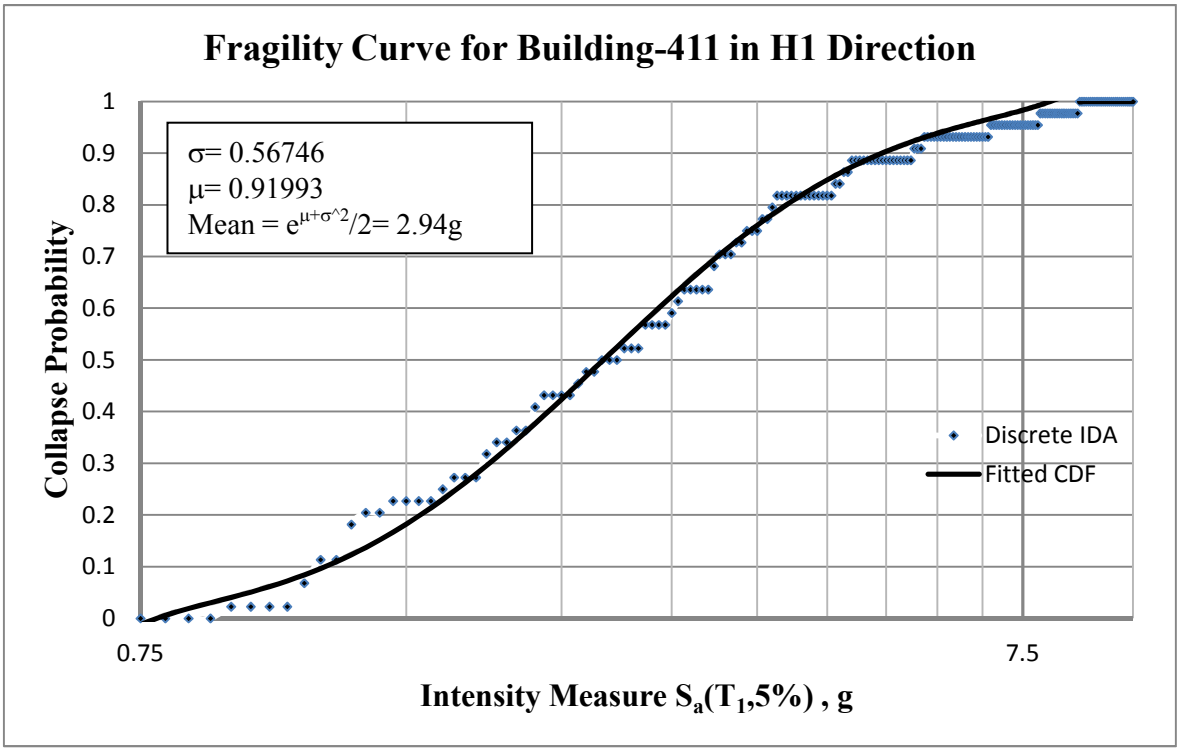

Figure 5.3. Probability distributions for building-411 in H1 direction.

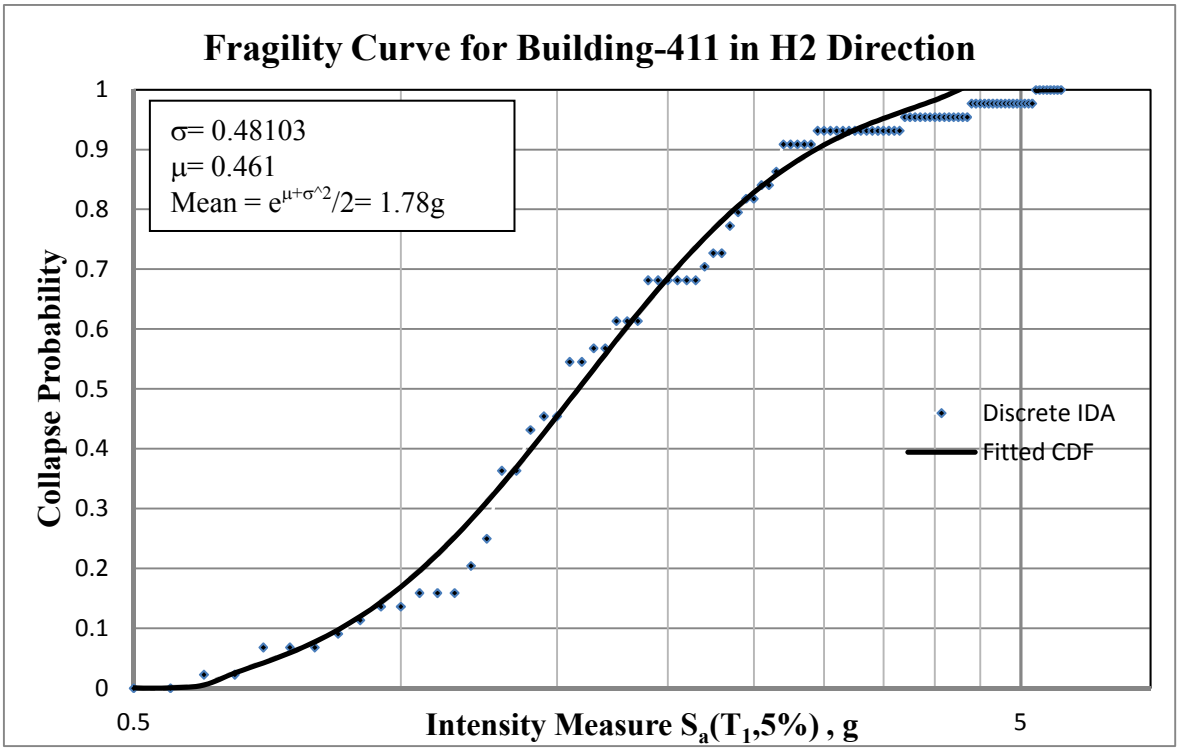

Figure 5.4. Probability distributions for building-411 in H2 direction.

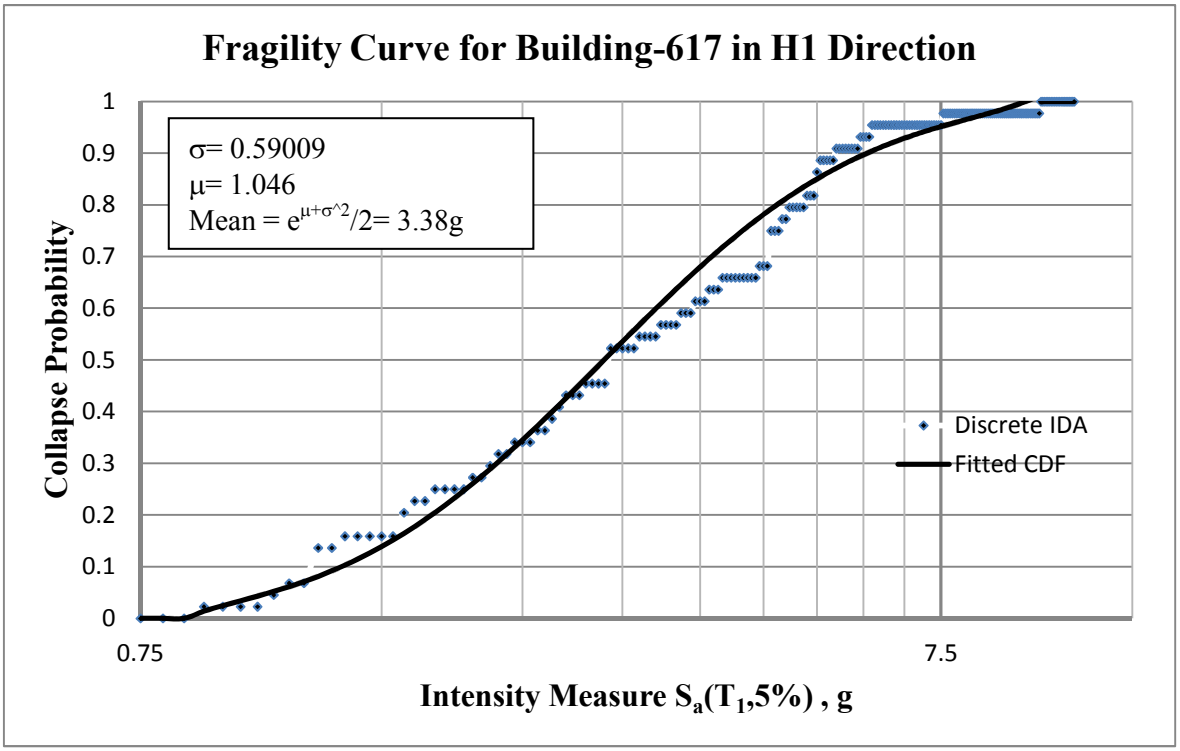

Figure 5.5. Probability distributions for building-617 in H1 direction.

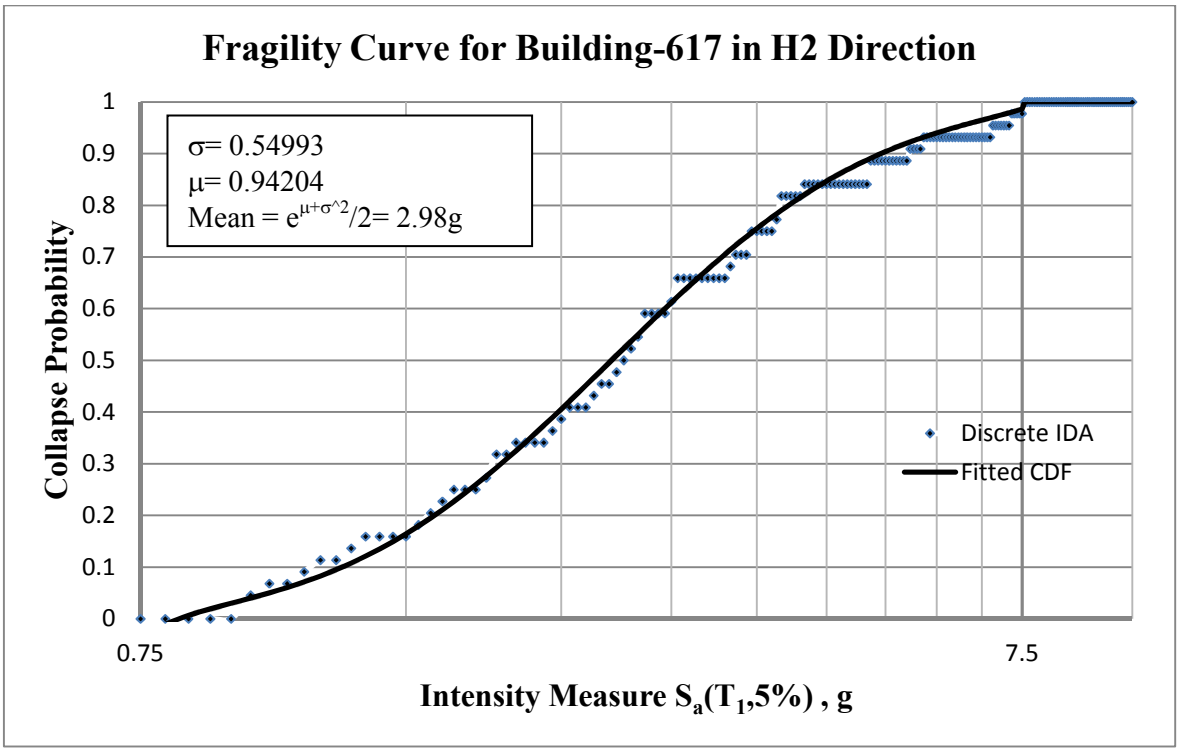

Figure 5.6. Probability distributions for building-617 in H2 direction.

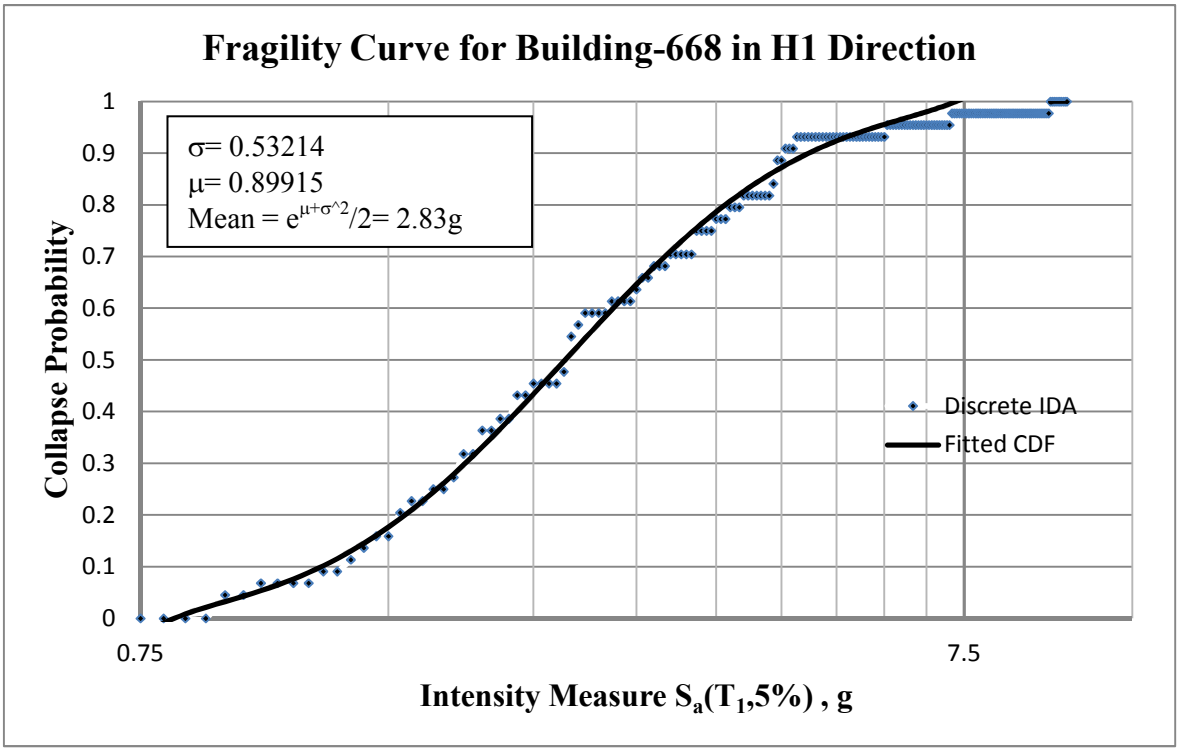

Figure 5.7. Probability distributions for building-668 in H1 direction.

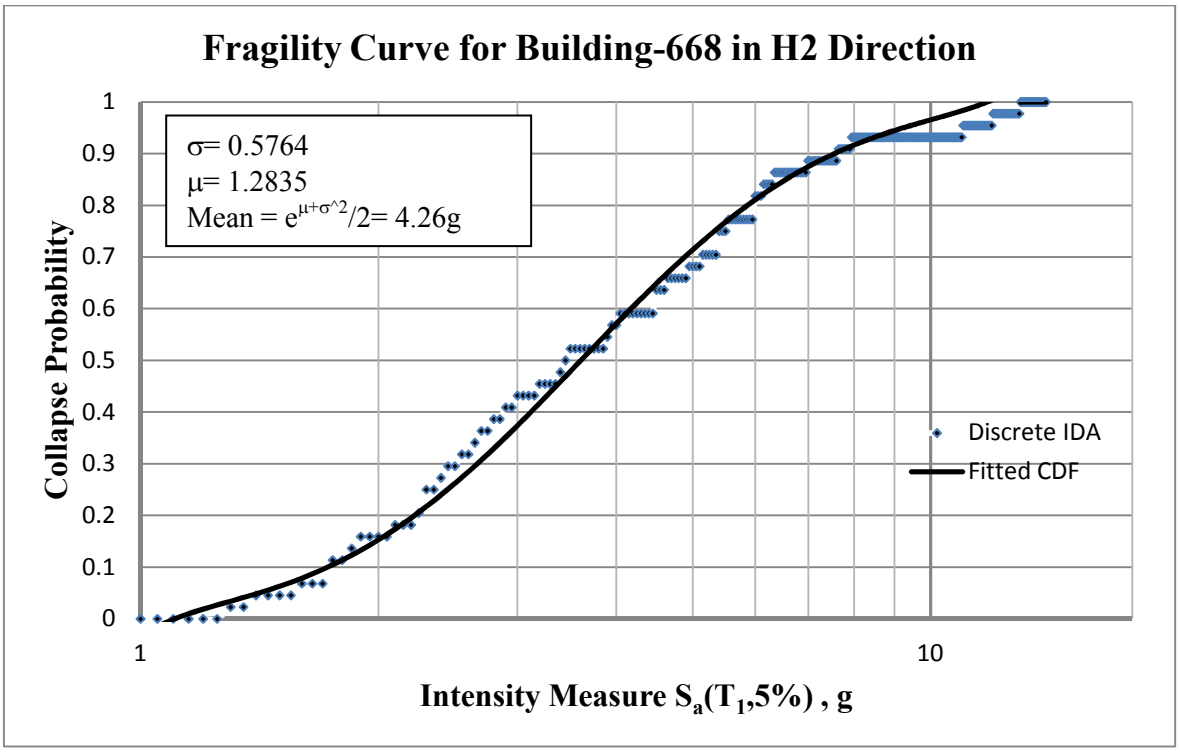

Figure 5.8. Probability distributions for building-668 in H2 direction.

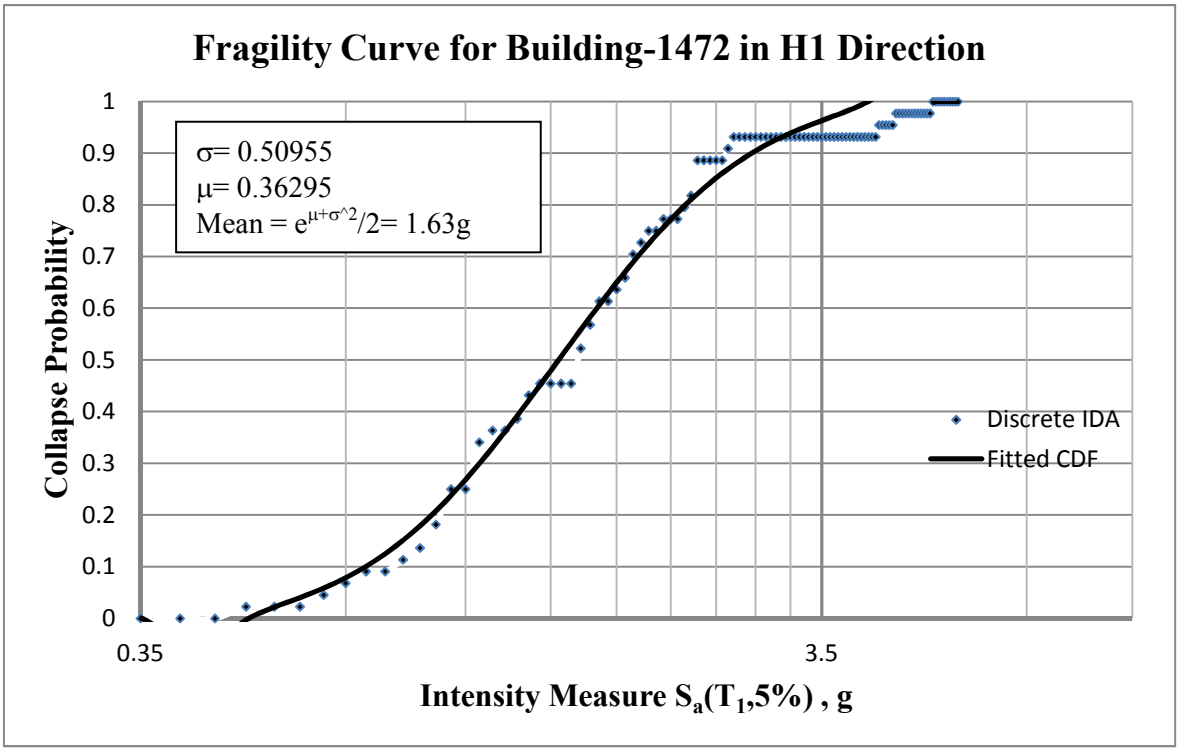

Figure 5.9. Probability distributions for building-1472 in H1 direction.

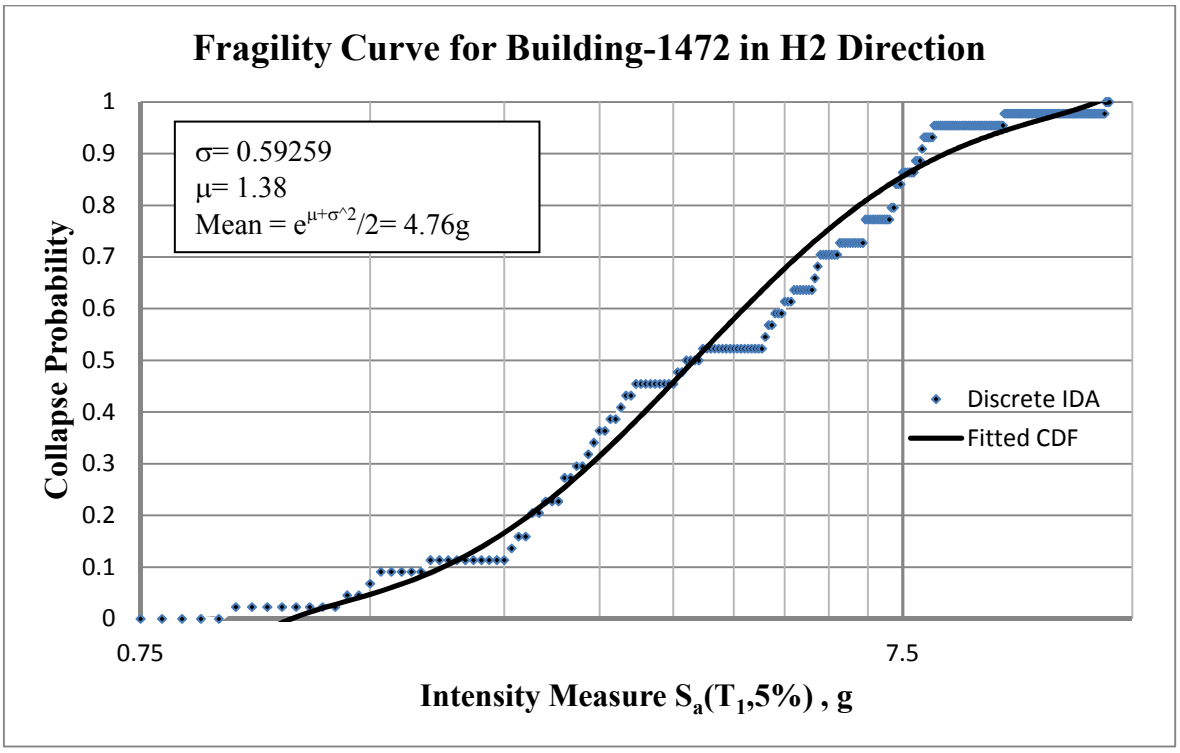

Figure 5.10. Probability distributions for building-1472 in H2 direction.

5.4. Estimation of the Collapse Risk

Fragility curve results estimated in the previous section and seismic hazard curves need to be combined in order to obtain mean annual frequency for any damage level. In this study the damage level is selected as collapse state resulted from dynamic instability. One of the required parameter in calculation of annualized probability of collapse, fragility curve in the form of a cumulative distribution function can be estimated from the results of incremental dynamic analyses. The other required parameter is the seismic hazard curve that represents the mean annual frequency of exceeding ground motion intensity measures at the seismic region. Also, five percent damped spectral acceleration at the first mode period of the structure ($S_a(T_1,5\%)$) is selected as the intensity measure of the ground motion which is the common variable for numerical integration.

Calculation of annualized collapse fragility requires integration of the fragility curve at collapse state with respect to hazard curve at seismic region which the structure is constructed (Eads *et al.*, 2013). This calculation is given in the following Equation 5.6;

$$\lambda_{collapse} = \int_0^{\infty} P(Collapse \quad im) \cdot \quad |d\lambda_{IM}(im)| \tag{5.6}$$

where *P(Collapse | im)* represents the probability of collapse on the condition that the structure subjected earthquake which intensities are *im* or larger than *im*. And, λ_{IM} represents the mean annual frequency of exceedence of intensity measure. The expression of the mean annual collapse frequency can be written in the form of Equation 5.7 by multiplying and dividing Equation 5.6 with *d(im)*;

$$\lambda_{collapse} = \int_0^{\infty} P(Collapse \quad im) \cdot \quad \left|\frac{d\lambda_{IM}(im)}{d(im)}\right| \cdot d(im) \tag{5.7}$$

where the first derivation of "$d\lambda_{IM}(im)$" with respect to "*d(im)*" represent the slope of the hazard curve. So, the Equation 5.7 can be solved numerically as it proposed in Equation 5.8;

$$\lambda_{collapse} = \sum_{i=1}^{\infty} P(Collapse \quad im_i) \cdot \quad \left|\frac{d\lambda_{IM}(im_i)}{d(im)}\right| \cdot \Delta im \tag{5.8}$$

where *Δim* is the increment of intensity measure. In this study, this increment is 0.05g as the quantity of five percent damped spectral acceleration at the first mode period of the structure ($S_a(T_1,5\%)$).

Moreover the collapse probability of a structure in "t" years can be calculated by assuming that the occurrence of earthquakes in time practices a Poisson process as in the Equation 5.9. The mean annual collapse frequency "$\lambda_{collapse}$" describe the mean collapse rate per year.

$$P_c(\text{in t years}) = 1 - \exp\left(-\lambda_{\text{collapse}} \cdot \text{t}\right) \tag{5.9}$$

Since the "$\lambda_{collpse}$" is small quantity for typical structures, the probability of collapse in one year is nearly equal to "$\lambda_{collapse}$". So, the probability of collapse in "*t*" years is ;

$$P_c(\text{in t years}) = 1 - \left(1 - \lambda_{\text{collapse}}\right)^{\text{t}} \tag{5.10}$$

By using this classical procedure calculated mean annual collapse frequencies and mean collapse risk over 50 years are given in the following Table 5.1 and Table 5.2 for discrete and fitted fragility curves respectively. In this table, the values are calculated by using real discrete probabilities representing collapse fragility curve.

Table 5.1. Collapse risk of the example buildings for discrete values.

Building Name	**Direction**	**Period (sec)**	**Mean Annual Collapse Frequency $\lambda_{collapse}$**	**Mean Collapse Probability Over 50 years $P_{collapse}$(in 50 years)**	
411	H1	0.906	1.3451E-04	6.7031E-03	(0.6703%)
	H2	0.673	6.4469E-04	3.1720E-02	(3.1720%)
617	H1	0.732	1.5365E-04	7.6529E-03	(0.7653%)
	H2	0.609	2.0399E-04	1.0147E-02	(1.0147%)
668	H1	0.659	1.8695E-04	9.3041E-03	(0.9304%)
	H2	0.859	4.0200E-05	2.0080E-03	(0.2008%)
1472	H1	0.549	1.1602E-03	5.6359E-02	(5.6359%)
	H2	0.923	4.1413E-05	2.0685E-03	(0.2069%)

Table 5.2. Collapse risk of the example buildings for fitted CDF.

Building Name	Direction	Period (sec)	Mean Annual Collapse Frequency $\lambda_{collapse}$	Mean Collapse Probability Over 50 years $P_{collapse}$(in 50 years)	
411	H1	0.906	1.8113E-04	9.0158E-03	(0.9016%)
	H2	0.673	7.1593E-04	3.5163E-02	(3.5163%)
617	H1	0.732	1.7977E-04	8.9480E-03	(0.8948%)
	H2	0.609	2.4849E-04	1.2347E-02	(1.2347%)
668	H1	0.659	2.3856E-04	1.1857E-02	(1.1857%)
	H2	0.859	6.5625E-05	3.2759E-03	(0.3276%)
1472	H1	0.549	1.3241E-03	6.4063E-02	(6.4063%)
	H2	0.923	4.3670E-05	2.1811E-03	(0.2181%)

5.5. A Simple Method to Estimate the Collapse Risk

Classical discrete solution of a fragility curve as described in previous section is a time demanding problem. This classical estimation of a fragility curve require utilizing many consecutive incremental dynamic analyses by conducting nonlinear response history analyses for all scale levels of each strong ground motion record. Also, to find the collapse intensity measure causing collapse within a predetermined tolerance level requires many sub-iterations.

On the other hand, if lognormal distribution assumption is accepted, the entire fragility curve can be clearly defined by two parameters: a median value and a standard derivation. Instead of these two independent variables, two random points on the cumulative distribution function can also exactly represent the log-normally distributed curve. In other words, estimation of collapse probability at only two intensity measure $S_a(T_1,5\%)$ points is enough to construct whole fragility curve. However; only two points never exactly represent the real discrete fragility curve through calculated probabilities at every intensity measure because of the dispersion of the real data. So, in order to evaluate the collapse risk of a building more precisely, these two representative points need to be chosen according to the slope of the hazard curve that effect the deaggregation of the mean annual collapse frequency "λ_c" (Eads *et al*., 2013).

The main steps of the proposed simple method to estimate the annual frequency of collapse "λ_c"(Eads *et al*., 2013).are:

- In order to find intensity measure that significantly contribute to collapse annual frequency "λ_c", approximate methods without conducting IDA analysis can be utilized to find initial estimate of the log-normally distributed fragility curve. Since this step is used to identify initial fragility curve, it is not necessary to have a proper estimation of the initial fragility curve.
- Integrate the collapse state cumulative distribution function representing the collapse probability as a function of the intensity measure $S_a(T_1,5\%)$ with respect to the hazard curve representing probability of occurrence of the intensity measure in selected seismic region. Only in that step, initial estimate of the log-normally distributed fragility curve which is calculated in the first step can be used. In this step, the annual frequency of collapse "$\lambda_{collapse}$" is calculated by using Equation 5.8 and the deaggregation of the annual frequency of collapse is estimated. From that deaggregation, IM_1 is determined such that the cumulative contribution of collapse in the total annual frequency shall be at least 90 %.
- All ground motions are scaled so that spectral acceleration of the records at the first mode period of the structure ($S_a(T_1,5\%)$) is equal to IM_1 which is estimated in previous step. Response history analyses are conducted for all these scaled set of data, and the real probability of collapse "$P(Collapse \mid IM_1)$ is calculated by dividing the number of the ground motions that collapse occurred to the total number of the ground motion used in the analysis.
- A more convenient collapse fragility curve is calculated with the help of the lognormal CDF assumption by using the $P(Collapse \mid IM_1)$ determined in previous step and the estimation of the dispersion parameter of fragility curve determined in the first step. By using this new fragility curve, the annual frequency of collapse "$\lambda_{collapse}$" is calculated from the Equation 5.8 and the deaggregation of the annual frequency of collapse is estimated. The IM_2 value is determined such that the cumulative contribution of collapse in the total annual frequency shall be at least 40 %.
- All ground motions are scaled so that spectral acceleration of the records at the first mode period of the structure ($S_a(T_1,5\%)$) is equal to IM_2 estimated in previous step. Response history analyses are conducted for all these scaled set of data, and The real probability of collapse "$P(Collapse \mid IM_2)$" is calculated.

- Based on lognormal distribution assumption, a new fragility curve is constructed by using coordinates of which are $(IM_1, P(Collapse \mid IM_1))$ and $(IM_2, P(Collapse \mid IM_2))$. After this step, the estimated initial dispersion parameter and the median collapse intensity calculated in the first step will no longer be used, so the approximate values selected in the first step remain as only an initial condition.
- The final annual frequency of collapse "$\lambda_{collapse}$" is calculated with Equation 5.8 by using the collapse fragility curve at previous step.

Additionally given the fact that $(IM_1, P(Collapse \mid IM_1))$ and $(IM_2, P(Collapse \mid IM_2))$ points are close each other, a new response history analyses can be performed at a third intensity level in order to update the fragility curve.

For the sample buildings used in the analyses, all the steps proposed in the study named ;"An Efficient Method for Estimating the Collapse Risk of Structures in Seismic Regions" (Eads *et al*., 2013); are applied, calculated and results are given in Table 5.3.

The estimated results obtained from "Incremental Dynamic Analysis" (IDA) procedure obtained by (Vamvatsikos and Cornelll, 2002) are plotted on the same graph with iterative fragility curves obtained from the procedure proposed by (Eads *et al*., 2013) defined in this section for comparison. Also, deaggregation of the annual frequency of collapse "$\lambda_{collapse}$" are plotted to show the highest contribution from which $S_a(T_1,5\%)$ value. These graphs are presented from Figure 5.11 to Figure 5.26 for all buildings studied in this thesis.

Table 5.3. Iteration results for example buildings.

Building Name		**411**		**617**		**668**		**1472**	
Direction		H1	H2	H1	H2	H1	H2	H1	H2
Period (sec)		0.906	0.673	0.732	0.609	0.659	0.859	0.549	0.923
Initial Values	$S_a(T_1,5\%)_{median}$	1.196	0.622	1.412	1.413	1.349	1.669	0.508	1.938
	σ	0.738	0.649	0.738	0.825	0.798	0.646	0.713	0.889
First Iteration	IM_1	2.40	2.00	2.50	2.25	2.25	3.35	1.85	2.55
	$P(C \mid IM_1)$	0.477	0.682	0.409	0.386	0.455	0.455	0.705	0.227
	$S_a(T_1,5\%)_{median}$	0.920	0.390	1.090	1.050	0.910	1.290	0.240	1.610
	σ	0.738	0.649	0.738	0.825	0.798	0.646	0.713	0.889
Second Iteration	IM_2	0.95	0.80	0.95	0.80	0.80	1.30	0.65	0.90
	$P(C \mid IM_2)$	0.023	0.068	0.023	0.000	0.000	0.000	0.045	0.000
	$S_a(T_1,5\%)_{median}$	0.901	0.471	0.941	0.791	0.791	1.271	0.361	0.891
	σ	0.475	0.468	0.107	0.496	0.461	0.510	0.471	0.611
Third Iteration	IM_3	1.70	---	2.95	1.50	1.55	1.95	1.20	1.35
	$P(C \mid IM_3)$	0.273	---	0.523	0.159	0.205	0.159	0.364	0.023
	$S_a(T_1,5\%)_{median}$	0.911	---	1.051	0.981	0.871	1.281	0.351	1.321
	σ	0.627	---	0.583	0.579	0.523	0.615	0.489	0.513
Target Values	$S_a(T_1,5\%)_{median}$	0.920	0.461	1.046	0.942	0.899	1.284	0.363	1.385
	σ	0.567	0.481	0.590	0.550	0.532	0.576	0.510	0.593

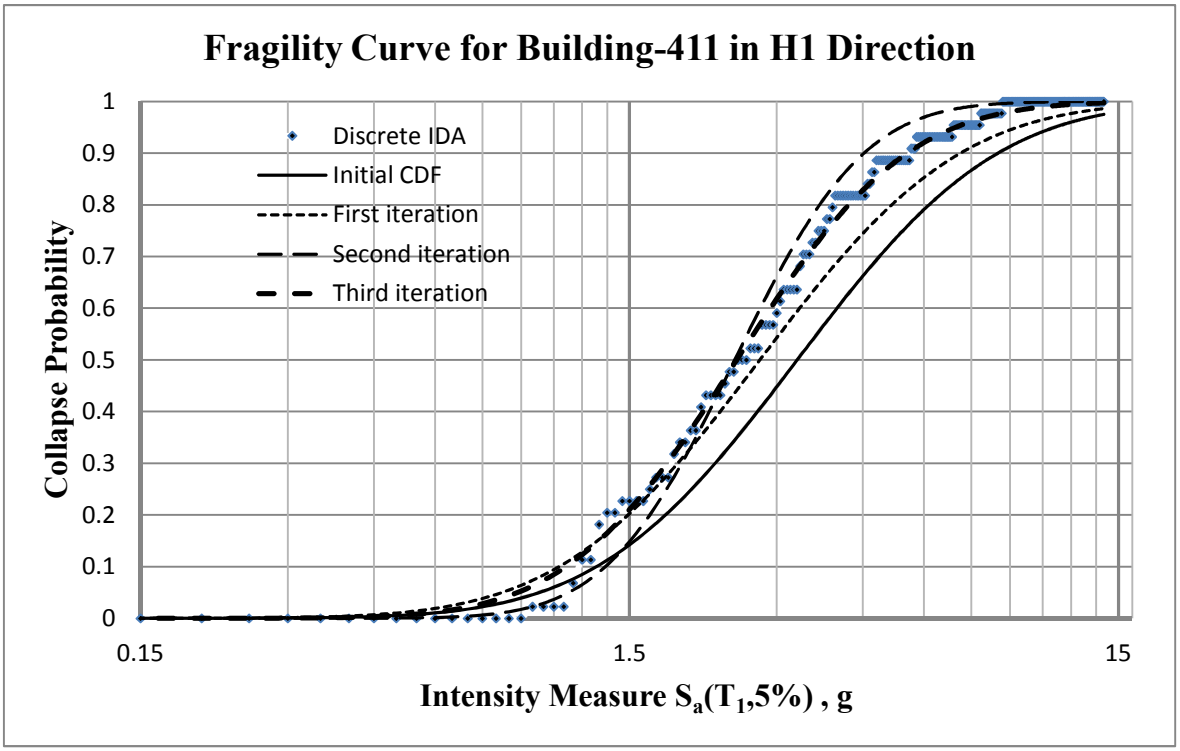

Figure 5.11. Iterative fragility curves for building-411 in H1 direction.

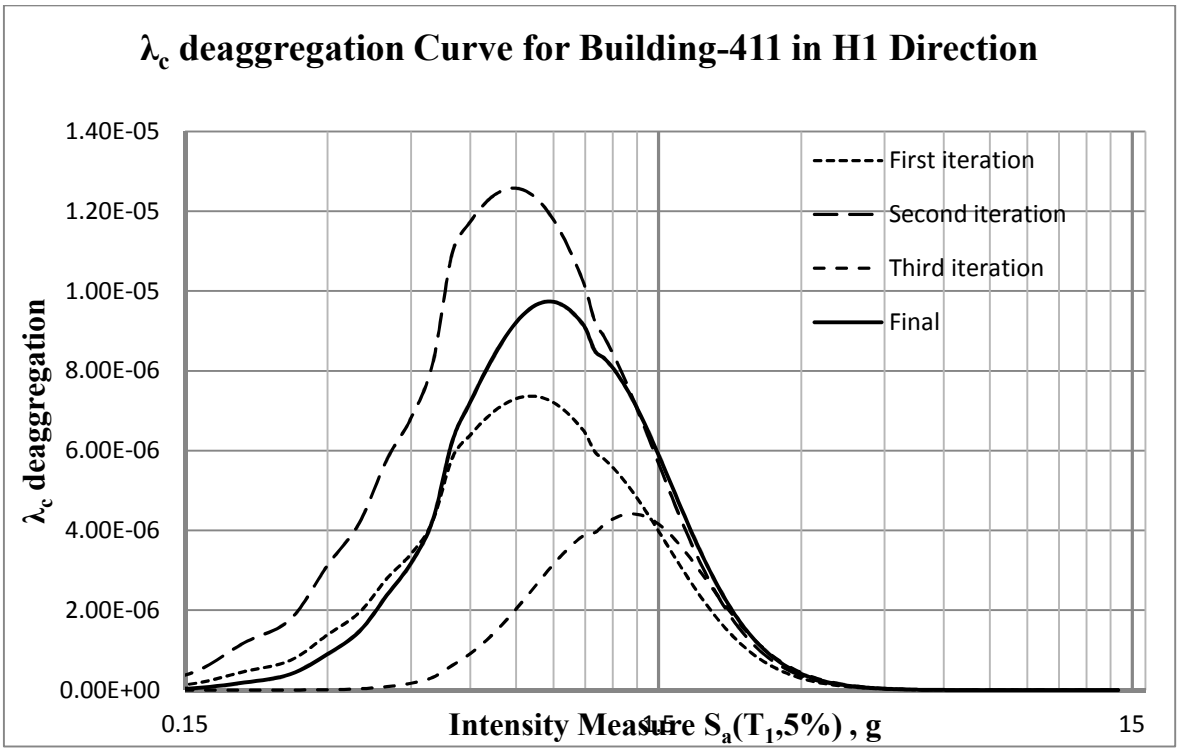

Figure 5.12. $\lambda_{collapse}$ deaggregation for building-411 in H1 direction.

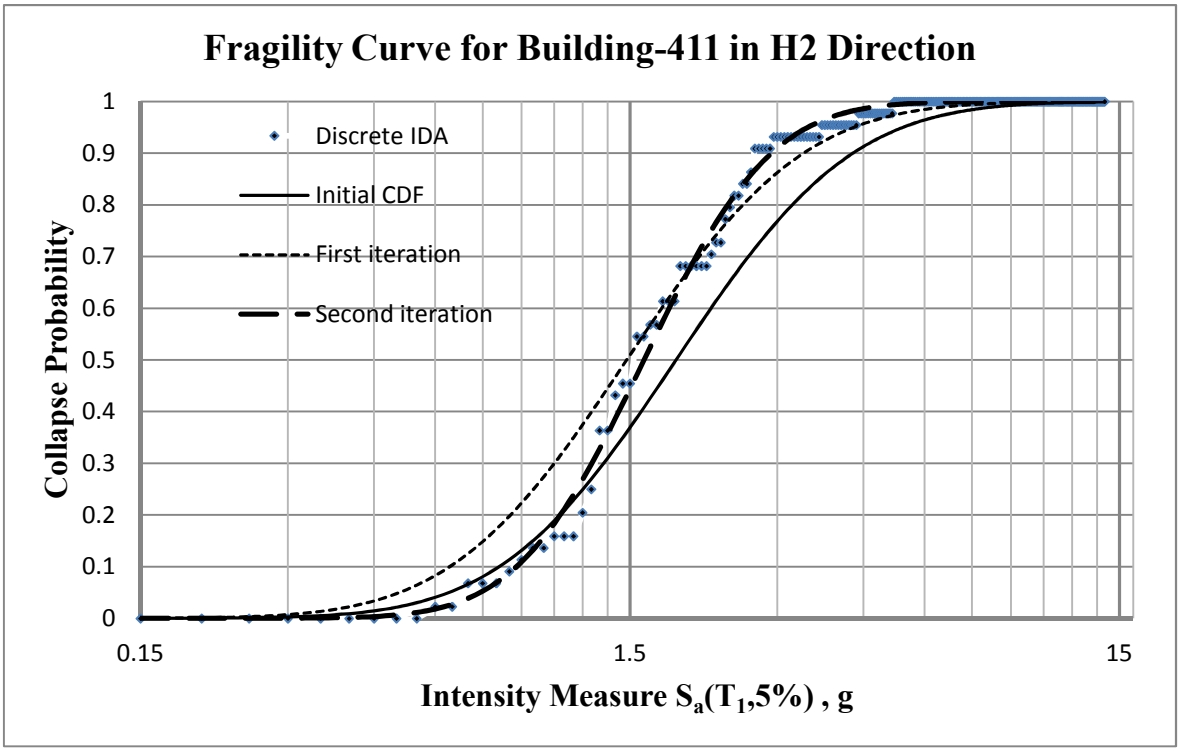

Figure 5.13. Iterative fragility curves for building-411 in H2 direction.

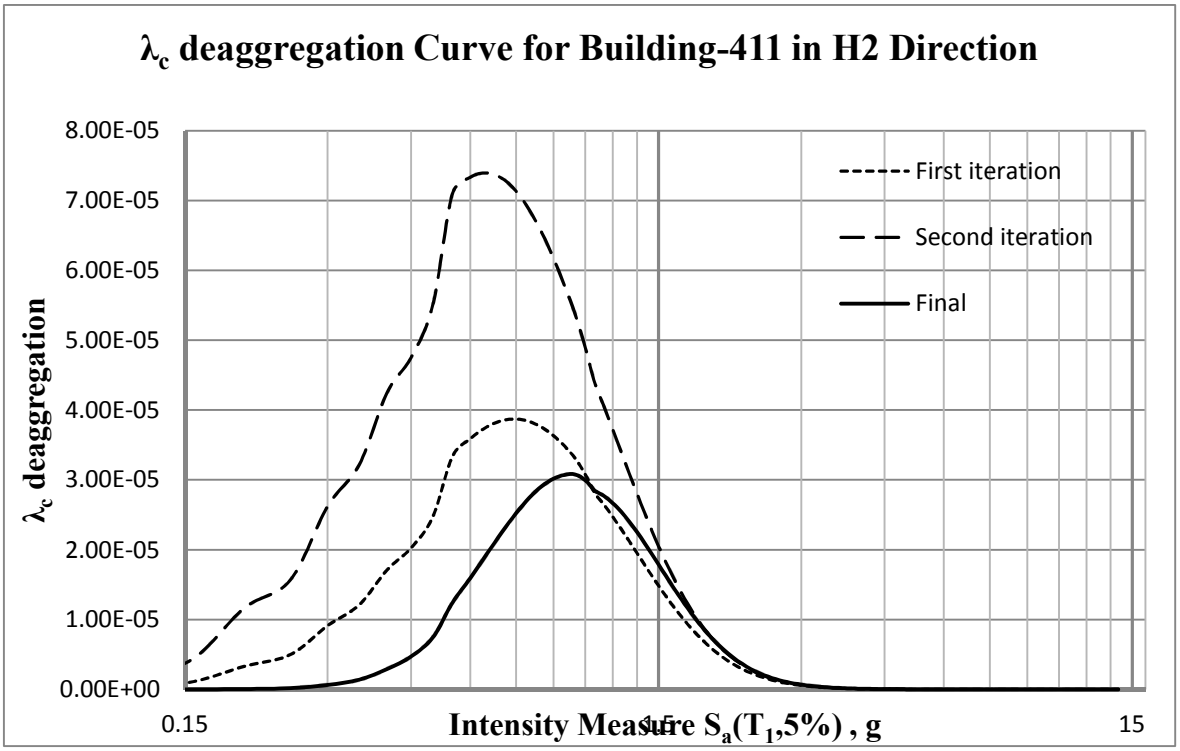

Figure 5.14. $\lambda_{collapse}$ deaggregation for building-411 in H2 direction.

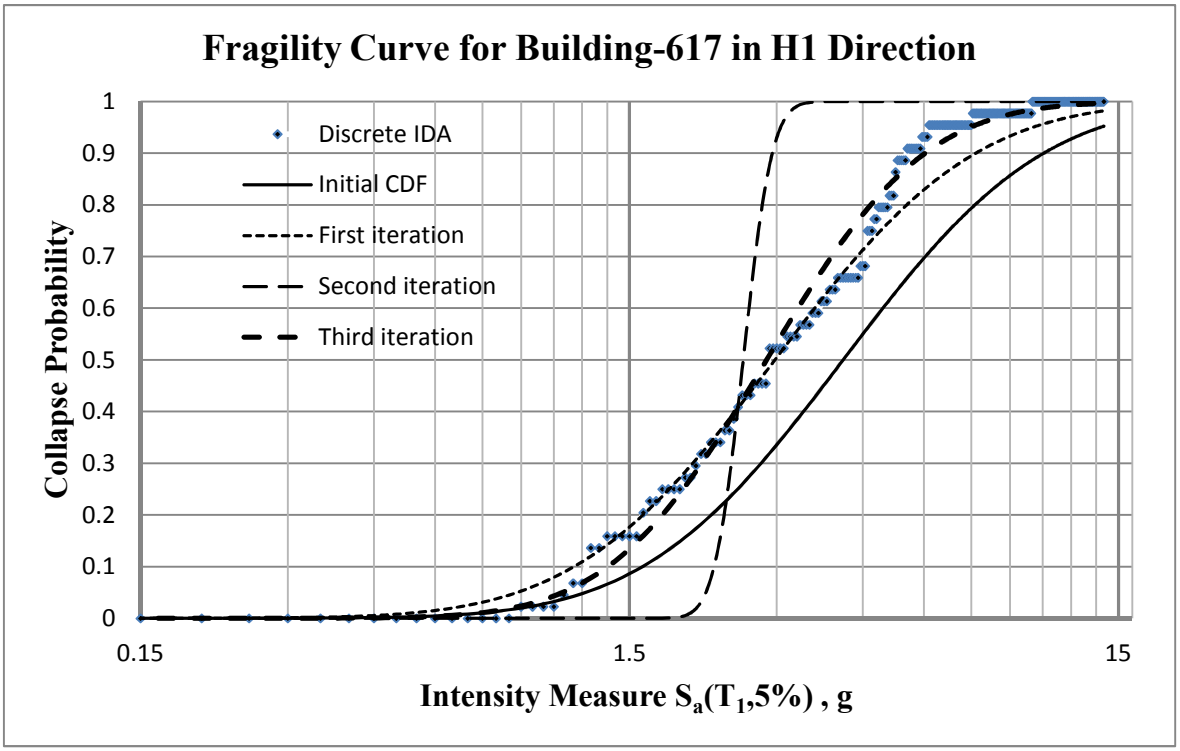

Figure 5.15. Iterative fragility curves for building-617 in H1 direction.

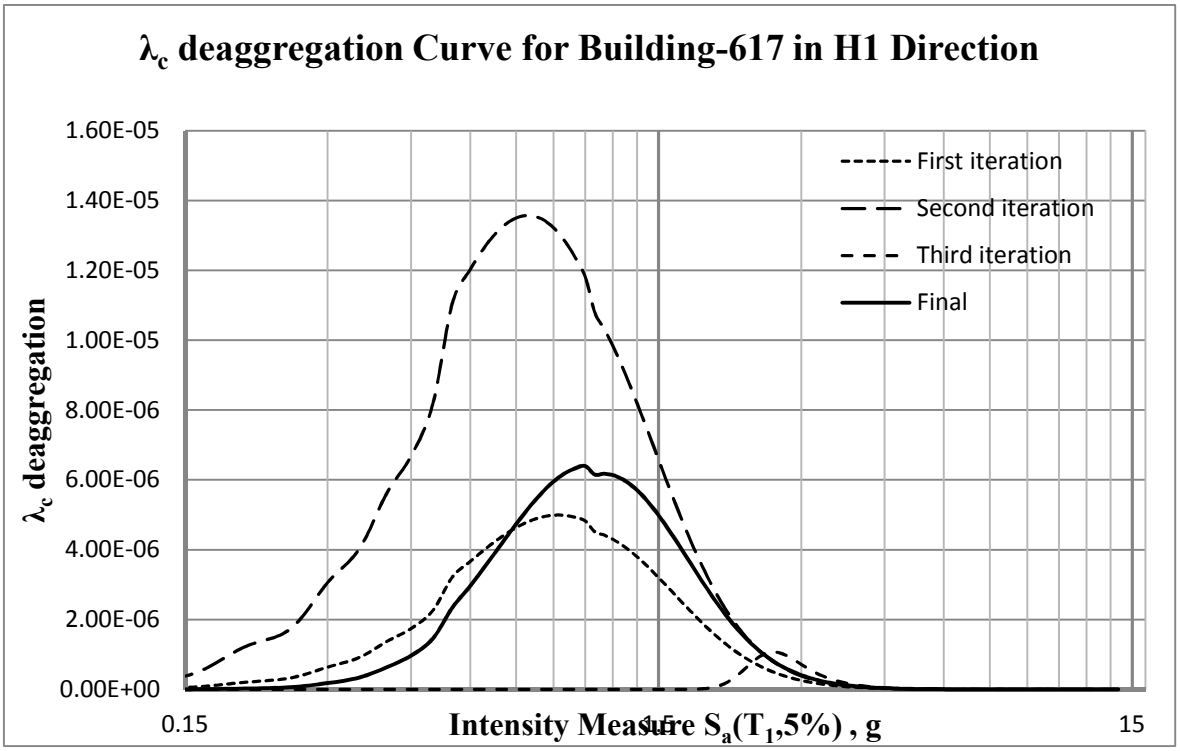

Figure 5.16. $\lambda_{collapse}$ deaggregation for building-617 in H1 direction.

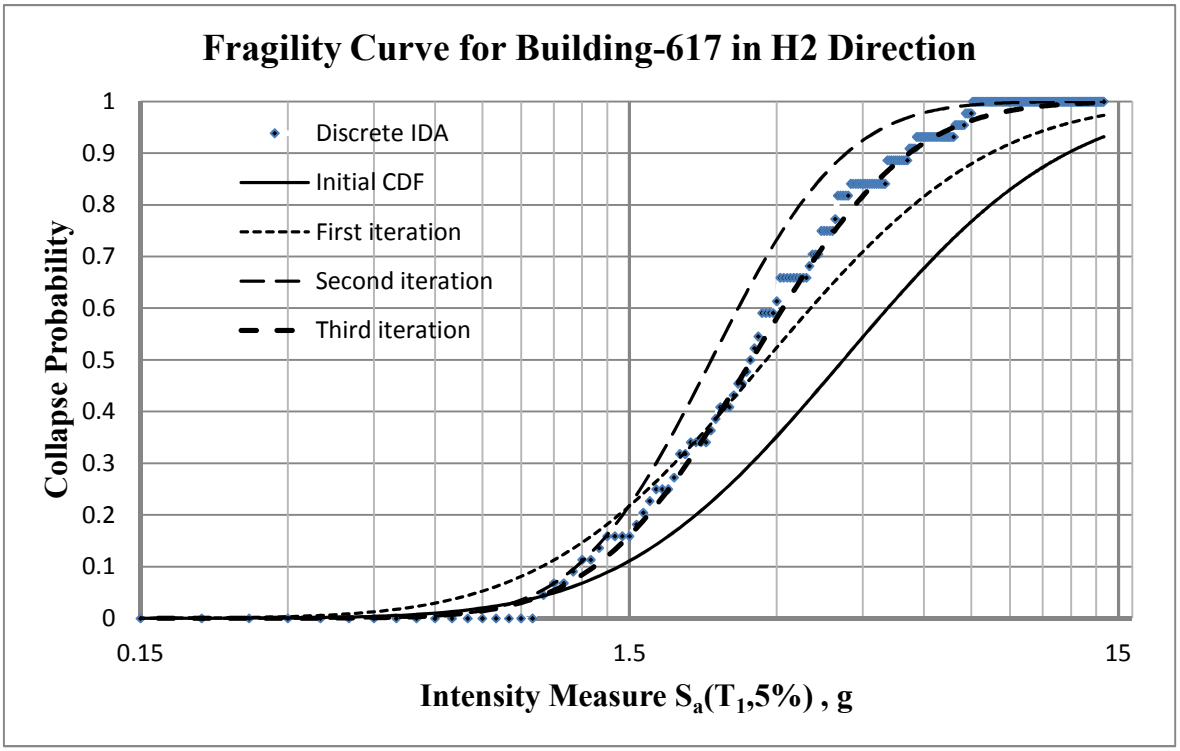

Figure 5.17. Iterative fragility curves for building-617 in H2 direction.

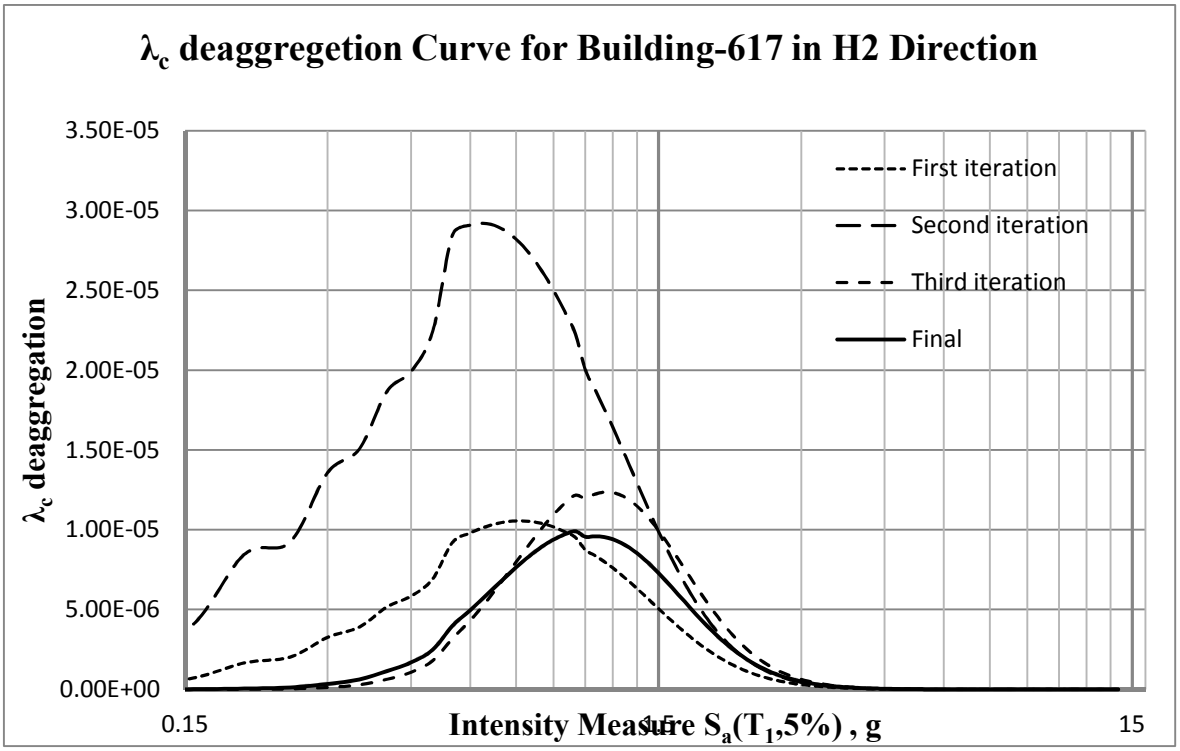

Figure 5.18. $\lambda_{collapse}$ deaggregation for building-617 in H2 direction.

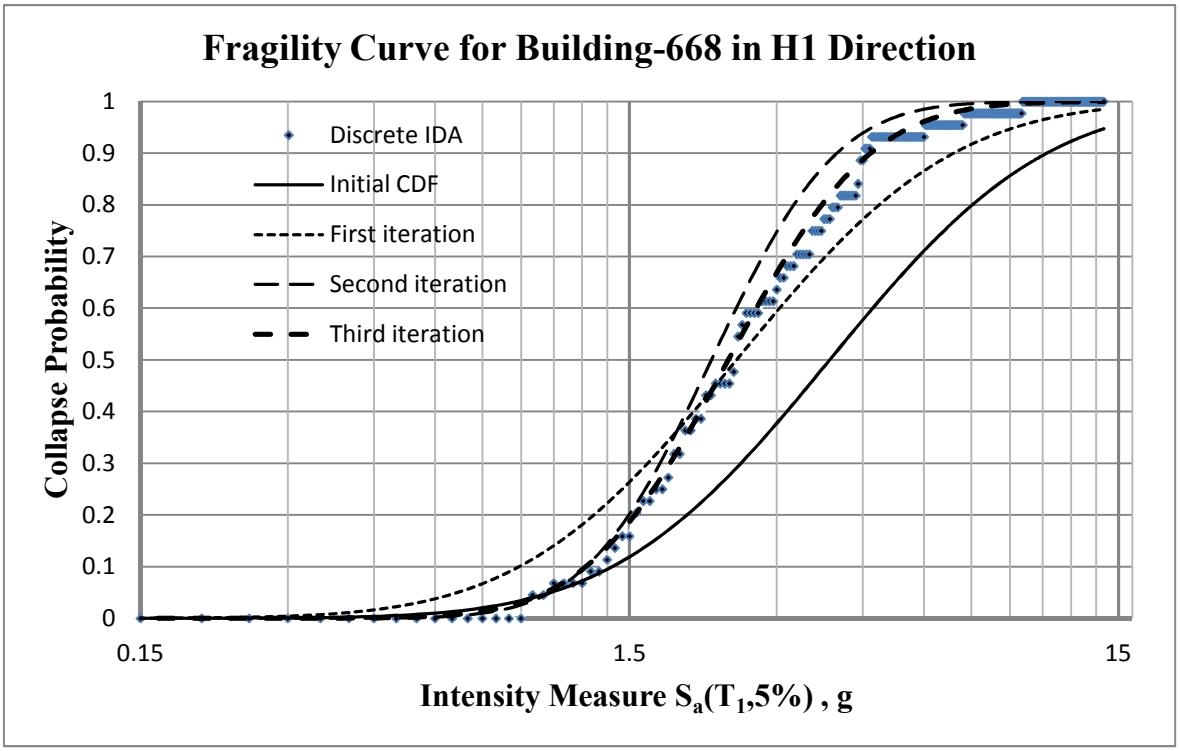

Figure 5.19. Iterative fragility curves for building-668 in H1 direction.

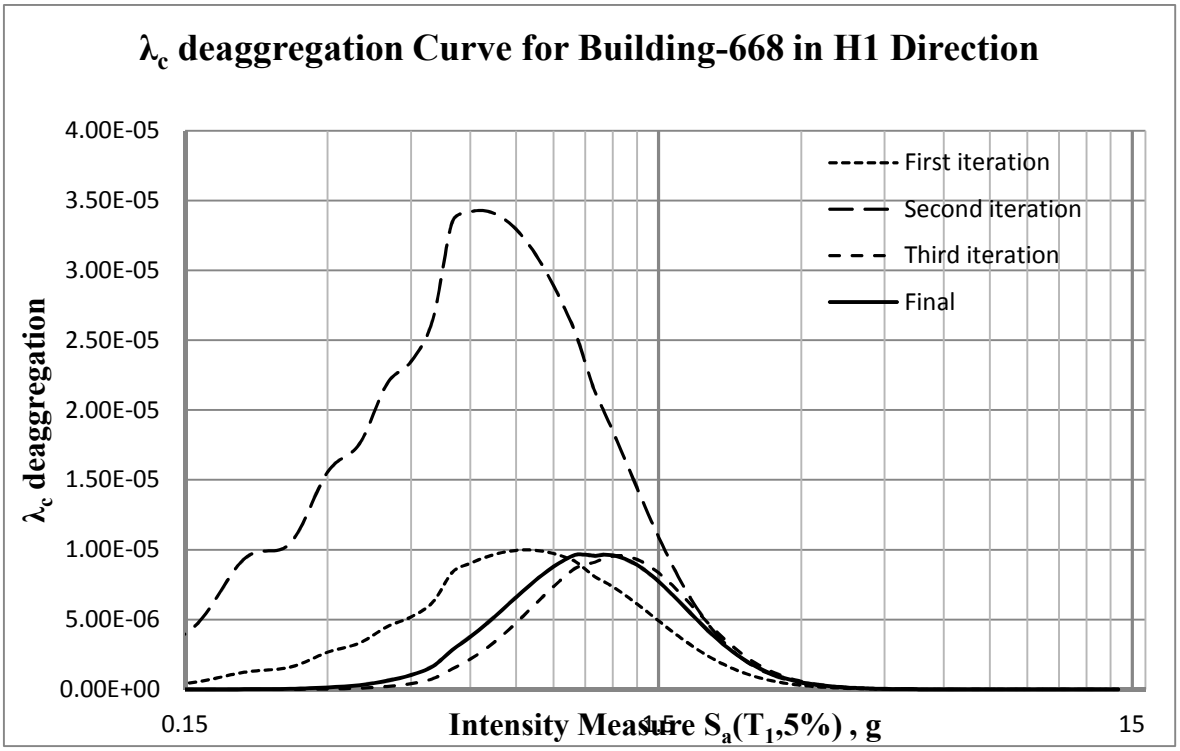

Figure 5.20. $\lambda_{collapse}$ deaggregation for building-668 in H1 direction.

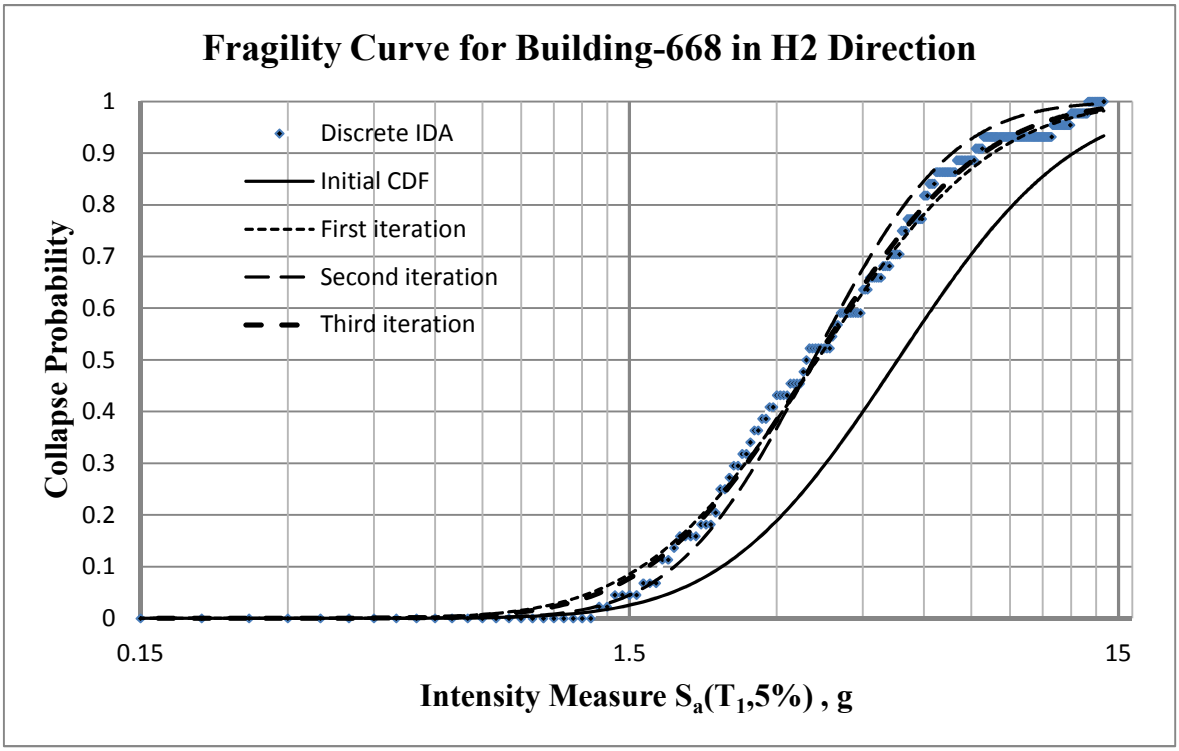

Figure 5.21. Iterative fragility curves for building-668 in H2 direction.

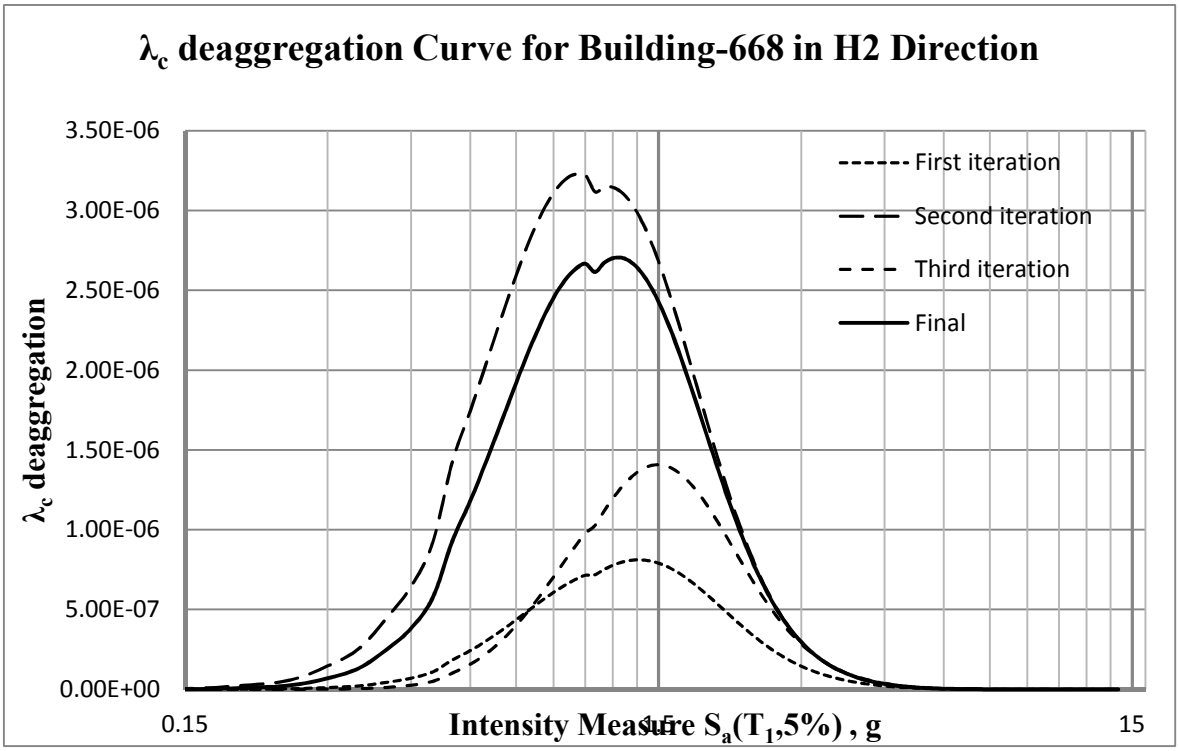

Figure 5.22. $\lambda_{collapse}$ deaggregation for building-668 in H2 direction.

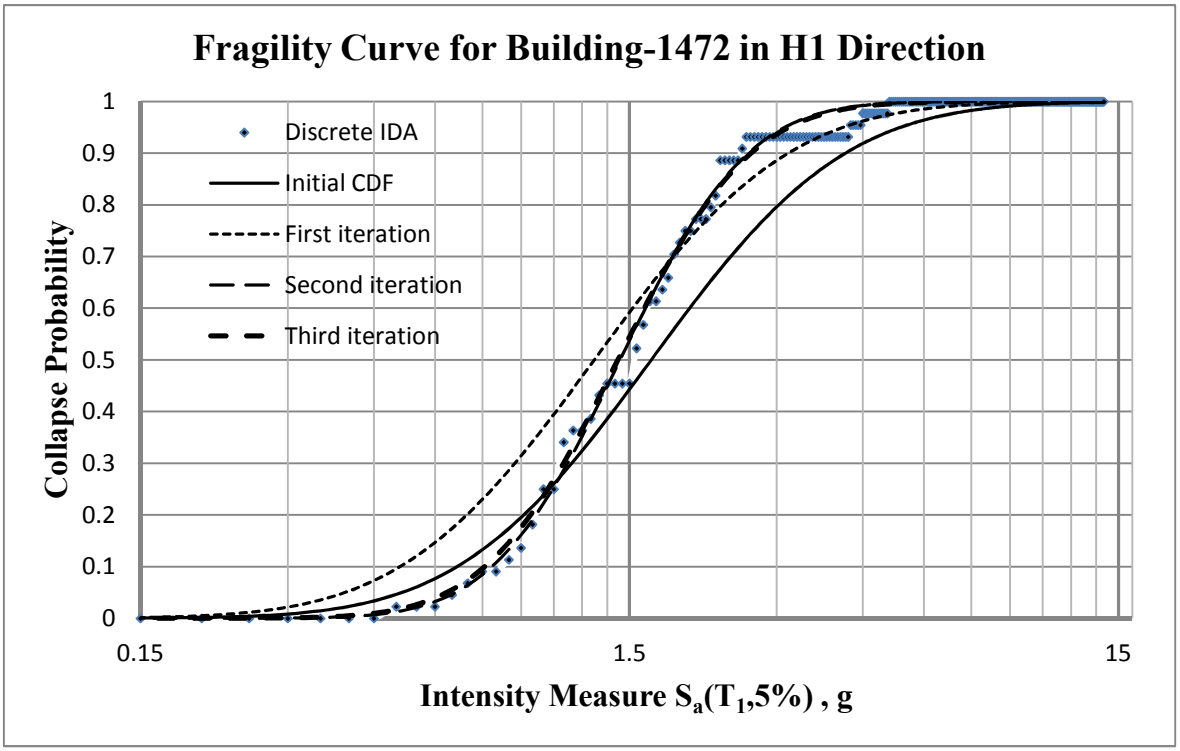

Figure 5.23. Iterative fragility curves for building-1472 in H1 direction.

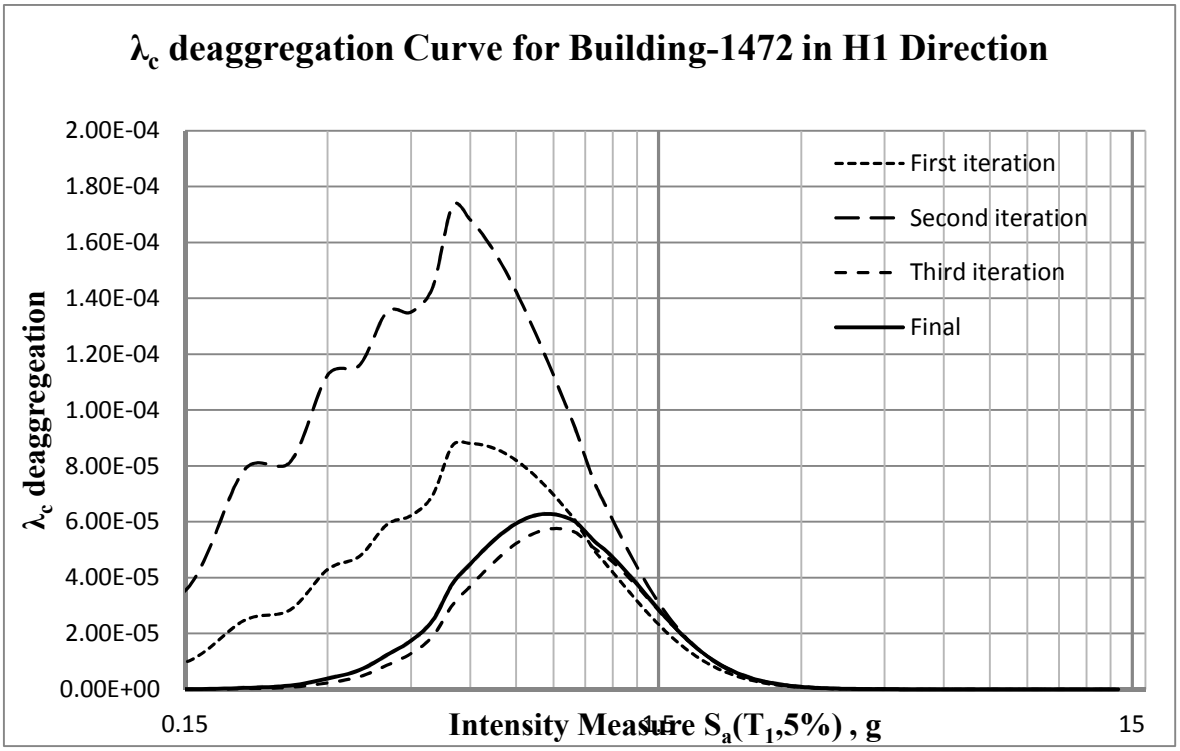

Figure 5.24. $\lambda_{collapse}$ deaggregation for building-1472 in H1 direction.

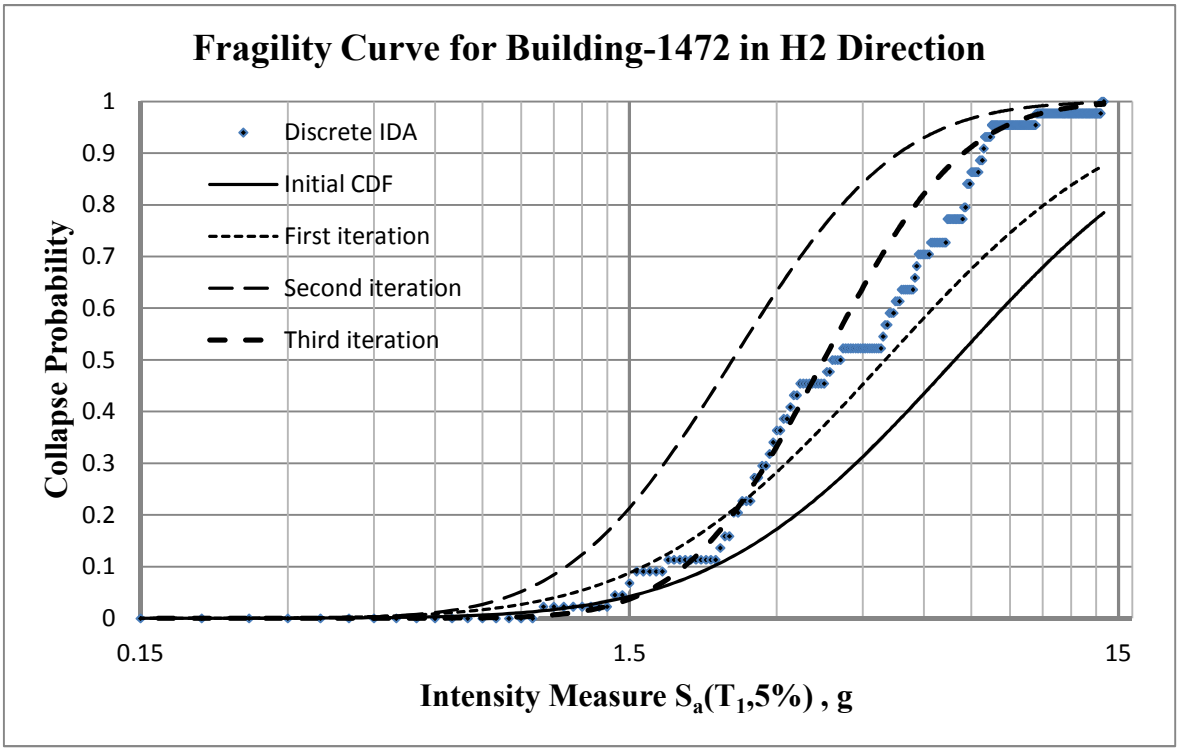

Figure 5.25. Iterative fragility curves for building-1472 in H2 direction.

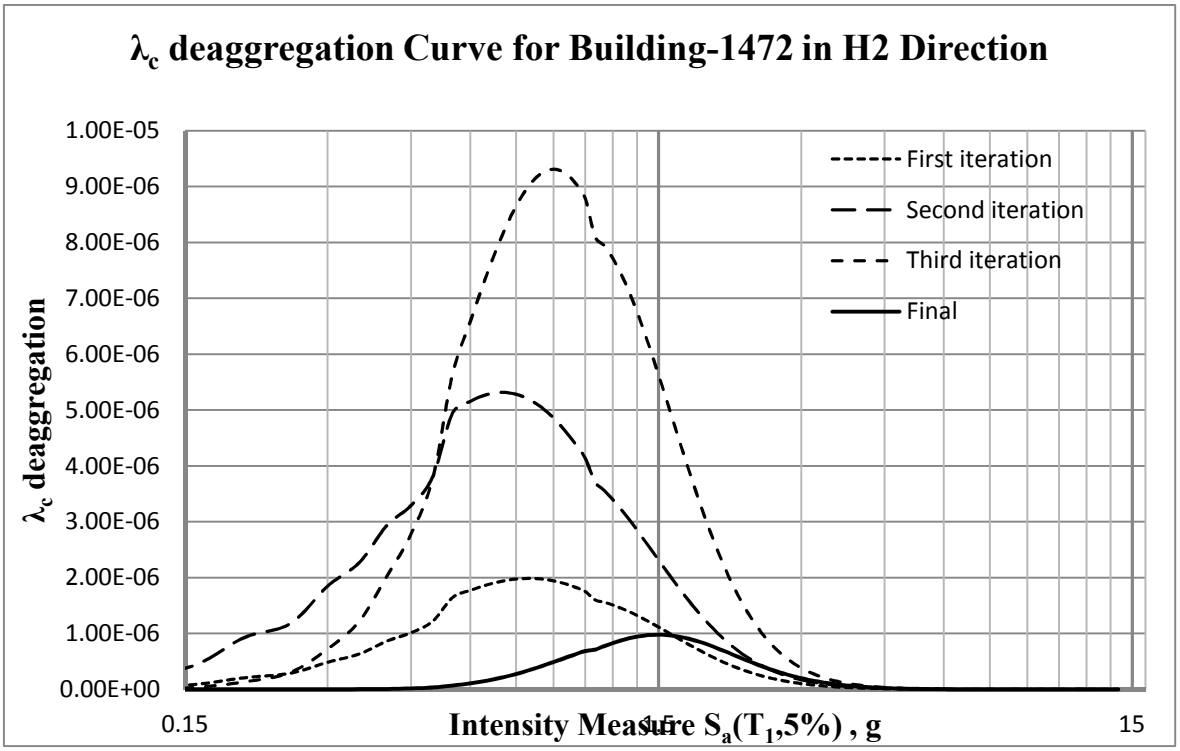

Figure 5.26. $\lambda_{collapse}$ deaggregation for building-1472 in H2 direction.

By using the classical procedure given in Section 5.4, calculated mean annual collapse frequencies and mean collapse risk in 50 years are given in Table 5.4. In this table, the values are calculated by using estimate fragility curves calculated iteratively in this section.

Table 5.4. Collapse probabilities of the example buildings for estimate fragility curve.

Building Name	**Direction**	**Period (sec)**	**Mean Annual Collapse Frequency $\lambda_{collapse}$**	**Mean Collapse Probability Over 50 years $P_{collapse}$(in 50 years)**	
411	H1	0.906	2.4200E-04	1.2027E-02	(1.2027%)
	H2	0.673	6.6709E-04	3.2805E-02	(3.2805%)
617	H1	0.732	1.7068E-04	8.4976E-03	(0.8498%)
	H2	0.609	2.5342E-04	1.2591E-02	(1.2591%)
668	H1	0.659	2.5012E-04	1.2428E-02	(1.2428%)
	H2	0.859	8.3044E-05	4.1436E-03	(0.4144%)
1472	H1	0.549	1.2893E-03	6.2429E-02	(6.2429%)
	H2	0.923	3.1740E-05	1.5857E-03	(0.1586%)

6. CONCLUSION

In this study IDA procedure is applied on a set of real three dimensional, non-linear numerical models of RC buildings through non-linear response history analysis. By using the actual design drawings of these real structures, the nonlinear design parameters such as framework plans, loads, material strength, longitudinal and transverse reinforcement detailing are applied to the non-linear model.

Four five-story reinforced concrete residential buildings used in this collapse risk analysis is selected from existing building stock of Bolu city which has been struck by 12th November 1999 Düzce earthquake with M_w=7.2 magnitude. All those four buildings are moment-resisting frame structures with monolithic beam-column connection. It can be stated that the selected structures can represent the regional engineering features for typical Turkish engineering practice.

In this study, sudden and excessive increment in the drift ratios is defined as the collapse state. The high drift values cause numerical convergence problem named as lateral dynamic instability in the nonlinear response history analysis.

The twenty-two pairs of two-component strong ground motions used in this study are obtained from the Far-field record set of the FEMA-P695 (2009). Also, both of fault parallel and fault normal components are applied each direction of the structure under consideration separately. Therefore, the total number of ground motions used in analyses has been increased to 44 and record-to-record (RTR) variability has been provided better. Uniform scaling procedure in time domain is preferred in order not to change the frequency content of the earthquake excitation. As such frequency content of earthquake data is not distorted by keeping phase information of the data intact.

Fragility curves which associate the probability of the selected damage level with ground motion intensity are presented in the form of log-normal cumulative distribution function. Studies show that fragility curve can be sufficiently well represented by two

parameters: a median value and a standard deviation. Mean annual frequency of the collapse is also estimated by integrating the fragility curve over the hazard curve

Classical discrete solution of a fragility curve as described in Section 5.3 is a time demanding problem. This classical estimation of a fragility curve require utilizing many consecutive incremental dynamic analyses by conducting nonlinear response history analyses for all scale levels of each strong ground motion record. On the other hand, if lognormal distribution assumption is accepted, the entire fragility curve can be clearly defined by two parameters: a median value and a standard derivation. Instead of these two independent variables, two random points on the cumulative distribution function can also exactly represent the log-normally distributed curve. In other words, estimation of collapse probability at only two intensity measure $S_a(T_1,5\%)$ points is enough to construct whole fragility curve.

These two classical and simplified methods estimate similar mean annual collapse frequency values with the order of 10^{-5} and 10^{-4}. These values obtained in the study are compatible with the conclusion of another study which assess the seismic performance of modern reinforced concrete moment frame building located in southern California (Haselton *et al*., 2007).

REFERENCES

ATC-13, 1985, *Earthquake Damage Evaluation Data for California Report*, ATC-13, prepared by Applied Technology Council, Redwood City, California, U.S.A.

Bowles, J.E., 1997, *Foundation Analysis and Design*, 5th edition, McGraw-Hill, New York, NY.

Campbell, K. W., 1997. "Empirical Near-source Attenuation Relationships for Horizontal and Vertical Components of Peak Ground Acceleration, Peak Ground Velocity, and Pseudo-absolute Acceleration Response Spectra", *Seismological Research Letters*, 68(1), 154–179.

Clough, R. W. and J. Penzien, 2003, *Dynamics of Sructures*, 3th Edition, Computer and Science Inc., Berkeley, CA.

Eads, L., E. Miranda, H, Krawinkler and D. Lignos, 2013, "An Efficient Method for Estimating the Collapse Risk of Structures in Seismic Regions", *Earthquake Engineering and Structural Dynamics*, Vol. 42, pp.25-41.

FEMA, 2009, *Effects of Strength and Stiffness Degredadion on Seismic Response,* FEMA P440A, prepared by the Applied Technology Council for the Federal Emergency Management Agency, Washington, D.C.

FEMA, 2009, *Quantificaton of Building Seismic Performance Factors,* FEMA P695, prepared by the Applied Technology Council for the Federal Emergency Management Agency, Washington, D.C.

Gutenberg, B. and C. F. Richter, 1954, *Seismicity of the Earth and Associated Phenomena*, Princeton University Press, 2nd edition.

Han, S. W., K. Moon and A. K. Chopra, 2010, "Application of MPA to Estimate Probability of Collapse of Structures", *Earthquake Engineering and Structural Dynamics*, Vol. 39, pp.1259-1278.

Haselton, C. B., Deierlin, G. C. 2007, "Assessing Seismic Collapse of Modern Reinforced Concrete Moment-Frame Buildings", *PEER Report 2007/08*, Pacific Earthquake Engineering Research Center (PEER), University of California, Berkley, CA.

Ibarra, L. F. and H. Krawinkler, 2005, *Global Collapse of Frame Structures under Seismic Excitations*, Report No. 152, The John A. Blume Earthquake Research Engineering Center.

Joyner, W. B., & Boore, D. M. 1981. "Peak Horizontal Acceleration and Velocity from Strongmotion Records Including Records from the 1979 Imperial Valley, California, Earthquake", *Bulletin of the Seismological Society of America*, 71(6), 2011–2038.

Matjaz, D. and P. Fajfar, 2004, "IN2- a Simple Alternative for IDA", *13th World Conference on Earthquake Engineering*, Computer and Science Inc., Vancouver, B.C., Canada.

Mander, J.B., M. J. N. Priestley, and R. Park. 1988. "Theoretical Stress-Strain Model for Confined Concrete.", *Journal of Structural Engineering*, Vol. 114, No.8, pp. 1804-1826.

NGA, 2008 *Next-Generation Attenuation (NGA) Models*, Pacific Earthquake Engineering Research Center, University of California, Berkeley, California. Available at http://peer.berkeley.edu/ngawest/nga_models.html/.

PEER, 2006, *PEER Next-Generation Attenuation (NGA) Database*, Pacific Earthquake Engineering Research Center, University of California, Berkeley, California. Available at http://peer.berkeley.edu/nga/.

PERFORM-3D *User Guide Nonlinear Analysis and Assessment for 3D Structures*, 2011, V5, Computer and Science Inc.,Berkeley, California, USA.

Tanırcan, G., 2010, *EQE520: Strong Ground Motion Lecture Notes*, Kandilli Observatory and Earthquake Research Institute, Department of Earthquake Engineering, Boğaziçi University, İstanbul, Turkey.

TS 500, Turkey, 2000, *Turkish Standards of Requirements for Design and Construction of Reinforced Concrete Structures – TS 500*, Turkish Standards Institute, Ankara.

Turkish Earthquake Code, Turkey, 2007, *Specification for Buildings to be Built in Seismic Zones*, Ministry of Public Works and Settlement Goverment of Republic of Turkey.

Tüzün, C., *A Seismic Vulnerability Analysis Procedure for Urban Loss Assessment*, PhD. Thesis, Kandilli Observatory and Earthquake Research Institute, Department of Earthquake Engineering, 2008.

Vamvatsikos, D. and C. A. Cornell, 2002, "Incremental Dynamic Analysis", *Earthquake Engineering and Structural Dynamics*, Vol. 31, pp.491-514.

Wilson, E. L. and A. Habibullah, 1987, "Static and Dynamic Analysis of Multi-Story Buildings, Including P-Delta Effects", *Earthquake Spectra*, Vol. 3, No. 2, pp. 289-298.

REFERENCES NOT CITED

Kappos, A.J.,M.S. Saiidi, M.N. Aydınoğlu, T. Isaković, *Seismic Design and Assessment of Bridges: Inelastic Methods of Analysis and Case Studies*, Springer,2012.

McGuire, R. K., *Seismic Hazard and Risk Analysis*, 1st Edition, Earthquake Engineering and Research Institute, Oakland, 2004.